SYNOPSIS OF PHASOR MONITORING APPLICATIONS FOR WIDE AREA CONTROL AND PROTECTION

A Thesis

by

AAQIB AHMAD PEERZADA

Submitted to the Office of Graduate and Professional Studies of
Texas A&M University
in partial fulfillment of the requirements for the degree of

MASTER OF SCIENCE

Chair Committee,	Miroslav M. Begovic
Committee Members,	Chanan Singh
	Tie Liu
	Sergiy Butenko
Head of the Department,	Miroslav M. Begovic

August 2018

Major Subject: Electrical Engineering

ABSTRACT

The phenomenon of voltage collapse in electric power systems has received a considerable amount of attention in the last decade. Although the occurrences of the voltage blackouts have decreased in the recent years, the problem of voltage stability still poses a considerable threat to the security and the reliability of modern electricity grids.

The ultimate objective of this thesis is to further investigate and expand upon the existing body of knowledge on the voltage collapse phenomenon and develop protection and control schemes for mitigating such undesirable events in modern electric grids. In doing so, the research done in this thesis work builds on an earlier work done in the area of Voltage Instability Prediction (VIP). Although proven to be a successful metric in determining the proximity of large nonlinear systems to a potential voltage instability event, much remains to be explored in the area of Voltage Instability Prediction.

In particular the issues of estimating the static stability margins, the locational dependence of accuracy of such VIP derived margins, the exploitation of redundant local measurements and a compelling argument in favor of combining/fusing the individual VIP margins into a single system-wide measure of voltage collapse margin form the main focus of investigation of this work. To lower the individual entropy of the VIP derived margins, a data fusion algorithm built on the foundations of Dempster-Shafer's evidential reasoning method is proposed. The research is concluded on a positive note with the final results further pushing the envelope of knowledge in the field of voltage stability studies in power systems.

DEDICATION

To my loving family.

ACKNOWLEDGEMENTS

I'd like to express my sincere gratitude for assistance and support provided to me in connection with this thesis to a number of people including :

First and foremost my supervisor Prof. Miroslav Bagovic for his valuable guidance and support in the absence of which this thesis would not have come to fruition. His careful observation of the development of this manuscript and of the articles published based on this work has been of great importance and instrumental in sculpting the principal facade of this work. In addition to honing my technical skills, Prof. Begovic's more intimate musings on love and life and on the importance of being earnest in the pursuit of scientific knowledge have been a source of great inspiration.

I'd also like to extend my appreciation to Ben Picone with whom I have shared many insightful discussions on the nature of the problem which eventually helped me to delve deeper and to better understand the complexities of several algorithms.

My colleague Dr. Reynaldo Nuqui for supporting this work and representing a part of it at the APAP conference held in South Korea in 2017.

My parents whose patience and unbridled love and support helped me to manoeuvre through various obstacles and never lose sight of my final goal.

Finally, my beautiful wife who continues to be my defense against nihilism and whose fierce love keeps many of my existential quandaries at bay. Every time I am faced with doubt or get bogged down by dogma, I turn to her in search of hope and purpose.

CONTRIBUTORS AND FUNDING SOURCES

This work was advised primarily by Prof. Miroslav Begovic, my graduate advisor with additional inputs from Prof. Chanan Singh and Prof. Tie Liu. The thesis committee consisted of Prof. Miroslav Begovic, ECE Department Head, Prof. Chanan Singh, ECE Past Department Head, Prof. Tie Liu and Prof. Sergiy Butenko.

The analysis depicted in Chapter 3, section 3.3 and Chapter 5, section 5.2 was conducted in part by Ben Picone of the ECE department. All other work for the thesis was completed by Aaqib Ahmad Peerzada independently. The graduate study was supported by a fellowship from Texas A&M University.

TABLE OF CONTENTS

LIST OF FIGURES

LIST OF TABLES

1. INTRODUCTION

This chapter provides a description of the background and gives a glimpse in to comprehensive body of the literature on the topic of voltage stability, starting with the classical approaches that were focused on the singularity of the Jacobian to the modern approaches more focused on the local measurements of current and voltage phasors. It attempts to provide an overview of the huge canvas of work done in the field of voltage stability starting from the early 1990s till the present date.

1.1 Background

In the planning and operation of Power Systems, voltage stability plays a pivotal role and has only accentuated in recent years, in terms of criticality and acting as a potential bottleneck to the successful operation of the entire power system. Voltage instability and by extension voltage collapse have received a considerable amount of attention in the last decade. Voltage collapse, and hence an electrical blackout, is the response of an electrical grid to the violations of several constraints that limit a large scale power grid's ability to transfer bulk electrical energy from the point of generation to the point of consumption. The mechanism of voltage instability and collapse was first identified by Russian scientists while working on the singularity of the Jacobian matrix in the power flow solution during early 1960s and 70s. Unlike angle stability, which was the first instability mechanism studied, voltage stability did evade the power system community for a while.

As the general understanding about the mechanism of voltage instability and collapse began to grow, a constant endeavor of the power system community has been to establish methods which could determine the proximity of a large power system to a potential voltage collapse situation. In recent years, given the rise of PMUs and the possibility of wide area monitoring of power systems, this line of work has witnessed an inflationary growth. One such successful

metric which has proven the test of time in determining the proximity of the system to a potential collapse scenario is the VIP, an acronym for Voltage Instability Predictor, which primarily senses the strength of the transmission network from the local measurements of current and voltage phasors. Although, VIP is one the first method devised for longer term voltage stability detection based on the local measurements, a significant body of literature exists on such techniques now, majority of which are presented in the form of either some variation of the original VIP formulation or derived from the the original VIP formulation. Work is currently being done on the versatility of the VIP formulation and several improvements have been made in the past couple of years.

1.2 Literature Review

Venikov et al. [4] use a modified Newton-Raphson algorithm to determine the point of voltage collapse. It is observed that voltage instability occurs when the system Jacobian matrix becomes singular. However, since the Newton's iterative process is executed in discrete steps, the solution can only be checked at each step. Thus, an interval between steps could contain a zero-crossing that would not be observed leading to a presumption of stability when the system in fact would have collapsed. Furthermore, under certain conditions, Newton's method may diverge when the system is in fact stable. To counter these problems, researchers propose a modified Newton's algorithm which makes it possible to approach the point of voltage collapse with accuracy. For large systems, this method could become quite time consuming.

The authors in [5] - [6] propose indices for voltage stability assessment based on the singularity of the Jacobian matrix also referred to as Modal Anaylis in [6]. The method relies on the calculation of the smallest number of eigen values and the corresponding eigen values of the system jacobian. While the eigen values reveal the system state in terms of the distance to the point of instability the eigen vectors can be used to assess the participation of the network elements. Based on the Modal Analysis a relationship between the voltage variation at node i and

the reactive power variation is established. The vulnerability of a particular nodal voltage to a possible scenario is established based on the magnitude of the corresponding eigen value and a system is deemed voltage stable when all the eigen values turn out to be positive. In addition, a measure of the participation by the network elements is made possible by the calculation of participation factors. This helps in outlining areas which are closer to the onset of voltage collapse and also helps in identifying branches with highest consumption of reactive power for a given incremental change in the system reactive load. The modal has been successfully applied to many large systems including the 3700 bus case. The applications as described in the paper are conducted as off-line studies and more work is required to fully investigate the potential of modal analysis for on-line stability assessment.

In [7] the authors review the method presented in [4] and arrive at some conclusions. The first one concerns with the stability of the load flow solution pair and the authors conclude that the solution which is given with the flat start is more stable than the exhaustive search multiple load flow calculation method. This article explores the relationship w between voltage stability and multiple load flow solutions from the view point of the static and /or semi-dynamic performances.

In [8], a mathematical explanation in the form of a saddle-node bifurcation is posited to model the phenomenon of voltage collapse. Central manifold theorem is invoked for studying the resulting dynamic processes and the proposed model is illustrated on a system which is made up of a generator connected to an infinite bus with a non linear load model. Similar bifurcation procedure has also been studies in [9], [10], [11], [12]. However, it is possible that the steady state equilibrium point can lose stability even in the absence of saddle-node bifurcation. The occurrence of such behavior, which is often attributed to Hopf Bifurcation, will affect the margin of stability in the sense that the distance to the collapse point will be less than one might expect if saddle-node bifurcation is taken as the only measure of voltage collapse. In the literature Hopf Birfucations have been reported before in power system models, in [13] where the authors illustrate sub-critical Hopf Bifurcations,in [14], a thorough analysis into local sta-

bility is provided as a result of Hopf Bifiurcation, another example is provided in [15] which the machine is modelled with a two axis representation and also in [16] where the authors illustrate a different type of degenerate Hopf Bifurcation with voltage control and a constant power load. In the study of chaos in power systems sub-critical and super-critical Hopf Bifurcations are encountered [17]. Hopf Bifurcations as a possible cause for voltage collapse have been reported in [18], [19], [20]. In [21], a degenrate Hopf bifurcation is illustrated on a system which consists of two generators and an infinite bus. Further references for bifurcations in power networks are [22], [23], [24], [25].

Hawkings et al. [26] propose an algorithm for assessing the remaining margin of a power system. This margin is expressed as the additional active power transfer which could be sustained. The algorithm monitors the voltage sensitivity elements of the Jacobian, $\frac{dV_i}{dP_i}$ and $\frac{dV_i}{dQ_i}$. The researchers state that a sign change in the inverse Jacobian (which heralds the system collapse) can be the result of a generator hitting its respective reactive power limit. Their proposed method predicts the precise collapse point by the following: 1) after observing a sign change, the inverse Jacobian is recalculated with the most recently limited generator restored back to a voltage-controlled bus. 2) If the elements are still negative, then they linearly interpolate between the current point and the point of the previous PV-PQ transition. Further up until 1996 before the advent of wide area measurement devices, the references [27], [28], [29], [30] document the work done on voltage stability till 1996. Majority of the work done in these references revolves around the maximum loadability conditions and development of methods to monitor voltage stability which are based on the singularity of the Jacobian. Further more important references which deal with the voltage stability assessment and the loadability limit margin are [31], [32], [33], [34], [35], [36], [37].

Vu, et. al [38] describe a system which utilizes local measurements sets of voltage and current phasors to estimate the closeness of a system to the occurrence of a possible instability. uses only local measurements to predict the proximity to voltage collapse. Except for the load bus in question, the rest of the transmission network is modelled by a stiff voltage source in

series with an equivalent system impedance, referred to as Thevenin impedance. For such a two bus representation, the Kirchhoff voltage equation states

$$V_L = E_{Th} - Z_{Th} I_L \tag{1.1}$$

Since E_{Th} and Z_{Th} are not directly observable and are complex numbers, the system contains four unknowns and is not directly solvable. Authors propose the use of a least-square algorithm to find the best solution based on this equation with multiple measurements. The system described by these researchers will become known as the Voltage Instability Predictor (VIP) and form the basis for much of the research contained in this report.

A difficulty of the VIP method pointed out by Corsi et al. [39] is that the equation (above) has infinite results unless the assumption is made that between two measurements, E_{Th} and Z_{Th} remain constant. However, when measurements are taken too close together, the corresponding matrix equation lends itself to a high probability of turning singular if there is no variation in observable parameters. An accurate result is only produced when there is significant system variation, which often happens too close to collapse for any meaningful action to be taken. As such [39] proposes a more robust algorithm for the purposes of identifying the Thevenin paramters. In this algorithm, the direction of change of and the amount variation in the Thevanin voltage is taken into account.

In [40], the analysis made in [38] is extended to include the voltage dependency of loads in the system Thevenin. It is concluded that the condition of maximum system loadability coincides with voltage instability. A metric to monitor the status of over excitation limiters is proposed for indication of the available system margin.

The problems of inclusion of all system loads in to a common system equivalence are dealt with in [41], wherein the authors propose a network decoupling transform to prevent the merging of all system loads in to a single equivalent. The objective is to break down a large complex

network with nonlinear and dynamic loads into a set of single networks. In [42] a linear indicator to voltage collapse is presented based on the multiplicity of the power flow. The authors propose the voltage collapse indicator to be $VCI = P/P_m$, where P_m is the maximum power that can be delivered to the load bus and is equal to $E^2/2X$, where E is the slack bus constant voltage and X is the line reactance. The linearity of the indicator makes the determination of the load margin to be $\delta P_m = P\,(1/VCI - 1)$.

Reference [43] makes use of Tellegen's theorem in conjunction with ad joint networks to compute the voltage stability index. The method provided an alternate way to estimate the equivalent model parameters of the Thevenin circuit. The main advantage of this method lies in the simplification of the estimation procedure.

Reference [44] proposes the use of a Voltage Collapse Indicator where the detection method is based on the critical lines as opposed to the use of critical nodes. The metric involves the use of the difference in the power flow at the sending and the receiving end of a line. The nature of the technique makes it possible to use it as a online monitoring tool as well as an offline monitoring tool. The method relies on the fact that close to a possible voltage collapse situation, the system line losses experience a nonlinear growth and exceed the system load demand. The situation is exacerbated by further increase in the load, as the extra generation is consumed in the lines because of increased losses, with losses taking up all the increased generation at the critical system loading. The metric can be used to locate lines in the system which show increased losses and thus could lead to the identification of the problem areas in a transmission network.

In [45], an online method for early detection of voltage instability is proposed. Voltage collapse prediction is made by making use of the bus voltage phasor and the corresponding system admittance matrix. The index can be computed at every PQ bus of the system and can take values in the range of zero to one. An index value close to 0 indicates a voltage stable node where as the index value close to 1, refers to an voltage unstable node.

Reference [46] presents another customized variation of the VIP impedances and proposes a stability index to determine the theoretical loadability limit of a network.The proposed indicator has the definition given by

$$VSM_s = \frac{(Z_l - Z_{th})^2}{Z_{th}^2 + Z_l^2 + 2Z_{th}Z_l\cos(\beta - \theta)} \tag{1.2}$$

where

β= Phase angle of Thevenin Impedance

θ=Phase angle of Load Impedance At the voltage collapse point the margin as indicated by VSMs reduces to zero.

Reference [47] posits the use of an online voltage stability analysis tool. This method is another variation of the original VIP method where the maximum real, reactive and apparent power is estimated to determine the stability index of a system. The stability index as presented in the paper is defined as

$$VSI = \min\left[\frac{P_{margin}}{P_{max}}, \frac{Q_{margin}}{Q_{max}}, \frac{S_{margin}}{S_{max}}\right] \tag{1.3}$$

Where

$$P_{max} = \sqrt{\frac{V_s^4}{4X^2} - Q\frac{V_s^2}{X}}$$

$$Q_{max} = \frac{V_s^2}{X} - P^2\frac{X}{V_s^2}$$

$$S_{max} = \frac{(1-\sin\theta)V_s^2}{2\cos^2\theta X}$$

Another customized variation of the VIP impedances algorithm is proposed in [48]. The proposed criterion relies on the change in the apparent power with respect to the change in the load admittance to determine $\frac{Z_L}{Z_S}$. The proposed metric can be easily computed and stays largely unaffected by the load characteristics. The data required can be easily extracted from the

local measurements made at a load bus and the metric can be reevaluated with every change in the system load.

Reference [49] establishes the use of a stability index referred to as Equivalent node voltage collapse index (ENVCI). As is common with the methods based on local measurements, this technique also requires the use of local voltage phasors. The advantages mainly lie in the computational ease offered by the method and benefit in being used as an on-line monitoring tool. The proposed index is given by

$$ENVCI = 2E_k V_n \cos\theta_{kn} - E_k^2 \tag{1.4}$$

When the index approaches zero in at least one node in a system, the system is assumed to move closer to the stability limit. The node with the least measure of the index is considered as the weakest node in the system.

Reference [50] is a lucid attempt at contextualizing the problem of voltage stability in power systems. The article summarizes the nature of the problem, driving forces behind instability and proposes some counter-measures to combat such voltage collapse situations. Some aspects of emergency control are also discussed with particular emphasis on load tap changer control and load shedding.

Reference [51] proposes the use of linear extrapolation of a stability index metric developed from the current and voltage phasors made available at a load bus to estimate the distance from the current operating point to a possible instability. The paper addresses the issues caused by the action of over-excitation limiters (OELs), line contingency and uneven load power transfer increase. The proposed stability index has the definition given by

$$VSI = \left[1 + \frac{I_i}{V_i}\frac{\triangle V_i}{\triangle I_i}\right]^{\alpha} \tag{1.5}$$

Where V_i and I_i refer to the votlage and the current phasors at the load respectively and

$\triangle V_i$ and $\triangle I_i$ refer to the changes in the voltage and the current when the load apparent power changes. The VSI varies from unity (at no load) to zero (at voltage collapse).

Reference [52] summarizes the key issues involved in the current and the upcoming generation of SPS and various emergency control schemes. Different equipment outages can lead to a potential black out scenario, as has often happened in many cases around the world. Under such a scenario, the need for a system which has the capabilities of combating such undesirable situations and can issue a timely prediction about an impending collapse scenario becomes crucial. Such a system should ideally perform actions that would revert the system back to the normal operating sate and minimize the impact of the disturbance. The authors propound that automatic load shedding is an improved solution than under-frequency load shedding. If the tasks are simple, local measurements suffice although for more complex requirements, it is deemed that communication of information which could either be from a central location or a remote substation is important. The paper reviews some basic disturbances in the power systems like the angle stability and voltage stability and reviews some of the remedial measures.

Reference [53] the authors propose a dynamic voltage collapse index with applications in wind generation. Like Solar PV, a wind generator connected to a distribution feeder can result in fluctuations in the power flow on the feeder. The variability associated with the wind power causes problems with the voltage regulation on such feeders. The effect of the shunt capacitors has been ignored in the derivation of the index, since voltage levels of distribution systems are low and line lengths are short. The authors define a parameter called Maximum Loadability Limit for a line carrying power from sending end bus to a receiving end bus. The MLI is defined as

$$MLI = \frac{V_i^2[(-r_{ij}P_j + x_{ij}Q_j) + \sqrt{(r_{ij}^2 + x_{ij}^2)(P_j^2 + Q_j^2)}]}{2(x_{ij}P_j - r_{ij}Q_j)^2} \tag{1.6}$$

where r_{ij}=Line resistance, x_{ij}=Line reactance and P_j, Q_j= Active and Reactive load at the receiving end

The authors in [54] propose a voltage stability indicator, VSI defined as

$$VSI = \frac{P_{max} - P_{calculated}}{P_{max}} \tag{1.7}$$

P_{max} can be found from the inequality

$$E^2(E^2 - 4PR - 4QX) - 4(QR - PX)^2 \geqslant 0 \tag{1.8}$$

where P and Q are the active and reactive load on the bus R and X are the Thevenin impedance parameters. The analysis is based on equating the sending end and receiving currents across the Thevenin equivalent and the load and arriving at the quadratic expression for the receiving end voltage in terms of V^2. The phasor equation of the equivalent Thevenin model of the system with respect to a particular load bus requires two sets of measurements of voltage and current phasors for making the system observable. However the disturbance needed to generate different measurement set of load bus voltage and current phasors should be on the load side and not on the source side. The authors propose a transformer tap position changes for obtaining two distinguishable sets of load bus voltage and current phasors. This change can be detected by the PMUs placed in the power network to produce two different sets of voltages and currents at the load bus and an equivalent model can be obtained. The issue of tap changers is addressed in the paper with either active change of direction or a proactive change of direction.

In [55] the authors discuss the issued related with the implementation of Synchrophasor measurements. The authors review the current limitation in implementing the efficient real-time protection and control schemes, expounding various issues like measurement systems, communication networks, Synchronized measurements, Computing resources, measurement hardware, monitoring of instantaneous phase angles and frequency applications of fast measurements and co-ordination and control techniques. Some of the issues having to do with the measurement of the phasors are delineated and the authors illustrate the affect of various com-

putational methods on the noisy steady state phase angle measurements. It is observed that the use of different techniques can possibly lead to conflicting situations. For deployment of PMUs on a large scale, it is imperative that the PMUs be subjected to certain testing requirements and be properly calibrated. Further, the challenges involved in the testing and calibration of PMUs are identified under the light of relevant standards.

In [56] the authors present an on line voltage stability assessment scheme using synchronized phasor measurements and periodically updated Decision Trees. The main focus of the investigation of the article are the problems caused by the severe disturbances. The authors propose the use of a three step decision tree scheme for on line voltage security assessment. The scheme entails conducting detailed post contingency voltage security analysis, periodically updating the DT's with the anticipated operating conditions for the next hour and continuously collecting the corresponding the PMU measurements.

In [57] the authors propose a load shedding algorithm which utlizes both voltage and frequency information provided by the PMUs. The main contribution of this paper is the consideration of reactive power along with the active power in the load shedding strategy. The authors propose the use of global triggers which consist of the λ_{min}, the minimum eigen value of the Jacobian matrix, f_c out of the normal frequency range and $\frac{df_c}{dt}$, the rate of change in frequency in the abnormal range of [-1.5,-0.2] Hz/s. Any of these triggers may initiate the load shedding. The authors propose the use of two indices for active and reactive power which are proportional to the total active and reactive power balance. The two indices contain the information about the frequency and the active power and voltage and reactive power respectively. An innovation of this paper lies in the use of reactive power to assess the reactive power load shedding in conjunction with the active power load shedding.

Reference [58] examines the feasibility of using the synchro-phasor measurements to develop a system wide voltage stability monitoring system.The voltage magnitude and the rate of voltage decline are considered as the two key criteria and a proposed synchro-phasor based

voltage stability monitoring index combines them by means of their weighted sum. The main innovation lies in the use of only time series data of the bus voltages for anticipating an impending voltage instability scenario, following a contingency or a load increase.

Reference [59] identifies some of the problems with the methods based on the impedance matching condition. Of particular significance is the inability of the impedance metric in issuing an early warning for an impending collapse situation. The difficulties involved in the extraction of the Thevenin impedance further compound the issues of the impedance matching methods. The detection scheme presented in the paper works on the measurement of controlled voltage of bulk power delivery transformers with load tap changers. The method works on the basis of a simple comparison of secondary voltages between two successive tap changes.

The authors in [60] attempt to deal with the long term voltage stability caused by the different equipment outages, usually a generating or a transmission item. The authors propose that by monitoring post disturbance voltages which can be extracted from the PMU measurements, a possible detection of the onset of voltage instability can be made. The underlying assumption is the high penetration of the PMU devices in the electrical grid in the future. The effects of OELs and LTCs are considered and the sensitivities are obtained in real time with a corresponding change in sign used as an indicator.

Reference [61] considers the issues posed by dynamic load models and constructs a stability index which is based on the state matrix determinant. The load model is of an induction motor in parallel with a constant impedance. Near the equilibrium point, linearization of the load model is carried out for the development of the stability index. The index has the features of

- Explicit network modelling is assumed to be factored in by WAMS measurements at different time steps.

- The proposed index is completely linear for all the margin values.

- The method is computationally less intense.

The authors in [62] propose the use of monitoring methods which is an extension of the methods based on wide area measurements facilitated by the use of PMUs. The underlying assumption is that the generators which is nearest to the load is capable of revealing system information which is comparable with the Thevenin voltage. The sum of the absolute values of the complex voltage is used to quantify the distance to the generator from a particular node. A Voltage stability index is defined

$$VSI_k = \frac{V_k}{\triangle V_k} \tag{1.9}$$

Where

V_k= Voltage at node k

$\triangle V_k$= Distance to the nearest generator

A major advantage of this method is that it could be implemented rapidly with a fast refreshment rate. However the method poses an increased computational burden under the changing system condition.

In [63], a model for the assessment of voltage stability in a transmission corridor, based on PMU measurements is presented. The authors contest that the proposed model is more detailed than the models based on a simple Thevenin model of a circuit with the retention of all transmission lines. Curve fitting techniques such a least squares technique is used to estimate the model parameters from the measurement samples obtained from PMUs. The model allows the use of boundary buses and the lines which directly connect the two nodes at a boundary. The model can be subdivided in to a generation center, the load center and the transmission center. It has been observed that the model presents a low compuational burden and has been tested on the IEEE 9 bus system.

Reference [64] is an attempt to refine the algorithm originally proposed in [62]. An index which quantifies the electrical distance is used to identify the nearest generator to a particular load. The model of the network is used to determine the relative eletric distance with a voltage drop defined by

$$\triangle V_i = \sum_{b=1}^{n_j-1} |V_b - V_{b+1}| = |V_g - V_i| \tag{1.10}$$

Where V_g and V_i are the voltage phasors at the nearest generator and the analyzed load bus. The sensitivity of the index is further increased by making use of a correction factor β. When the proposed index approaches a value of unity, the system becomes voltage unstable. This method does however require the use of PMU at each load bus, the feasibility of which is up for debate.

Reference [65] improves upon the traditional L-index by consolidating an equivalent model for a generator in to the voltage stability analysis. In order to fully capture the time variant behavior of the generating devices, time varying internal voltages and impedance are used. Assuming the knowledge of certain generator parameters, the authors propose to estimate the parameters of the Thevenin model by using only one system state. Like in previous mentioned indices, as the value of the index approaches unity, it signifies critical voltages.

Reference [66] investigates some of the advantages associated with the reduction of voltages in relation with avoiding the addition of new capacity as well as increasing the stability margins. Voltage reduction involves the act of regulating substation voltages in order to operate the feeders at minimum acceptable voltage levels. With the addition of reactive support along a distribution feeder, an improvement in the minimum feeder voltage is possible. It is observed that the effects of the voltage reduction are often dictated by the behavior of the dominant customers on the feeder. The paper studies the cost benefit analysis and the voltage stability effects which can be improved as a results of

1. The reduction of active powers made possible by the practice of voltage reduction.

2. Load reactive powers are offset by the use of reactive support along a feeder. The range of load power factors is normally between 0.99lagging and0.99 leading.

Reference [67] proposes a framework to address the challenge of voltage stability after a contingency, by utilizing a coordinated control strategy of the FACTS devices installed in different areas in a power system. The article discusses the response strategy which is executed by having a coordinated control of several FACTS devices in order to compensate for the reactive power. Reactive power compensation elevates the depressed voltages in a power network and presents an easy solution method to combat situations which lead to depressed voltages in a power system. The authors seem to propose that line compensation utilizing FACTS devices allows for a more robust voltage control following a severe disturbance. This method has the advantage of not interfering with the system topology or the availability of the generators. The article illustrates the coordinated control strategy of different FACTS devices for accomplishing reactive power compensation to improve the system stability margin.

The article [68] deals with the on line estimation of the Thevenin Equivalent when system states are changing. The tracking of the Thevenin Impedance based on the equation $\overline{E}_{th} - \overline{Z}_{th}\overline{I} = \overline{V}_L$ is valid when the Thevenin voltage stays constant between two phasor measurements. If a disturbance occurs (system side changes), the Thevenin voltage changes and estimation process is hindered. The article proposes a statistical way of computing the Thevenin Impedance when system side changes happen using the local measurements. The Thevenin impedance as computed by considering the system side changes is expressed as

$$\overline{Z}_{th} = \frac{-COV[\triangle\overline{V}_L \triangle\overline{Z}_{app}]}{COV[\triangle\overline{I}_L \triangle\overline{Z}_{app}]} \tag{1.11}$$

Where $\triangle\overline{V}_L$ and $\triangle\overline{I}_L$ represent the changes in the voltage and current phasors at the load bus and $\triangle\overline{Z}_{app}$ represents the change in the apparent load impedance between two successive measurements. For estimating the Thevenin Equivalent at different system conditions, the article proposes the use of Recursive Least Squares technique, using the impedance as obtained

by using the statistical expression as the initial guess to track the system stability.

Reference [69] includes a framework to examine the weakest branch in a network. A weakest branch is defined as the heavily loaded branch in a distribution network. The stability indicator is developed by equating the sending and receiving end current, and is defined as

$$VSI = \frac{4Q_j}{V_s^2 X_i}(R_i^2 + X_i^2) \tag{1.12}$$

where Q_j is the reactive power flowing in the receiving node and $R_i and X_i$ are the resistance and the reactance of the branch. In line with the previous methods, in oder to maintain the voltage stability the proposed index should be less than unity. If the value of VSI exceeds unity then the branch is unstable. The effectiveness of the proosed VSI is tested on the 11kV radial distribution systems consisting of 12 buses. The branch with the least value of the VSI is the closest to the instability.

In [70] the authors extend the previous analysis on on line estimation of Thevenin Impedance using statistical methods and develop a framework for under voltage load shedding. The authors argue in the favor of under voltage load shedding, positing that it presents a viable economical solution to the challenge of voltage instability while also providing protection for unusual disturbances which are not considered while designing the planning and operation procedures. This article first expounds on the Thevenin Equivalent estimation considering system side changes and then discusses the placement of UVLS relay based on modified maximum power transfer. In this article the authors propose the use of an indicator L for deciding the UVLS relay placement. The indicator L is defined as

$$L = \left| 1 + \frac{\overline{V}_0}{\overline{V}_1} \right| = \frac{\overline{S}_1}{\overline{Y}_{11}.\overline{V}_1^2} \tag{1.13}$$

Where $\overline{S}_1$ is the apparent power injected in to the network at load bus. $Y_{11} = Y_L + Y_Q$ is the self admittance of the load bus. $\overline{V}_1$ is the bus voltage and $\overline{V}_0 = -\frac{Y_L}{Y_L + Y_Q}.V_2$

A larger value of the L metric signifies more sensitivity to changes in the load. The authors argue it would prove to be effective to place the UVLS relay at buses which have larger L values. The amount of the load shedding is determined by the study of the P-Q curve derivation. By using the equation of the voltage at the receiving end of the line, for a given P the value of Q that forces the system to operate at the verge of collapse is obtained. Certain numerical examples and case studies are presented for the UVLS relay placement based on the L indicator values.

In [71], Phasor measurement units (PMUs) are utilized for estimating the real time stability margin in a load area which is supported by multiple tie lines. The authors suggest that the method is more resilient to the changes occurring in the phase angles of the external system and tie line flow power factor. It is observed that the assumption of "$constant\theta$" in the Thevenin voltage phasor can result in inaccuracies in the proper identification of equivalent Thevenin impedance which would further contaminate the estimated measures of the loading margin. Another potential issue with the impedance matching criteria is the possibility of reaching of active and reactive limits at different times under the conditions of changing tie line power factors. A non-pocket load area is replaced by a fictitious bus with an equivalent voltage phasor $\overline{V}$ and an equivalent tie-line current phasor $\overline{I}$. The changes in the Thevenin voltage phase angle θ are considered and the impedance matching criteria is modified and impedance indices are defined as Z_S, Z_P and Z_Q to be security limits of Z_L in terms of the power transfer limits of S, P and Q. Z_L is defined as $\frac{\overline{V}}{\overline{I}} = Z_L\angle\phi$.

Only when ϕ is constant, $Z_S = Z_P = Z_Q$ and $\overline{S}_{ax} \triangleq S_{max}\angle\phi = P_{max} + jQ_{max}$. Otherwise the total S,P and Q of the monitored tie lines may meet their limits at different times. In the paper the authors argue that it advisable to estimate S_{max}, P_{max} and Q_{max} seperately to identify the limiting factor on voltage stability. An impedance index is defined in the paper

$$Z_T^S = Z_S + (Z_T - Z_S)\left|\frac{1-\left(\frac{Z_S}{Z_L}\right)^\gamma}{1+\left(\frac{Z_S}{Z_L}\right)^\gamma}\right| \tag{1.14}$$

Simulations have been carried out on a two bus system and IEEE 39 bus system and it is shown

that the new approach gives estimates the Thevenin parameters more accurately than the old approach.

In [72] the authors propose a new method to estimate the Thevenin parameters based on the Schmidt's orthogonalization transformation. The authors argue that the method is more accurate in tracking the Thevenin parameters providing more precision than the conventional methods. Schmidt's orthogonalization transformation solves a general least squares equation of the form $C\hat{\theta} = d$ where C is the coefficient matrix. The method involves the use of unit column vectors which combine with the rows of the coefficient matrix and produce row vectors which are not linearly dependent. The authors claim that when Thevenin parameter equations are severely ill-conditioned then the Schmidt's orthogonalization transformation loses stability. The method has been tested in a real world system with data obtained from PMUs and the authors claim that a precise estimation of the Thevenin parameters was achieved.

In [73] the authors propose to calculate the voltage stability power margins and their visualization in the P-Q plane. The voltage stability boundary is computed in real-time with the assumption of a parabolic P-Q curve. Starting from the impedance matching criteria of the VIP the authors develop an index for calculating the MVA,MW and MVAr distance to the collapse point. The maximum MVA corresponding to the current values of the Thevenin Parameters is defined as

$$S_{max} = \frac{E^2\sqrt{1+\tan^2\Phi}}{2[R_t + X_t\tan\Phi \pm \sqrt{(R_t^2+X_t^2)(1+\tan^2\Phi)}]} \tag{1.15}$$

based on the constant power factor. The loading margin is then computed as

$$\triangle S = S_{max} \tag{1.16}$$

The voltage stability boundary is defined by a parabolic equation of the form

$$Q_t = a^2 P_t + bP_t + c \tag{1.17}$$

and it is claimed by the authors that in principle only measurement is sufficient to determine the coefficient a, b and c. The Nordic test system has been used for calculating the stability margins and the authors claim that the method is easy to implement in real time and offers a simple and a clear interpretation of the results. The method also takes advantage of the fast PMU sampling enabling timely detection of the changes in the system.

Reference [74] compares different algorithms for estimating the Thevenin Impedance. Since the impedance matching condition indicates the onset of an imminent voltage collapse it is very important to have a fast and accurate estimation of the Thevenin Impedance. In this paper the author compare four major algorithms used for estimating the Thevenin Equivalent namely Least Square technique introduced by [38], the adaptive technique introduced by [39], algorithm based on the coupled single port circuit and an estimation technique which is based on Tellegen's theorem. Two different scenarios are created. In the first scenario, New England system is used and in the second scenario, 140 Bus NPCC system is used. In the analysis the authors contest that the algorithm based on the least squares technique seems to work better in assessing a voltage collapse scenario. However the comparison has not been tested on larger systems which would have been a more rigorous test of the algorithms.

A smart relay scheme based for long term voltage instability is proposed in [75]. The method called VIP++ is based on the local area measurements and seeks to improve the robustness and observability of the conventional VIP as proposed in [Begovic seminal]. The VIP++ is an expansion of the previous VIP and it improves the estimation by adding the knowledge from the surrounding area of the load bus. The VIP++ looks at two load buses and measures the current and voltage at both load buses and assumes a known admittance between the two. Two methods of VIP++ are explored in the paper. One of the methods assumes a constant load gradient at the load buses and the other method assumes a sudden increase in the load at one bus. When the system is far from collapse the VIP++ method gives an approximate distance to the point of collapse. As the system trajectory moves close to the collapse point the method becomes more accurate. This is true for both the alternatives. The authors claim that the method

can be expanded to include more known load buses.

In [76], a more intuitive index referred to as the "power margin" is proposed which is based on the linear forecast of the V-I characteristics obtained at a load bus. The distance to the possible collapse is quantified in terms of apparent power. Power margin from the current operating point is expressed as

$$\triangle S = \frac{(V_t - Z_{th} I_t)^2}{4 Z_{th}}. \tag{1.18}$$

The linear forecast index has been tested on the AEP southern transmission region which consists of 22,000 miles of High voltage lines, including 2022 miles of 765,000-volt lines. In the paper, the authors claim that the forecast stays optimistic if there are no topology changes.

Reference [77], discusses a method which makes use of the local measurements obtained from the PMUs to assist in the online identification of the equivalent Thevenin parameters at a particular node. The errors associated with the measurement are taken into account and so are the changes that seem to occur on the system side. The article includes an analysis of the effects of the changes that happen on the system side and the corresponding impact on the determination of the equivalent system parameters. Similar measurement based indices are also proposed in [78], [79], [80], [81].

In [82], extrapolation based on a cubic spline is proposed for estimating the steady state voltage stability limit. It is expected that the use of a spline extrapolation should increase the accuracy of determination of the loading margin. The method invovles similar assumptions found in all the local measurement based techniques and employs a spline function with three data points given by

$$Q_j(x) = a_j + b_j(x - x_j) + c_j(x - x_j)^2 + d_j(x - x_j)^3 \tag{1.19}$$

This makes possible the estimation of loading margins expressed as the percentage of base

apparent load of the system. Voltage stability margin is expressed as $VSM_s = \frac{P_s^M(k)}{P_s(k)}$, where $P_s(k)$ is the load power of the system at the measuring point k and $P_s^M(k)$ is the summation of all the margins at all the load buses, at measuring point k.

Reference [3], modifies the original VIP formulation to include the systems with pronounced longitudinal topology, represented by a transmission corridor (called flowgates). PMUs which are installed at the receiving end of flowgates are made use of to obtain the local phasor measurement samples. Given the measured data sets at two consecutive events of system loading, the paramters are identified as

$$Z_{th} = \frac{V_2 - V_1}{I_1 - I_2} \tag{1.20}$$

$$E_{th} = V_2 + I_2 Z_{th} \tag{1.21}$$

Where E_{th} and Z_{th} are Thevenin voltage and Thevenin impedance, respectively. (V_1, I_1) and (V_2, I_2) are two measurements sets respectively.Voltages V_1 and V_2 are two snapshots of the bus voltages, whereas the currents I_1 and I_2 are obtained at the same instants as follows: $I = (S_{flowgate}/V)^*$, where $S_{flowgate}$ is the apparent power injected into the bus at the receiving end of the flowgate (through the flowgate). The flowgate VIP differs in the use of $S_{flowgate}$ instead of S_{load}.

In [83], a voltage collapse proximity indicator is proposed based on the $\mathbf{Z}$ bus network. For a network with n buses, the Thevenin's equivalent impedance looking into the port between bus i and the ground is $Z_{ii}\angle\beta$. Therefore, at load bus i, the Thevenin's equivalent impedance is $Z_{ii}\angle\beta$ and therefore for permissible power transfer to the load at bus i we must have $Z_{ii}/Z_i \leq 1$ where $Z_{ii}\angle\beta = i^{th}$ diagonal element of the impedance matrix $\mathbf{Z} = \mathbf{Y}^{-1}$ and $Z_i\angle\phi_i$ is the impedance of the load. The algorithm involves the computation of the load flow at the operating point to obtain system power and voltage profile, followed by linearizing the system load and generator active and reactive powers, by representing them as shunt elements with appropriate

signs. The admittance matrix **Y** is evaluated and inverted to obtain the impedance matrix **Z**.The Thevenin Impedance seen at node i is determined and the distance to the point of collapse is calculated using the proximity indicator.

Reference [84] reports an investigation on the application of Artificial Neural Networks in Voltage Stability Assessment. The authors make use of an energy function to generate sample patterns for ANN training, testing and design of the ANN architecture. The voltage stability is studied using the energy method and sensitivity analysis of the jacobian. The ANN employed is a multi level network with error back propagation. It consists of an input layer, one or more hidden layers and an output layer. The voltage stability of the power system is governed by real power, reactive power and the voltage profile of the buses. Understandably these variables are chosen as inputs to the ANN. The energy method is used to identify the stable equilibrium point and the unstable equilibrium point by solving the load flow equations. These are then substituted in the energy function to estimate the stability margins. For the hidden layer, one layer with five hidden neurons are chosen. For the output layer one neuron is required since the end goal is the estimation of a single system margin which would serve as a proximity indicator for the entire system. The computation of the sensitivities is performed by the inversion of the jacobian matricies corresponding to both the stable equilibrium and the unstable equilibrium point. The sensitivities of the energy margin with respect to the system variables provide important information affecting voltage stability and the most effective direction to maximize voltage stability. The system load is generated by using a random number generator and then the load is distributed among the load buses by using some distribution factors. However for practical size systems this scheme is not feasible due to large number of loads and generators.

In [85], a method for analyzing the voltage stability limit is presented using Artificial Neural Networks. It is proposed that the methods based on artificial neural networks present increased robustness that even extends into the contingency situations. The measurements samples of local current and voltage phasors can be used to estimate the available system margin in real-time which then can be used to trigger emergency control actions. One important distinction

made in this paper is in the use of the input variables for calculating the stability margin. The authors propose the use of voltage magnitudes and phase angles obtained from the PMU measurements for calculating the stability margin. The relationship patterns or the mapping between input and output parameters, which could be ($V_0, \theta_0, P_0 and Q_0$ and P_{margin}, respectively need to fed to the neural network. Such inter dependencies are generated by a CPF proram. The ability to capture the nonlinear behavior of the power system is a major advantage of the methods based on ANN. Several approaches in this direction have been pursued with each iteration of the ANN application differing only in the use of input vector. Reference [86] propose the use of active and reactive power injections at all PQ buses as a way to formulate the input vector. In [87], input vector formulation differs in the addition of voltage magnitude at generation load buses. References [88] and [89] use different variation of the input vector formulation with varying degrees of success.

There are also attempts being made to use genetic algorithms to train ANN for accurate estimation of the stability but by far the majority of the researchers have relied on the Thevenin Equivalent for the prediction of the collapse and the corresponding margin estimation. Local measurements taken at a load bus offer a very simple way to quantify the system margin. The computational burden is kept at a minimum with very little need for an elaborate communication infrastructure. The simplicity of the approach however does limit the accuracy of the model.

The phenomenon of voltage instability and collapse has been studied extensively and the literature pertaining to the subject is quite exhaustive. Nevertheless, it is hoped that that this reference list provides the reader with sufficient background and motivation to further peruse the contents of this thesis. Additional important references are cited throughout this document.

1.3 Contributions

The main contribution of this work lies in the formulation of VIP derived security margins for large scale power systems and the characterization of such security margins based on the individual sensitivities of the VIP locations. Furthermore, a possibility of a consolidation framework of the VIP derived margins, expressed in the form of data fusion has also been proposed in this work. Several techniques which extend the basic VIP algorithm and enable the estimation of the security margins based solely on the local measurements of current and voltage phasor have been developed with varying degrees of accuracy. Since this work builds on an earlier body of work done on the VIP, the fundamental assumptions stay the same.

The distribution of the VIP margins does not seem to follow any statistical patterns which makes it necessary to characterize such distributions using some external properties. One such characterization based on the gradient of the bus voltage to the changing local load has been found useful and enough empirical evidence has been collected to validate its use in large systems. Such characterization seems to be impervious to changing system conditions or topology and based on the evidence collected from different systems, tends to get stronger as the system approaches the critical load beyond which the power flow solutions become unfeasible.

Owing to a lack of any statistical distribution, a fusion based method for the consolidation of the VIP derived security margins is explored. This enables the estimation of the overall system security margin at a low computational cost and with higher accuracy than the individual security margins.

1.4 Outline of the Thesis

The thesis is organized as follows:

Chapter 2 This chapter gives a general description of the VIP formulation. The method is presented along with some algorithms for calculating the mode parameters. The application on

the IEEE 39 bus system is discussed briefly.

Chapter 3 This chapter delves deep in to the algorithms used for estimating the stability margins from the VIP formulation. Three such methods of estimating the VIP margin distribution are presented and a comparative analysis of the accuracy of these methods is presented. Additionally, the algorithm for the calculation of true system margin based on the repeated load flow studies is also shown.

Chapter 4 This chapter focuses on the characterization of the VIP margin distribution as well as on the effect of changing system conditions and topology on such margin distributions. A couple of indices are presented for characterizing VIP margins and a thorough assessment of the efficiency of sensitivity based characterization is presented as tested on the IEEE 118 bus system. Additionally, a generator based sensitivity metric is also presented to determine the role of generators in maintaining voltage stability.

Chapter 5 This chapter introduces the idea of data fusion based on Dempster Shafer evidential reasoning. The fundamental principles of the theory are explained and a working implementation is presented on a simple 4 bus system with two VIP locations.

Chapter 6 This chapter presents the results of data fusion as tested on a variety of standard IEEE test cases.

Chapter 7 The final chapter provides a holistic summary of the work done and offers several conclusions as well as possible future directions for this work.

2.1 Introduction

Figure 2.1 shows a power system being represented by a two bus Thevenin Equivalent connected with the local load bus. For a constant power load, the loadability limit coincides with the maximum delivarable power to a load. At critical loading of the system, the absolute values of the load impedance and the Thevenin impedance are equal.

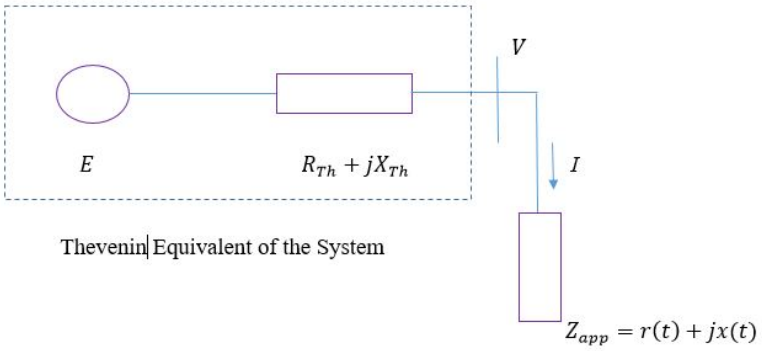

Figure 2.1: Thevenin Equivalent Model of a network as seen from a load bus

The complex power injected at the load bus is

$$S = V I^* \tag{2.1}$$

$$S = V\left(\frac{E_t - V}{Z_t}\right)^* \tag{2.2}$$

We can express the Thevenin Voltage, Thevenin Impedance and the load voltage as:

$$E_t = E_t e^{(j\delta_E)}, V = V e^{(j\delta V)}, \text{and} Z_t = Z_t e^{(j\theta_Z)} \tag{2.3}$$

Equation (2.2) can now be written as

$$S = Ve^{j\delta_V}\left(\frac{E_t e^{j\delta_E} - Ve^{j\delta V}}{Z_t e^{j\theta_Z}}\right)^* \tag{2.4}$$

$$S = Ve^{j\delta_V}\left(\frac{E_t e^{-j\delta_E} - Ve^{-j\delta V}}{Z_t e^{-j\theta_Z}}\right) \tag{2.5}$$

$$S = \left(\frac{E_t V}{Z_t}\right)e^{j(\theta_z+\delta_V-\delta_E)} - \left(\frac{V^2}{Z_t}\right)e^{j\theta_z} \tag{2.6}$$

This can be further simplified as

$$P + jQ = \frac{EV}{Z_t}\cos(\delta_V - \delta_E + \theta_z) + j\frac{EV}{Z_t}\sin(\delta_V - \delta_E + \theta_z) - \frac{V^2}{Z_t}\cos\theta_z - j\frac{V^2}{Z_t}\sin\theta_z \tag{2.7}$$

$$P + jQ = \frac{EV}{Z_t}\cos(\delta_V - \delta_E + \theta_z) - \frac{V^2}{Z_t}\cos\theta_z + j\left(\frac{EV}{Z_t}\sin(\delta_V - \delta_E + \theta_z) - \frac{V^2}{Z_t}\sin\theta_z\right) \tag{2.8}$$

Then we can write for the real and reactive power as:

$$P = \left(\frac{E_t V}{Z_t}\right)\cos(\delta_V - \delta_E + \theta_z) - \frac{V^2}{Z_t}\cos\theta_z \tag{2.9}$$

$$Q = \left(\frac{E_t V}{Z_t}\right)\sin(\delta_V - \delta_E + \theta_z) - \frac{V^2}{Z_t}\sin\theta_z \tag{2.10}$$

Equations (2.9) and (2.10) can be combined together to yield

$$\left(\frac{E_t V}{Z_t}\right)^2\cos^2(\delta_V - \delta_E + \theta_z) + \left(\frac{E_t V}{Z_t}\right)^2\sin^2(\delta_V - \delta_E + \theta_z) = (P + \frac{V^2}{Z_t}\cos\theta_z)^2 + (Q + \frac{V^2}{Z_t}\sin\theta_z)^2 \tag{2.11}$$

Using the trigonometric identity $\sin^2\lambda + \cos^2\lambda = 1$, we can write further

$$\left(\frac{E_t V}{Z_t}\right)^2 = P^2 + \left(\frac{V^2}{Z_t}\right)^2\cos^2\theta_z + 2P\frac{V^2}{Z_t}\cos\theta_z + Q^2 + \left(\frac{V^2}{Z_t}\right)^2\sin^2\theta_z + 2Q\frac{V^2}{Z_t}\cos\theta_z \tag{2.12}$$

To make the equation simple and remove all the clutter, we can make use of changing the

variable, $V^2 = U$. Then equation (2.12) reduces to

$$\frac{U^2}{Z_t^2} + \frac{U}{Z_t}(2(P\cos\theta_z + Q\sin\theta_z) - E^2) + (P^2 + Q^2) = 0 \tag{2.13}$$

$$U^2 + U((2(P\cos\theta_z + Q\sin\theta_z)Z_t) - E^2) + Z_t^2 S^2 = 0 \tag{2.14}$$

Changing the variable back to V, yield the following quadratic equation in V^2

$$(V^2)^2 + ((2(P\cos\theta_z + Q\sin\theta_z)Z_t) - E^2))V^2 + Z_t^2 S^2 = 0 \tag{2.15}$$

The solutions of equation (2.15) are given by

$$V^2 = \frac{\frac{2}{Z_t}\left(\frac{E^2}{2} - (P\cos\theta_z + Q\sin\theta_z)\right)}{2\left(\frac{1}{Z_t}\right)^2} \pm \frac{\sqrt{\left[\frac{2}{Z_t}\left(\frac{E^2}{2} - (P\cos\theta_z + Q\sin\theta_z)\right)\right]^2 - 4\frac{S^2}{Z_t^2}}}{2\left(\frac{1}{Z_t}\right)^2} \tag{2.16}$$

$$(V^2) = \frac{E^2 - 2Z_t(P\cos\theta_z + Q\sin\theta_z) \pm \sqrt{(E^2 - 2Z_t(P\cos\theta_z + Q\sin\theta_z))^2 - 4(Z_t^2 S^2))}}{2} \tag{2.17}$$

We notice the presence of multiple solutions. At the point of voltage collapse the two solutions come together and coalesce in to a single solution. Mathematically this can be characterized by making the discriminant equal to zero in (2.16).

$$(E^2 - 2Z_t(P\cos\theta_z + Q\sin\theta_z))^2 - 4(Z_t^2 S^2) = 0 \tag{2.18}$$

$$E^2 - 2Z_t(P\cos\theta_z + Q\sin\theta_z))^2 = 4(Z_t^2 S^2) \tag{2.19}$$

$$E^2 - 2Z_t(P\cos\theta_z + Q\sin\theta_z) = 2Z_t S \tag{2.20}$$

Substituting (2.20) into (2.16) we have

$$V^2 = Z_t S \tag{2.21}$$

which can be expressed as:

$$Z_t = \frac{V^2}{S} = Z_{app} \tag{2.22}$$

Hence the maximum power transfer and hence the point of collapse is reached when the apparent load impedance is equal to Thevenin Impedance in absolute value. [38]

The procedure makes no assumption on the nature of the load. The load impedance is simply a ratio of current and voltage phasors sampled at a particular system load. The expression (2.22) stays true regardless of the load characteristic. In Figure 2.2, as the transmission system is weakened which signifies increased load on the system, the apparent load impedance moves closer to the Thevenin circle and voltage instability is said to occur when the load impedance trajectory breaches the Thevenin circle.

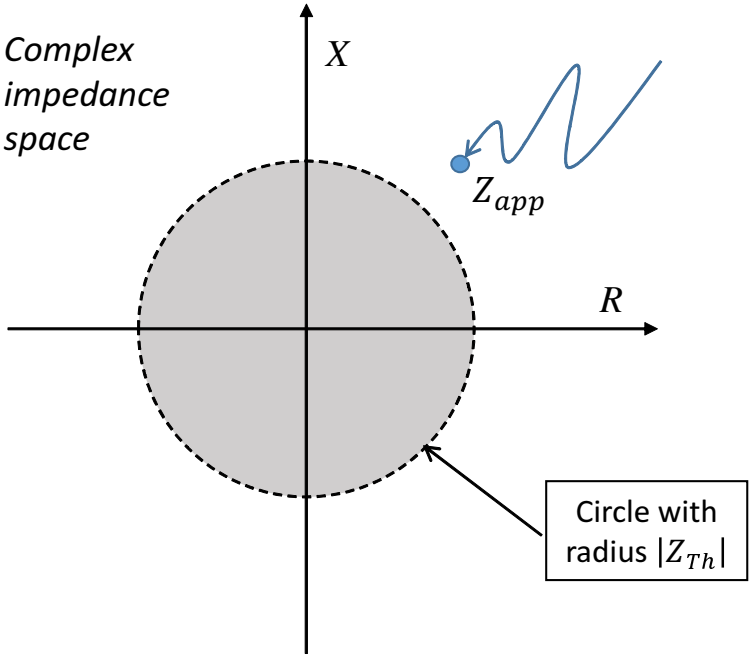

Figure 2.2: Load Impedance and Thevenin Circle [1]

The distance between the two impedance trajectories can thus serve as a running indicator which could be quantified into a measure of the available system margin. Since the Theve-

nin model approximates a large complex network with possibly thousands of equipment, the status of any of which could change at any given time, the Thevenin circle thus is a time varying entity.

2.2 Tracking the Thevenin Equivalent

Tracking the Thevenin Equivalent is most important for determining the distance to the point of collapse. Various methods have been proposed in the literature to track the Thevenin equivalent. The tracking is based on the following equation:

$$E_{thev} - Z_{thev} I = V \tag{2.23}$$

2.2.1 Cartesian Coordinates

Denote $E_{thev} = E_r + jE_i$, $Z_{thev} = R_{thev} + jX_{thev}$, $I = I_r + I_i$ and $V = V_r + V_i$, Equation (2.23) can be rewritten in the matrix form with real and imaginary parts as [38]

$$\begin{bmatrix} 1 & 0 & -I_r & I_i \\ 0 & 1 & -I_i & -I_r \end{bmatrix} \begin{bmatrix} E_r \\ E_i \\ R_{thev} \\ X_{thev} \end{bmatrix} = \begin{bmatrix} V_r \\ V_i \end{bmatrix} \tag{2.24}$$

where the sub-scripts r and i represent the real and the imaginary parts. From this equation we can easily determine that the system is under-determined or under-constrained, in the sense that there are four unknowns (variables) and only two equations for solving them. In a strict sense an under-determined system has no solutions or infinitely many solutions. So the system can be either consistent if the rank of the augmented matrix is equal to the rank of the coefficient matrix, and can also have a unique solution if the rank is equal to the number or unknowns, or the system can be inconsistent if the rank of the augmented matrix is greater than

the rank of the coefficient matrix. For the system represented by equation (2.24), the augmented matrix is

$$(A|B) = \begin{bmatrix} 1 & 0 & -I_r & I_i & | & V_r \\ 0 & 1 & -I_i & -I_r & | & V_i \end{bmatrix} \tag{2.25}$$

while the coefficient matrix is given by

$$\begin{bmatrix} 1 & 0 & -I_r & I_i \\ 0 & 1 & -I_i & -I_r \end{bmatrix} \tag{2.26}$$

For the system in consideration, measurements for the voltage and current phasors, obtained from MATPOWER, indicate that the rank of the augmented matrix and the coefficient matrix is always equal as the system dynamics change, making the system consistent with however an infinitude of solutions. For estimating a solution we make use of the Least squares method, which in essence finds the smallest of the solutions. For our system we can represent the equations in the form:

$$A\vec{x} = \vec{b} \tag{2.27}$$

where

$$A = \begin{bmatrix} 1 & 0 & -I_r & I_i \\ 0 & 1 & -I_i & -I_r \end{bmatrix} \vec{x} = \begin{bmatrix} E_r \\ E_i \\ R_{thev} \\ X_{thev} \end{bmatrix} \tag{2.28}$$

and

$$\overrightarrow{b} = \begin{bmatrix} V_r \\ V_i \end{bmatrix} \tag{2.29}$$

The assumption of constancy of Thevenin parameters is often challenged by the changing systems conditions. Further the inclusion of all loads in to a system equivalence, all of which are uniformly changing at a given period of time, contaminates the estimation of the model parameters. To account for this, a suitable data window needs to be selected to suppress large system changes which might results in conflicting VIP actions.

2.2.2 Least Squares Method

From equation (1.30) we can observe that the matrix A is a $(n \times m)$ matrix with $n < m$. In this case there are fewer constraints than unknowns, and the system is under-determined, with an infinite number of solutions. We can pick one of these solutions by finding the smallest one. That is we can minimize $\overrightarrow{x}$,subject to the constraint $\overrightarrow{b} = A\overrightarrow{x}$.The method of Lagrange multipliers has us add a term to the quantity to be minimized:

$$||\overrightarrow{x}||^2 + \lambda^T(\overleftarrow{b} - A\overrightarrow{x}) \tag{2.30}$$

Differentiating w.r.t x, and setting the term equal to zero, yields

$$2\overrightarrow{x} - A^T\lambda = 0 \tag{2.31}$$

We can't just solve for λ since A is not a square matrix, but we can pre-multiply by A to obtain:

$$2A\overrightarrow{x} - AA^T\lambda = 0 \tag{2.32}$$

and using $\overrightarrow{b} = A\overrightarrow{x}$ gives:

$$2\overrightarrow{b} = AA^T\lambda \tag{2.33}$$

$$\lambda = 2(AA^T)^{-1}\overrightarrow{b} \tag{2.34}$$

and hence

$$\overline{x} = A^T(AA^T)^{-1}\overline{b} \tag{2.35}$$

This method involves the inversion of this matrix (AA^T), which consists of the measurements of current, and with badly scaled matrix (A),the algorithm will be subjected to numerical problems. These problems can either be overcome by increasing the number of measurements, n.

2.2.3 Delta Method

To solve the for the Thevenin network parameters we can apply Kirchoff's voltage law to the circuit in figure 2.1

$$\overline{E}(k) - \overline{Z}_T(k)\overline{I}(k) = \overline{V}(k) \tag{2.36}$$

This equation refers to the current measurement sample of $(V(k), I(k))$. A similar equation can be written for a measurement sample taken at a previous instant i.e $k-1$ as

$$\overline{E}(k-1) - \overline{Z}_T(k-1)\overline{I}(k-1) = \overline{V}(k-1) \tag{2.37}$$

Simulations on bulk systems have shown that the Thevenin parameters approximate to be constants between two successive sufficiently close (allowing a change in load) measurement samples. This fact has also been extensively reported in literature. Using this observation we can

write for the Thevenin Impedance

$$\overline{Z}_T(k) = \frac{\overline{V}(k-1) - \overline{V}(k)}{\overline{I}(k) - \overline{I}(k-1)} \tag{2.38}$$

and for the Thevenin Voltage as

$$\overline{E}(k) = \frac{\overline{V}(k-1)\overline{I}(k) - \overline{V}(k)\overline{I}(k-1)}{\overline{I}(k) - \overline{I}(k-1)} \tag{2.39}$$

These equations contain phasor quantities for the voltages, current and impedance. Two measurement samples were considered for producing an estimate of the Thevenin impedance. In principle the number of measurement samples can be increased, which translates to using a larger data window. If we have $'n'$ measurement samples we will have $'n'$ equations.

$$E(n) - Z_T(n)I(n) = V(n) \tag{2.40}$$

$$E(n-1) - Z_T(n-1)I(n-1) = V(n) \tag{2.41}$$

$$\vdots$$

$$E(2) - Z_T(2)I(2) = V(2) \tag{2.42}$$

$$E(1) - Z_T(1)I(1) = V(1) \tag{2.43}$$

Assuming constancy of Thevenin Equivalent, we can write

$$\begin{bmatrix} \triangle I(n) \\ \triangle I(n-1) \\ \vdots \\ \triangle I(3) \\ \triangle I(2) \end{bmatrix} Z_T(n) = - \begin{bmatrix} \Delta V(n) \\ \Delta V(n-1) \\ \vdots \\ \Delta V(3) \\ \Delta V(2) \end{bmatrix} \tag{2.44}$$

This can be solved by using the Least squares as explained in section 1.3.2.

2.3 VIP applied to Test Systems

The VIP algorithm is tested on the IEEE 39 bus Test System, by making use of equations (2.38) and (2.39). The Thévenin Impedance is assumed to be constant between the two sets of measurements. It is important to note that this assumption makes the system observable and a solution can be determined, although this makes the system vulnerable to false estimations as has been explained in the previous section. The simulations are done using MATPOWER package by running a series of power flow programs with increasing loading at each iteration till the point of collapse is reached.

Figure 2.3 shows the impedances observed at a particular bus in the IEEE 9 bus test system. The top line in represents the variation of apparent load impedance. The load increase is evident by the decaying load impedance profile. The top line represents the Thevenin impedance which increases gradually.

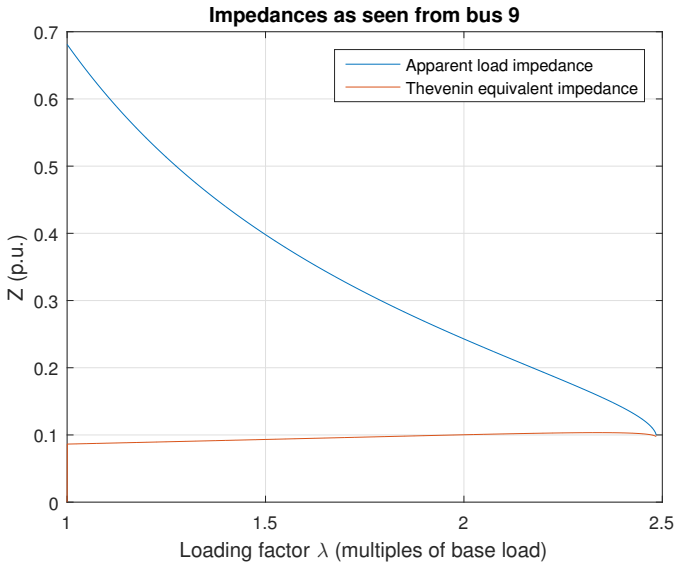

Figure 2.3: Sample impedance plot for IEEE 9 bus system

Figure 2.4 shows the impedances observed at a particular bus in the IEEE 39 bus test system. Thevenin impedance again tends to rise gradually, but at certain loading factors, there are sharp

increases. These instants coincide with the PV-PQ transitions of certain generators. When a generator reaches its reactive limit, it transitions to a PQ bus which is reflected by the sharp rises in the Thevenin Impedance of the system.

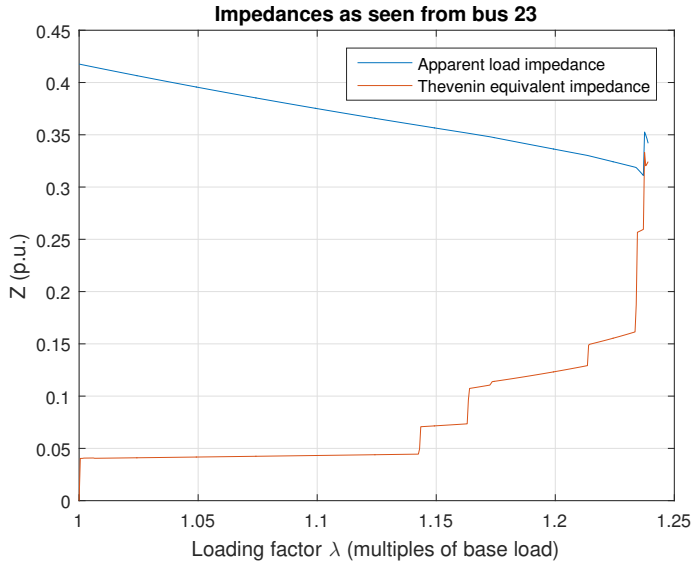

Figure 2.4: Sample impedance plot example for the IEEE 39 bus system

Base case load for this simulation is $247.5 + j84.6$MVA. The critical loading factor is $\lambda_c = 1.2395$. At λ_c times the base load voltage deteriorates rapidly the system enter a collapse triggered by the violation of generation and transmission limits. The impedance curves of all the load buses share the same profile.

The voltages in the system progressively decline as the stress on the transmission system builds. As the transmission system is loaded, the power drawn by the loads increases which results in higher currents flowing in the lines. The higher currents increase the stress on the transmission system while also resulting in decreased voltages at the local buses because of increasing voltage drops along the lines. The generators which are the dominant reactive power reserves in the system also start to run out of their reserves, as each generator hits its respective reactive limit. Ultimately owing to the deficiency of the reactive power in the system, the voltages fall below the minimum acceptable level and the system enters a state of voltage collapse. Figure 2.5 shows the voltage profile of all the buses of IEEE 39 bus test system. Note that

the voltage of the PV buses remains constant until the generators hit their reactive limits and voltage becomes a variable and drops while bus makes the transition to a PQ bus.

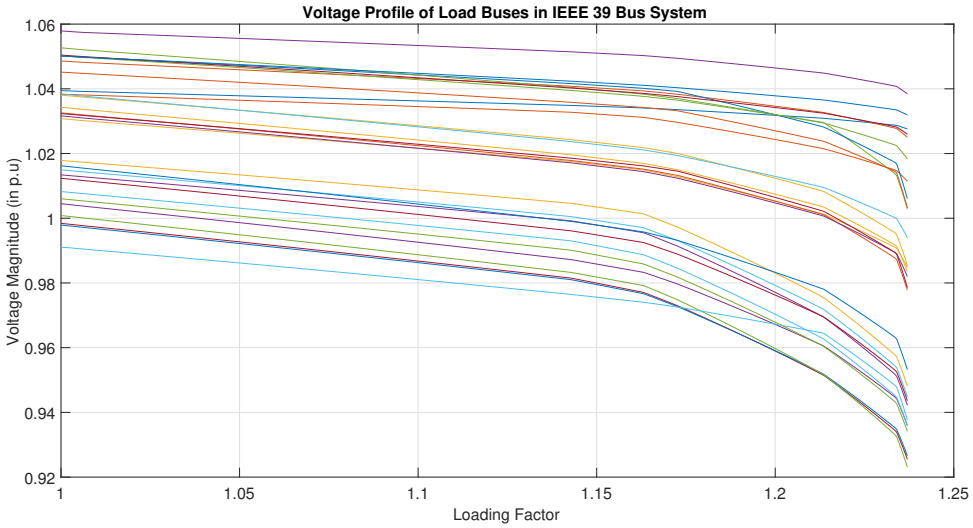

Figure 2.5: Voltage Profile for all buses in IEEE 39 Bus System

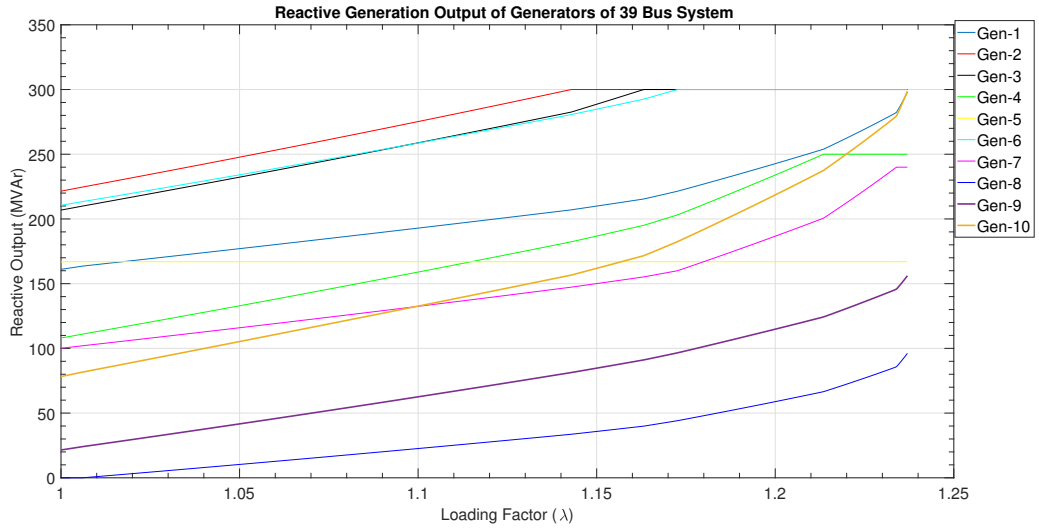

Figure 2.6: Reactive power of generators plotted against increased loading

2.3.1 SVC added to Generators-Effect on loadability limit

Figure 2.6 represents the reactive power output of the generators as a function of the loading factor. Generator reactive limits have a great impact on the onset of voltage instability [90].

However there are various corrective measures that can be taken to enhance the reactive capability of the system by individual generators with SVCs. SVCs can greatly impact the reactive capability of the generator thereby also allowing the system to withstand higher loading. Having SVCs added to the generators affects the critical loading factor at which the the load impedance at a local bus merges with the Thevenin Equivalent. In IEEE 39 bus system simulations are carried out by placing an SVC at each generator one at a time and observing the effects on the critical loading factor as well as the PV-PQ transitions.

The following figures, obtained from MATPOWER simulations illustrate this fact.

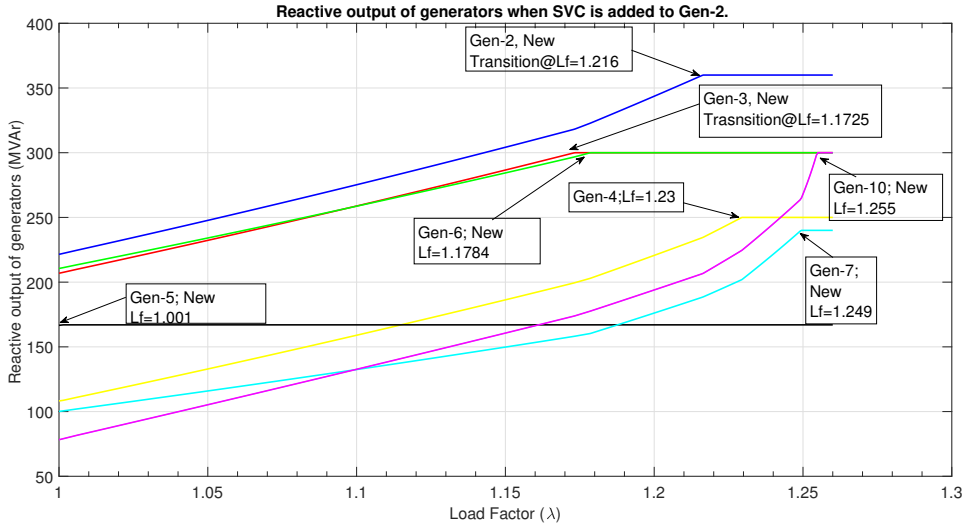

Figure 2.7: Reactive power output of generators plotted with System Loading, when SVC support is added to Generator-2

Similarly SVC support can be added to other generators and the affect on the stability limit can be observed. Different generators influence the loadability limit in different ways, depending on the magnitude of their reactive capability.

Figure 2.8 plots the reactive power output curves of generators when SVC is added to generator-3.

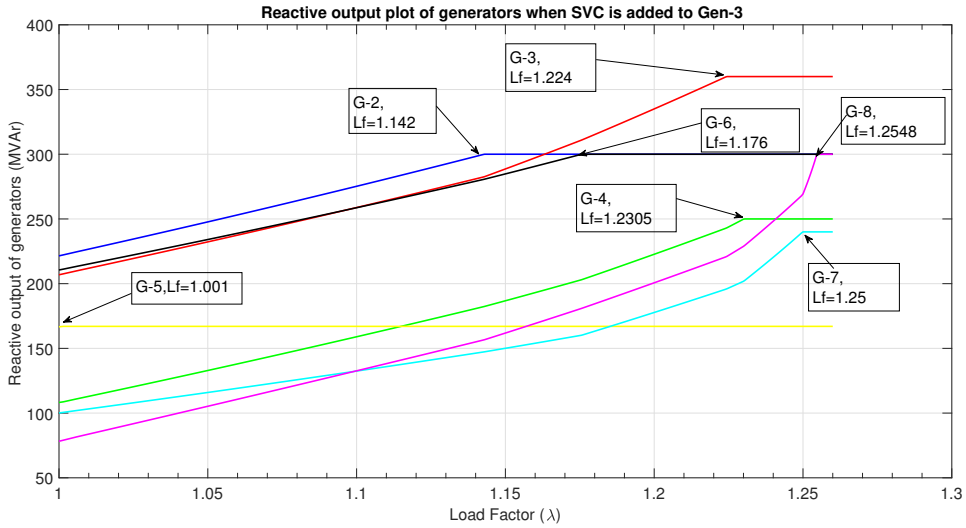

Figure 2.8: Reactive power output of generators plotted with System Loading, when SVC support is added to Generator-3

The following plots depict the same characteristics when SVC's are added to different generators.

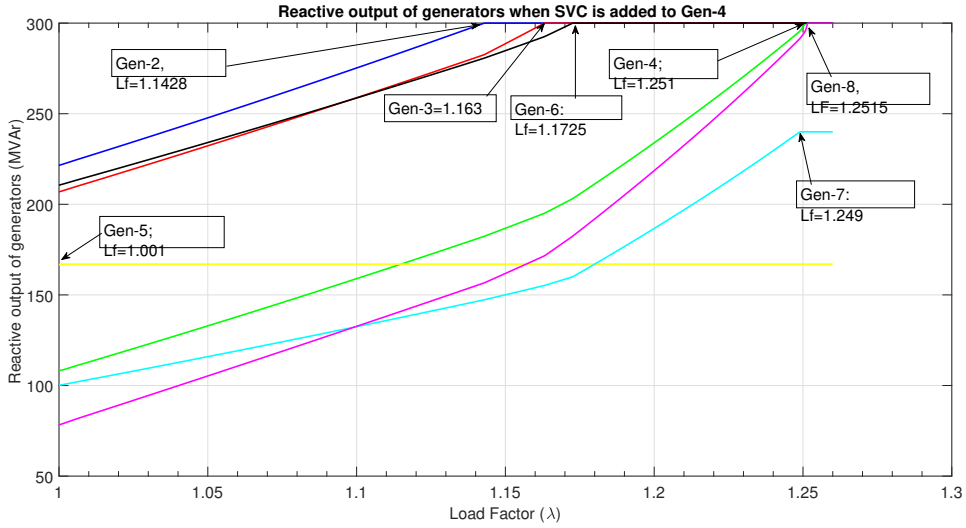

Figure 2.9: Reactive power output of generators plotted with System Loading, when SVC support is added to Generator-4

.

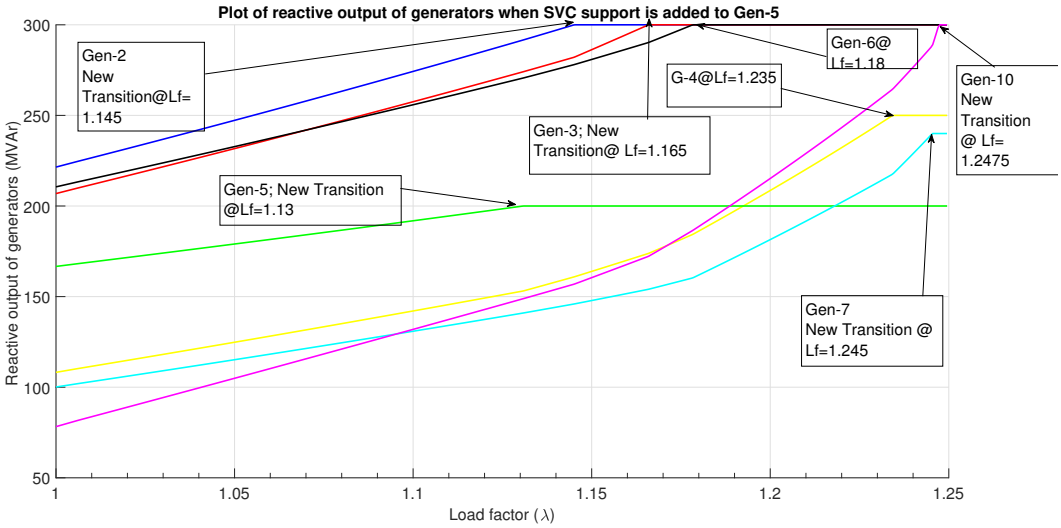

Figure 2.10: Reactive power output of generators plotted with System Loading, when SVC support is added to Generator-5

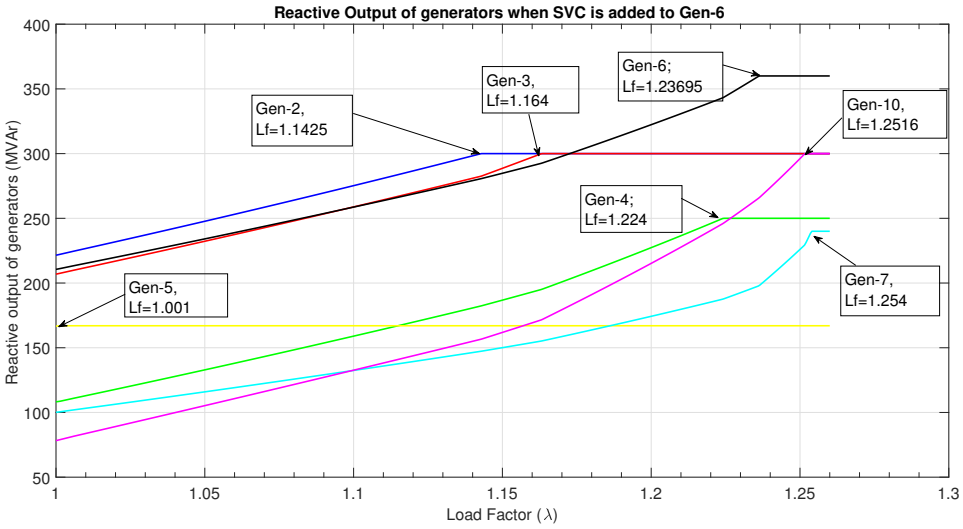

Figure 2.11: Reactive power output of generators plotted with System Loading, when SVC support is added to Generator-6

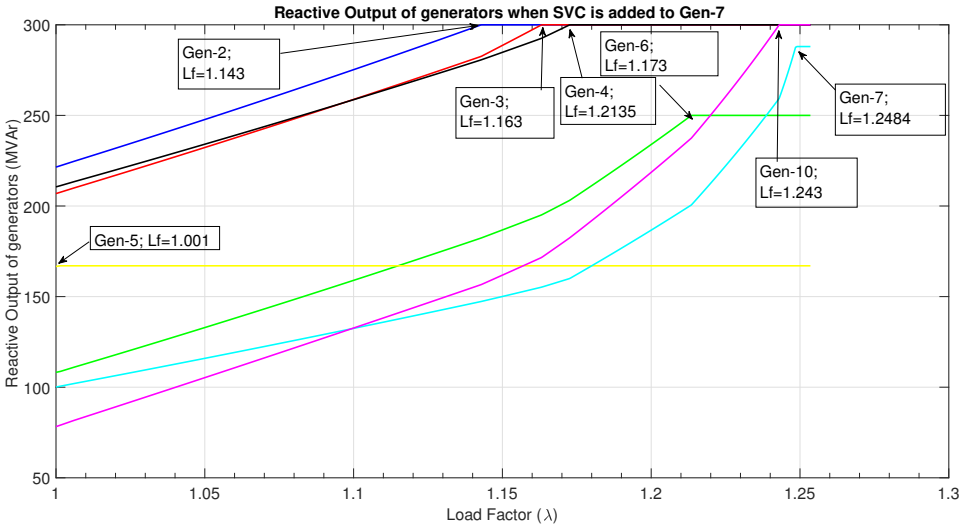

Figure 2.12: Reactive power output of generators plotted with System Loading, when SVC support is added to Generator-7

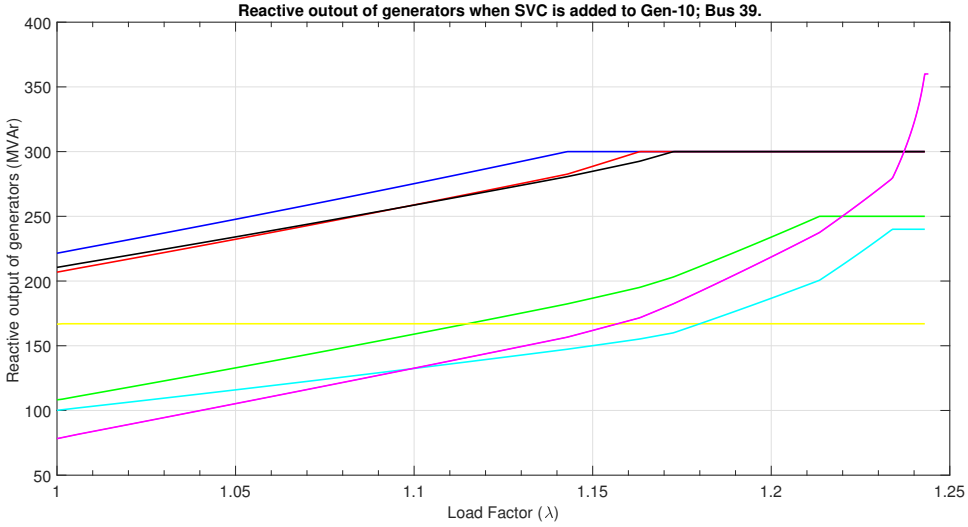

Figure 2.13: Reactive power output of generators plotted with System Loading, when SVC support is added to Generator-10

.

From the plots simulated for the reactive output of the generators and the corresponding impedance changes as a function of loading factors, certain inferences can be drawn. Table 2.1 lists some of the observations in tabular form:

Table 2.1: New critical loading factors and PV-PQ Transitions

Number	20% SVC support added at	New Critical Point	New PV-PQ transition	Previous PV-PQ transition
1	Generator-5; Bus 34	k=1.249	Lf=1.131	Lf 1.0015
2	Generator-2; Bus 31	k=1.261	Lf=1.216	Lf=1.143
3	Generator-3; Bus 32	k=1.256	Lf=1.224	Lf=1.163
4	Generator-6; Bus 35	k=1.256	Lf=1.236	Lf=1.173
5	Generator-4; Bus 33	k=1.254	Lf=1.251	Lf=1.213
6	Generator-7; Bus 36	k=1.253	Lf=1.248	Lf=1.234
7	Generator-10;Bus 39	k=1.243	Lf=1.243	Lf=1.237

Previous Critical Loading factor=1.2395

From the above table we find that if SVC support is added to individual generators, one at a time, it changes the critical point at which the voltage collapse takes place. In all the cases the critical point shifts to the right of the x- axis, hence increasing, although the increase is different for different generators. Some generators shift the critical point more than the others, while for some the change is more or less the same. If we look at the reactive data for the generators, we find that those generators which have almost similar reactive limits, affect the critical point in more or less the same manner, with slight variation and those generators which have significant difference in their reactive limits, the effect on the critical point is significant.

For example if we take a look at the reactive limits of Genrator-5 and Generator-2, we find that the $Q_{g,max}$ and$Q_{g,min}$ values for these generators are:

$$Generator-5(Bus-34) = \begin{cases} Q_{g,max} = 167MVAr \\ Q_{g,min} = 0MVAr \end{cases} \tag{2.45}$$

$$Generator-2(Bus-31) = \begin{cases} Q_{g,max} = 300MVAr \\ Q_{g,min} = -100MVAr \end{cases} \tag{2.46}$$

When 20 percent reactive support is added to these generators individually one at a time,

they affect the critical point differently, with generator-2 pushing it further than generator -5. Similarly when the reactive limits are similar or very close, the difference in the critical point is very slight.

Another important observation are the instants at which the PV-PQ transitions take place of the individual generators which are supplied with additional reactive support. It is seen that in every case the PV-PQ transition is delayed than in the previous case where there was no reactive support. Without the reactive support the generators hit their reactive limits early while as with the reactive support the transition is delayed. This is also intuitive because if the generator can supply more reactive power, it will take longer (more load), for it run to run out of its reactive reserve. The loadability of the system is hence increased by adding more reactive support. However because of the limits of the transmission system, there is only a limited quantity of power that can be transferred, and the system enters a collapse as soon as the transmission limits are violated.

2.4 Estimation Problems and Data Requirements

VIP models the external system seen from the point of measurement as a Thévenin equivalent. The two equivalent parameters are the Thévenin emf $E_T h$, and Thévenin impedance $Z_T h$, . Once the external system parameters are identified, metrics for distance from the operating point to the point of collapse can be determined. In particular, the loading margin can be derived from the two system equivalent parameters. Although VIP suffers from some identification problems, particularly in the estimation of the model parameters, such problems are overcome by sampling discrete time sequence of voltage and current phasors. Between two sufficiently close sampling events, system parameters show nearly constant characteristics in the absence of topology-changing events such as equipment outages of generator PV-PQ transitions. The assumption of constancy of the Thévenin model allows parameter identification and facilitates determination of the system equivalent impedance and voltage.

The VIP method trades speed and resilience of using local measurements for the complexity of calculating accurately the stability margins of large nonlinear systems in the absence of almost all of the state information. Thus, by using one of the many customized variations of the VIP impedances, which are calculated from the discrete time sequence of voltage and current phasors, it is possible to make an estimate about the power margin to voltage collapse.Such an estimate however is not an accurate representation of the power margin because of the inherent simplicity of the algorithm, which becomes a liability of this method. Fortunately, in a VIP network such a liability can be offset by making use of the multiplicity of data, obtained from across the system, which is an asset. Any meaningful exploitation of this redundancy can, in principle, reduce some of the inaccuracies associated with this method.

The length of the data window chosen for sampling the time sequence measurements of voltage and current phasors is critical for optimal estimation of model parameters. The measurements are sampled at time instants or loading instants, which allow a change in the operating point while at the same time maintaining the quasi-constant nature of the system equivalent. Achieving this trade-off between sufficiently closely spaced sampling instants and measurably different system conditions is critical in obtaining meaningful information from the measurements. Figure 2.14 captures the effect of sampling discrete time sequence measurements at different sampling rates. Increasing the length of the data widow between two successive phasor measurements results in inaccurate estimation of system thevenin impedance which ultimately can lead to erroneous results.

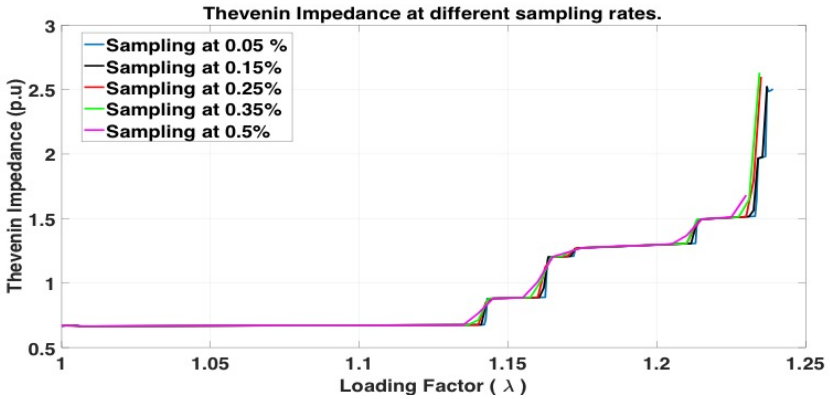

Figure 2.14: System Thevenin Impedance at different sampling rates

The parameter identification of the Thevenin Equivalent model is impacted by various internal (VIP Algorithm and Choice of Parameters) and external (Transients and Disturbances) factors. Different customized versions of VIP use different numerical approaches for parameter identification and the identification accuracy depends on factors like length of sampling window and the assignment of weight factors. The external factors have to do with the modelling of a time variant system with respect to accuracy and sensitivity. The VIP modelling technique ignores the fast dynamics which may render it inappropriate when system experiences fast dynamics. The system Thevenin Impedance may undergo constant changes due to various transients and as such false triggering is possible. Since power systems are time-variant systems with gradual or abrupt changes in the form of transients, it is important to distinguish the system transients in order to issue a block signal to and stop the VIP calculation. Figure 2.15 represents a sudden change caused by a transient event across the system. The VIP estimation should be blocked between instants $j\&j+1$, or otherwise the VIP will incorrectly assume that the system is at or close to instability.

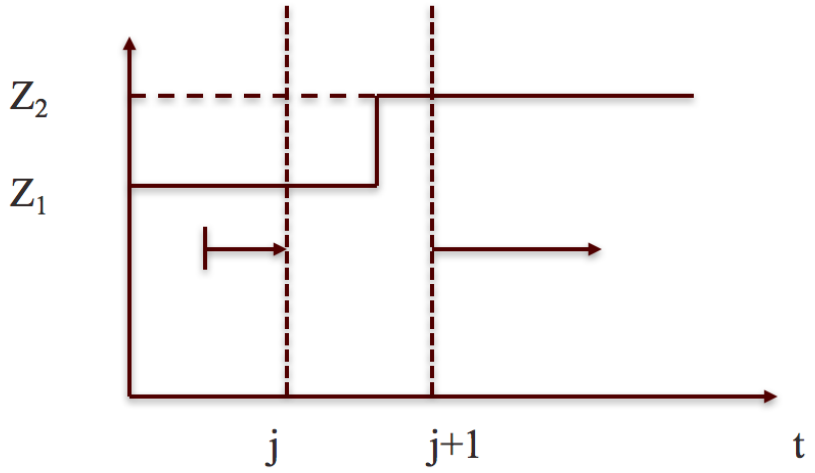

Figure 2.15: Abrupt Change in Thevenin Impedance

The impedance circle of Figure 2.2 would resemble a cylinder with varying surface area when seen as a function of time. The discontinuous controls such as controls of LTCs and over excitation limiters (OXLs) can cause short dynamic processes which can be magnified by the

voltage sensitive equipment. Such events could alter the surface area of the impedance cylinder which may or may not result in false triggering voltage instability. In [40], recursive least algorithm with a forgetting factor is used to weigh the effect of new changes to the system state. For time invariant systems the longer the window size, higher is the accuracy of estimation. For time variant systems, a longer window size would make the estimation less sensitive to system changes. In a given sampling window the VIP algorithm assumes an identical Thevenin model applied to all system states. However if there are multiple distinct system conditions included in the data window, the existence and uniqueness of the VIP estimate is not guaranteed. Since the change in load is important for VIP to be able to produce an estimate, it becomes necessary to distinguish system changes caused by a change in load from those caused by transient processes. The applicability of VIP to different system conditions (load ramping, fast dynamics etc) and the choice of VIP parameters (sampling frequency, window size, forgetting factor etc) are still open issues, up for discussion in designing VIP based applications.

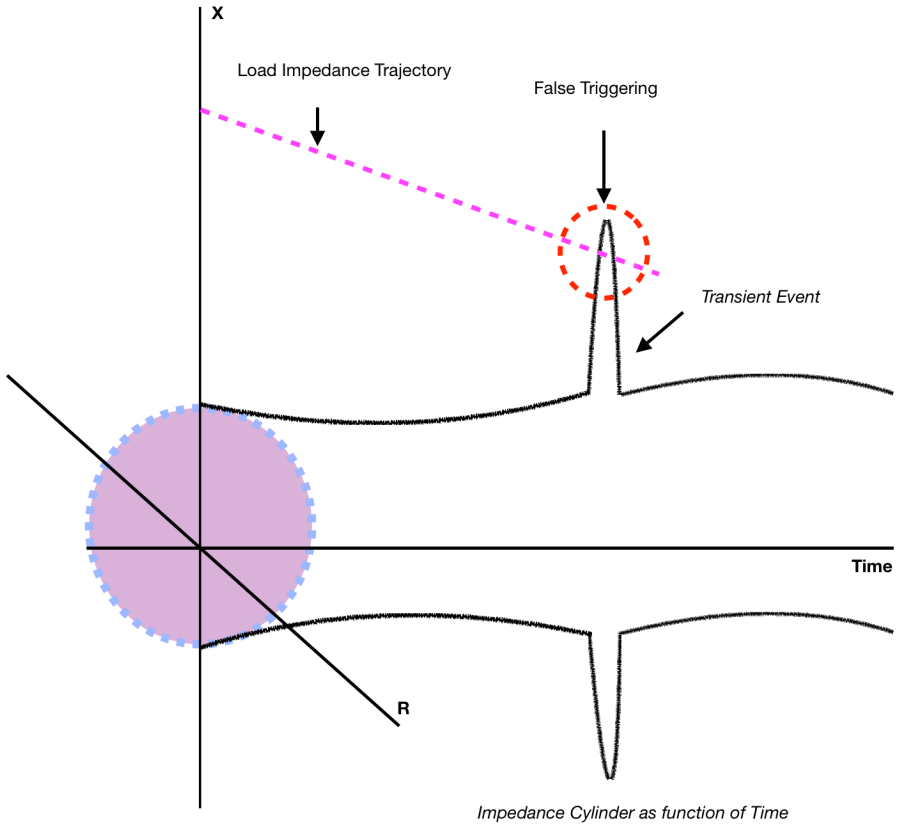

Figure 2.16: False Triggering initiated by a Transient Event

Yang Song in [91] lists the detailed actions of the VIP algorithm in response to different system conditions. The actions are tabulated in Table 2.2

Table 2.2: VIP actions to different system conditions

System Condition	VIP actions
Steady State	No evaluation and report the last calculation results
Discontinuous Changes and Transients	VIP calculation blocked
Subsequent Transients	Use LS algorithm to obtain initial guess and then use recursive VIP to update VIP results

3.1 Impedance Margins

For a constant power load, the point of collapse corresponds to the point of maximum power transfer which suggests that the impedance trajectories of the load and the Thevenin Equivalent meet at the point of collapse. Based on this fact several indices can be constructed to estimate the distance to the point of collapse from the current operating point. Various indices have been proposed in the literature to track the stability margin. The methods based on the impedance matching criteria are based on the equivalence of the absolute values of the load impedance and the Thevenin impedance at the point of collapse. This realization makes it natural to use the difference between the two impedance trajectories as a means to quantify the system margin. Such a quantification of system margin is fast and does not rely on the accurate calculation of singularities of large dynamic systems. Figure 3.1 illustrates the estimated trajectories of $|Z_i^L|$ and $|Z_i^{th}|$.

The challenge lies in estimating the Impedance trajectories. The trajectories can be estimated by using a linear regression technique, and the coefficients of the resulting polynomial can be fitted by linear least squares or nonlinear least square techniques. The accuracy of the regression is affected by the number of data samples used for estimating the curve. The Thevenin equivalent is for the most part a constant impedance curve,and the new 'Thevenin equivalent system' is not changing by much when PV-PQ transitions (or other topology-changing contingencies) do not occur. [1]

[1] Part of the data reported in this chapter is reprinted with permission from "Locational Accuracy of VIP Indices for Voltage Collapse Margin Estimation-Begovic, Miroslav, et al. (2018)-Proceedings of the 51st Hawaii International Conference on System Sciences| 2018"

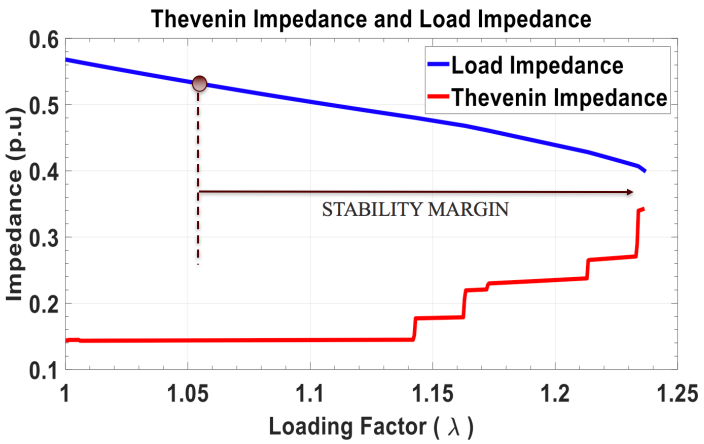

Figure 3.1: Trajectories of Load Impedance and Thevenin Equivalent

.

3.1.1 Linear Regression

Linear regression is a curve fitting technique to model a relationship between two variables. A linear polynomial is fitted to the measure data and the error between the observed data and the fit is minimized in least square sense. A linear regression line has the equation

$$y = a + bX \tag{3.1}$$

where X is the explanatory variable Y is the dependent variable. The slope of the line is b and a is the intercept. Least square method, in spite of several performance issues with data containing big outliers, is the most common method for fitting a regression line. This method aims to minimize the sum of squares of the errors to account for positive as well as negative deviations. A point on line has zero deviation. Since the deviations are squared and then summed it does not lead to cancellation of positive and negative values. It is possible that the relationship between the two variables under consideration is also influenced by a third variable which is ignored in the model. Such hidden variables can be identified by examning a time series plot of the data.

The difference between the two impedances can serve as a running indicator for margin estimation. The impedances can be plotted in MATPOWER, by running a series of power flow simulations with increasing loading at every iteration. A difference plot,given by Figure 3.2, indicates that as the loading on the system is increased the difference between the two impedances approaches zero.

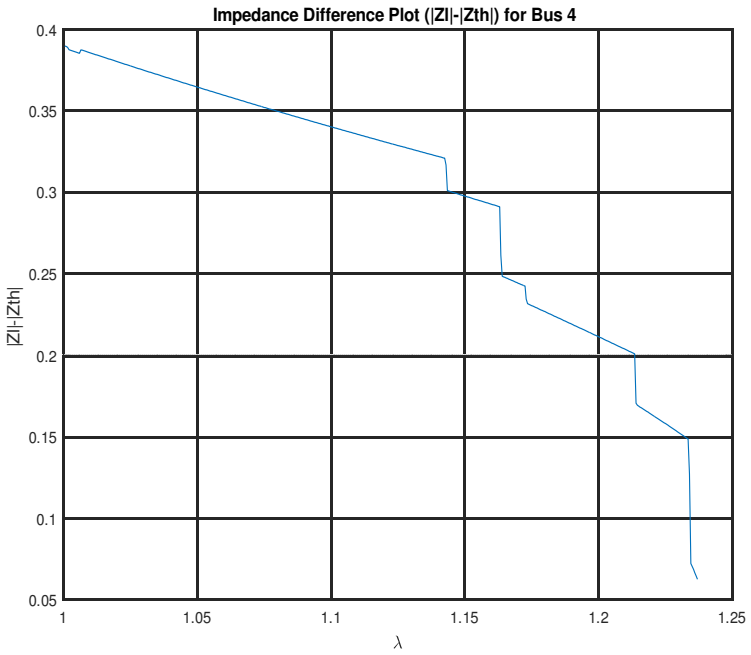

Figure 3.2: $|Z_L| - |Z_{th}|$ curve

The values of the curve shown in figure 3.2, can be used to estimate the critical load factors, using a linear regression model. Using a linear regression model requires a data set of two samples at measuring instants, k and $k-1$. By using the phasor measurements values for current and the voltage at the local bus, for two successive time instants, an estimate of the Thevein Impedance can be made in principle, which can then be fitted in to a regression model as explained in the previous section, to yield a theoretical estimate of the critical load factor.

3.1.2 Extrapolation using Linear Regression

The margins can also be calculated from the difference between the measured load impedance and the Thévenin impedance. In this method, the maximum power is calculated from a linear extrapolation of two subsequent measurements of $\Delta Z_k = Z_{L,k} - Z_{th,k}$, where $Z_{L,k}$ is the observed load impedance (calculated by V_D / I_D and $Z_{th,k}$ is the Thévanin impedance at loading factor λ_k.

Let λ_c be the point maximum loading factor where $\Delta Z_k = 0$. In other words, when $k \rightarrow c$ then $Z_{L,c} \rightarrow Z_{th,c}$ thus $\Delta Z_c = 0$. Using the point-slope form of a linear function, we have,

$$\Delta Z_k - \Delta Z_c = \frac{\Delta Z_k - \Delta Z_{k-1}}{\lambda_k - \lambda k - 1}(\lambda_k - \lambda_{k-1}) \tag{3.2}$$

Which, when solved for the definition of the margin, $\lambda_c - \lambda_k$, results in,

$$M_Z \equiv \lambda_c - \lambda_k = \frac{\Delta Z_k}{\Delta Z_k - \Delta Z_{k-1}}(\lambda - \lambda_{k-1}) \tag{3.3}$$

The results of the impedance margin estimation are shown in figure 3.3

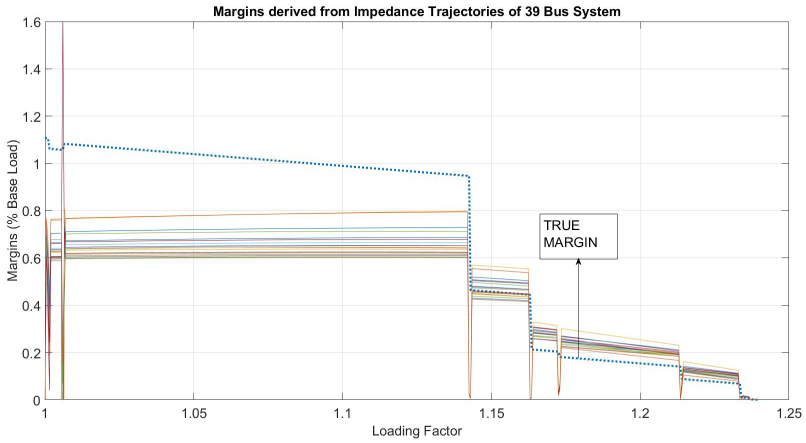

Figure 3.3: Margin estimates using the impedance margin method of IEEE 39 Bus System

3.1.3 Reactive Power Reserve Index-In terms of System Loading

The actions of the Over Excitation limiters induces discontinuities in the system stability margin, which in the absence of which is a monotonously linearly decreasing function of the system loading. As a transmission network is increasingly stressed, such generator transitions tend to have more damaging consequence on the system stability. This makes it necessary to monitor the reactive reserves of the generators and deploy sufficient control actions when such reserves are nearly exhausted.

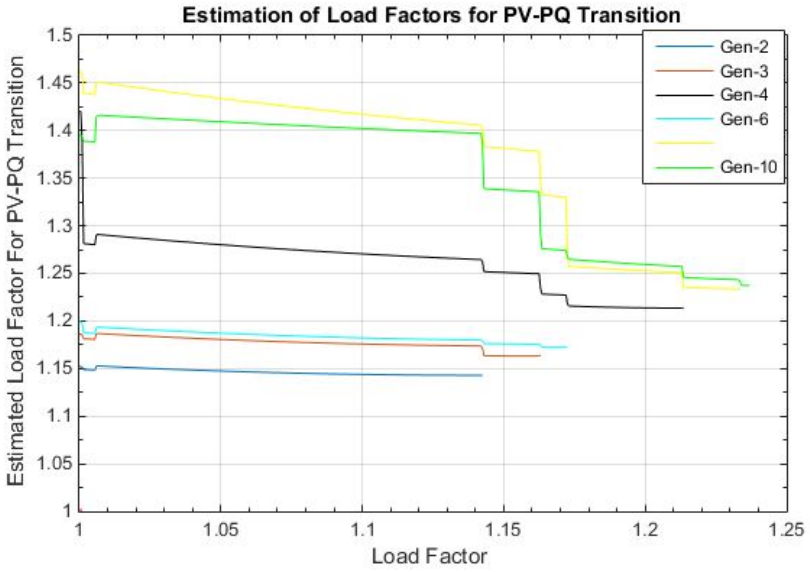

Figure 3.4: Estimated PV-PQ transitions as a functions of Load Factor

Assuming a quadratic regression model, the PV-PQ transition of a generator can be estimated by monitoring its reactive power reserve, $Q_{gi,max} - Q_{gi,k}$, the load factor at which reactive power of unit i will be exhausted as

$$Q_{g,max} = a_1 L_{f,i}^{*2} + a_2 L_{f,i}^{*} + a_3 \tag{3.4}$$

$$L_{f,i}^{*} = -\frac{a_2 \pm \sqrt{a_2^2 + 4a_1(Q_{gi,max} - a_3)}}{2a_1} \tag{3.5}$$

The coefficients $a_1, a_2 and a_3$ are determined by the regression model and they represent the

coefficients of the second degree polynomial used for extrapolating the reactive power curve. The estimated loading factor for the PV-PQ transitions is obtained from the intersection of the extrapolating curve and the maximum reactive limit of the generator. Therefore the next occurrence of the PV-PQ transition is estimated by

$$L_i^* = min\{L_{f,i}^*\} \tag{3.6}$$

The estimated margin for the next PV-PQ transition is

$$RPRI_k = min\{L_{f,i}^* - L_{fk}\} \tag{3.7}$$

A linear regression model can also be used for estimating the PV-PQ transitions. Assuming a linear regression model, the load factor at which the reactive power of generator-i, will be exhausted is

$$Q_{g,max} = aL_{f,i}^* - b \tag{3.8}$$

$$L_{f,i}^* = \frac{Q_{g,max} + b}{a} \tag{3.9}$$

Equation (2.9) gives the estimated load factor for PV-PQ transition of generator-i. The occurrence of the next PV-PQ transition is the same as given by equation (2.5) and Equation (2.7), gives the reactive power reserve index. Every time the $RPRI_k$, gets close to zero, a generator may reach its reactive power limit.

Milosevic [40] estimates the time to next PV-PQ transition by monitoring the reactive power reserve, $Q_{g_i,max} - Q_{g_i,k}$, for each generator g_i at each time t_k. We can modify this model to fit our approach by tracking the reactive power reserve at a given load factor, λ_k. If we assume a linear

reactive power increase, then the reactive power reserve will run out when,

$$\lambda_{g_i}^* = \lambda_k + \frac{Q_{g_i,max} - Q_{g_i,k}}{\frac{\Delta Q_{g_i,k}}{\Delta \lambda_k}} \tag{3.10}$$

The next PV-PQ transition event will occur at load factor

$$\lambda_g^* = \min_{i \in \alpha_{PV}} \{\lambda_{g_i}^*\} \tag{3.11}$$

The reactive power reserve index (RPRI) can then be defined by

$$RPRI_k = \min_{i \in \alpha_{PV}} \lambda_{g_i}^* - \lambda_k \tag{3.12}$$

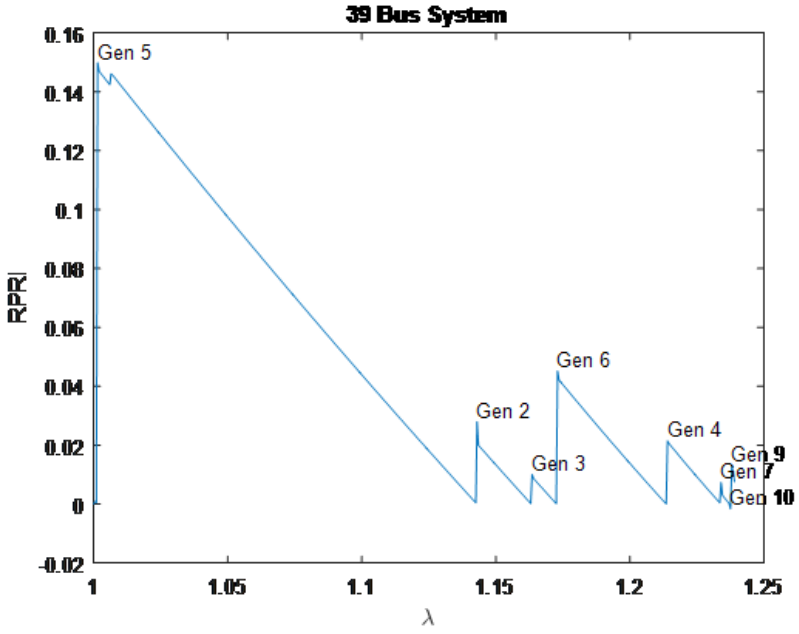

Figure 3.5: Reactive power reserve index

Figure 3.5 shows the results of the RPRI prediction algorithm. The process of determining the voltage stability margin at a load bus i and the approximate control actions can be summa-

rized in the following steps:

- Perform local phasor voltage and current measurements at the current load factor,λ_k.
- From the local measurements, estimate the Thévenin parameters for the two bus equivalent.
- From the Thévenin equivalent, estimate the critical load factor for the current loading.
- From the estimated load factor, calculate the estimated margin available.
- From the received information on reactive power reserve of each generator, estimate the next PV-PQ transition L_i^*
- If the system margin is low, below a certain chosen threshold and generators are expected to reach their respective reactive limits, control actions in the form of reactive reserves must be deployed. Load shedding is resorted to if such control actions fail to bring the system back to normal operating state.

3.2 Complex Power Margins

3.2.1 Linear Forecast of V-I characteristics

The power margin ΔS is defined as the difference between the power consumed at any given VIP and the forecast maximum power consumed at that bus before voltage collapse

$$\Delta S = S_D - S_{D,max} \tag{3.13}$$

In [76] the authors have calculated the power margin using a linear extrapolation of the slope of the V-I curve calculated at the present time to its maximum forecast [1, 76].

At the present time the slope is calculated by

$$\frac{V_k - V_{k-1}}{I_k - I_{k-1}} = -Z_{th} \tag{3.14}$$

A linear forecast satisfies the following relationship:

$$V - V_k = -Z_{th}(I - I_k) \tag{3.15}$$

Thus the forecast power is quadratic with respect to I:

$$S_D = VI = -Z_{th}I^2 + (Z_{th}I_k + V_k)I \tag{3.16}$$

The maximum will occur at the bifurcation point that occurs when the discriminant goes to zero:

$$S_{D,max} = \frac{(V_k + Z_t h I_k)^2}{4 Z_t h} \tag{3.17}$$

Thus the power margin is

$$\Delta S = \frac{(V_k + Z_{th}I_k)^2}{4Z_{th}} - V_k I_k \tag{3.18}$$

$$\Delta S = \frac{(V_k - Z_{th}I_k)^2}{4Z_{th}} \tag{3.19}$$

The conventional steady state voltage stability analysis identifies the tip of the nose curve (fig. 3.6) as the point of maximum loadability and hence signal the onsets of the voltage collapse for a constant power load. Power margin can thus be evaluated by estimating the difference between the present operating point and the tip of the nose curve.

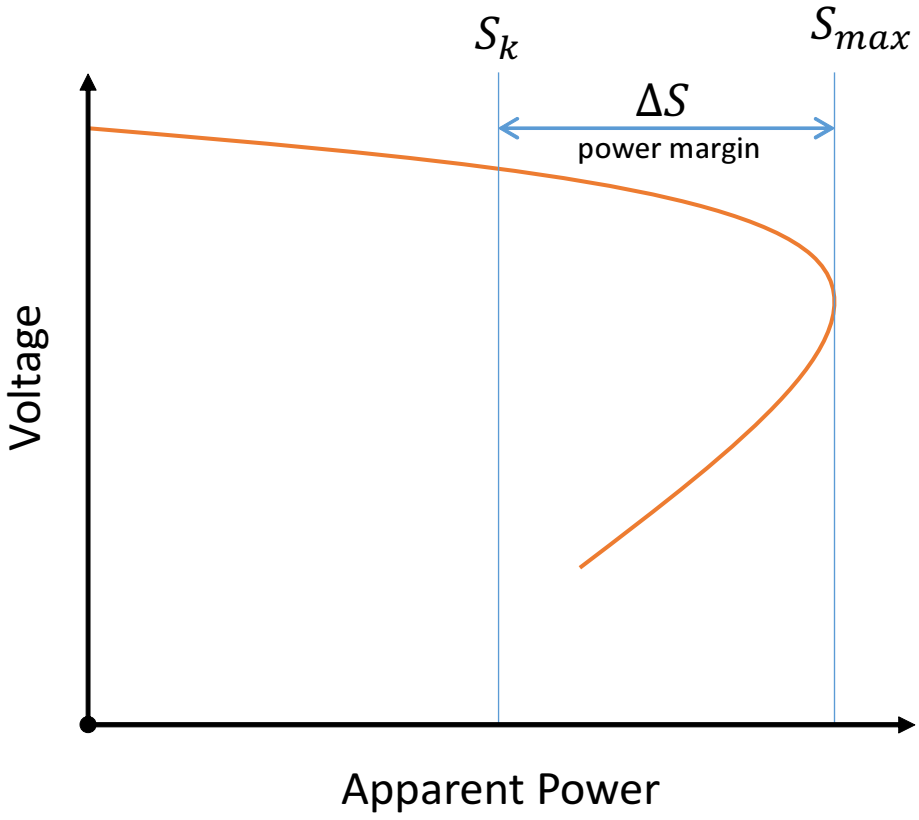

Figure 3.6: Power Margin

An alternate derivation of the equation of maximum deliverable power and hence the power margin can be derived by considering the Figure 3.7 making use of the estimated Thevenin Impedance and the current and voltage phasors at time instant, k.

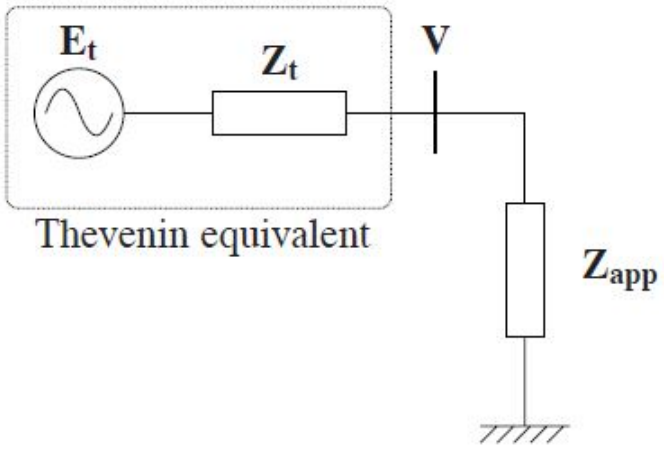

Figure 3.7: Local Bus and the rest of the system treated as Thevenin Equivalent

Figure 2.1 has been reproduced here (fig. 3.7) for the purpose of analysis. The load impedance is denoted by:

$$Z_L = R_l + jX_l \tag{3.20}$$

Where

R_l= Load Resistance

X_L= Load Reactance

Specifying a load power factor of $cos\phi$ is equivalent to having a load impedance of the form

$$Z_L = R_l + jX_l = R_l + jR_l tan\phi \tag{3.21}$$

The current $\overline{I}$ is given by

$$\overline{I} = \frac{\overline{E_t}}{(R_t + R_l) + j(X_t + R_l tan\phi)} \tag{3.22}$$

The load active power is given by

$$P = R_l I^2 = \frac{R_l E^2}{(R_t + R_l)^2 + (X_t + R_l tan\phi)^2} \tag{3.23}$$

The extremum condition is

$$\frac{\partial P}{\partial R_l} = 0 \tag{3.24}$$

Which is equivalent to

$$|Z_l| = |Z_t| \tag{3.25}$$

The optimal load resistance and reactance are then given by

$$R_{l,maxP} = |Z_t| cos\phi \tag{3.26}$$

$$X_{l,maxP} = |Z_t| sin\phi \tag{3.27}$$

The complex power injected in to the load is

$$S_l = I^2 |Z_l| = |Z_l| \frac{E_t^2}{(R_t + R_l)^2 + (X_t + R_l tan\phi)^2} \tag{3.28}$$

The maximum complex power injected in to the load

$$S_{max} = |Z_l| \frac{E_t^2}{(R_t + |Z_t| cos\phi)^2 + (X_t + |Z_t| sin\phi)^2} \tag{3.29}$$

$$S_{max} = |Z_l| \frac{E_t^2}{R_t^2 + |Z_t|^2 cos^2\phi + 2R_t|Z_t| cos\phi + X_t^2 + |Z_t|^2 sin^2\phi + 2X_t|Z_t| sin\phi} \tag{3.30}$$

$$S_{max} = |Z_l| \frac{E_t^2}{R_t^2 + X_t^2 + |Z_t|^2 (R_t cos\phi + X_t sin\phi)} \tag{3.31}$$

$$S_{max} = |Z_l| \frac{E_t^2}{2|Z_t|^2 + 2|Z_t| \left(\frac{R_t^2}{||Z_t} + \frac{X_t^2}{|Z_t|} \right)} \tag{3.32}$$

At the loadability limit

$$|Z_t| = |Z_l| \tag{3.33}$$

$$\Rightarrow S_{max} = \frac{E_t^2}{4|Z_t|} \tag{3.34}$$

The complex power injected at a time instant ,k

$$|S_k| = |V_k||I_k| \tag{3.35}$$

The complex power margin is then given by

$$|\Delta S| = |S_{max}| - |S_k| \tag{3.36}$$

$$|\Delta S| = \frac{E_t^2}{4|Z_t|} - |V_k||I_k| \tag{3.37}$$

The Kirchoff Voltage law dictates

$$E_t = |V_k| + |Z_t||I_k| \tag{3.38}$$

Hence

$$|\Delta S| = \frac{(|V_k| + |Z_t||I_k|)^2}{4|Z_t|} - |V_k||I_k| \tag{3.39}$$

$$|\Delta S| = \frac{(|V_k| - |Z_t||I_k|)^2}{4|Z_t|} \tag{3.40}$$

Where

(V_k, I_k) is the current measurement set.

Z_t is the estimated Thevenin Impedance.

Alternatively the power margin at any loading factor can also be represented in terms of the difference between the maximum power deliverable and the power that is being delivered. Reflecting back on 3.31 we can write for the maximum deliverable power

$$S_{max} = \frac{E_t^2}{2} \frac{1}{|Z_t + (R_t \cos\phi + X_t \sin\phi)|} \tag{3.41}$$

Where

S_{max}= Maximum Deliverable Power at a bus.

E_{Th}, Z_{Th}= Estimated Thevenin Parameters at the critical point.

R_{Th}, X_{Th}= Real and imaginary parts of estimated Thevenin Impedance.

ϕ= Load Power Factor angle.

Margin would then be given as;

$$\triangle S = S_{max} - S_k \tag{3.42}$$

In terms of base load percentage, the margin can be expressed as

$$\triangle S = \frac{M_p}{S_{BaseLoad}} \tag{3.43}$$

Where

M_p= Margin in terms of power

Margin as expressed as in 3.42 has been used to estimate the bus stability margins in this work. The accuracy of equation 3.42 in predicting S_{max} depends on the constancy of the Thevenin parameters. VIP algorithm has the implicit assumption of the constancy of the Thevenin parameters which is an ideal assumption. In the real world the thevenin parameters drift as the system conditions change which introduces estimation errors in equation 3.42.Using this method power margins of a simple two bus system can be estimated and plotted as the system loading is increased. For a system with two load buses, figure 3.8 plots the power margins as a function of system loading.

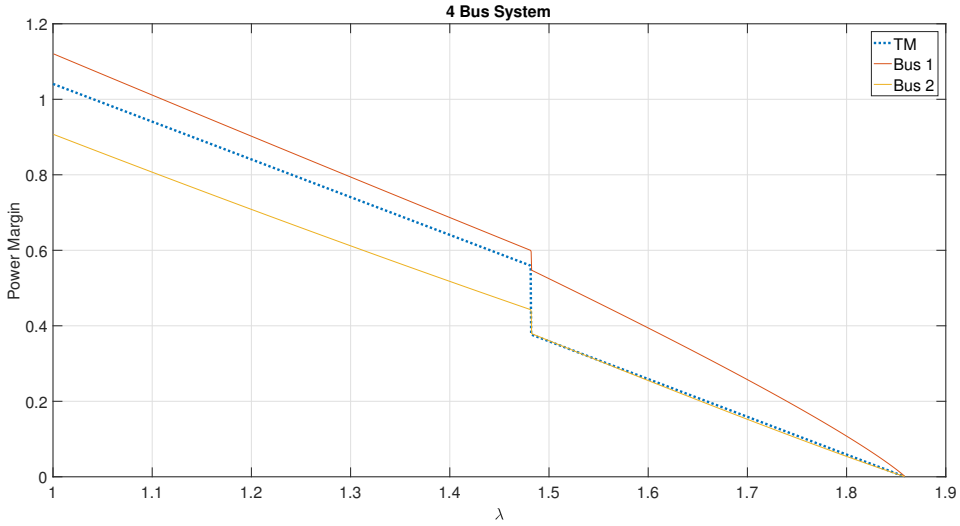

Figure 3.8: Power margins for Two Load Bus system

3.2.2 Power Margins for IEEE 39 Bus Test System from the Linear Forecast of V-I characteristics

Equation 3.41 can be applied to the IEEE-39 Bus system, and the power margins are computed as illustrated in Figure 3.9.

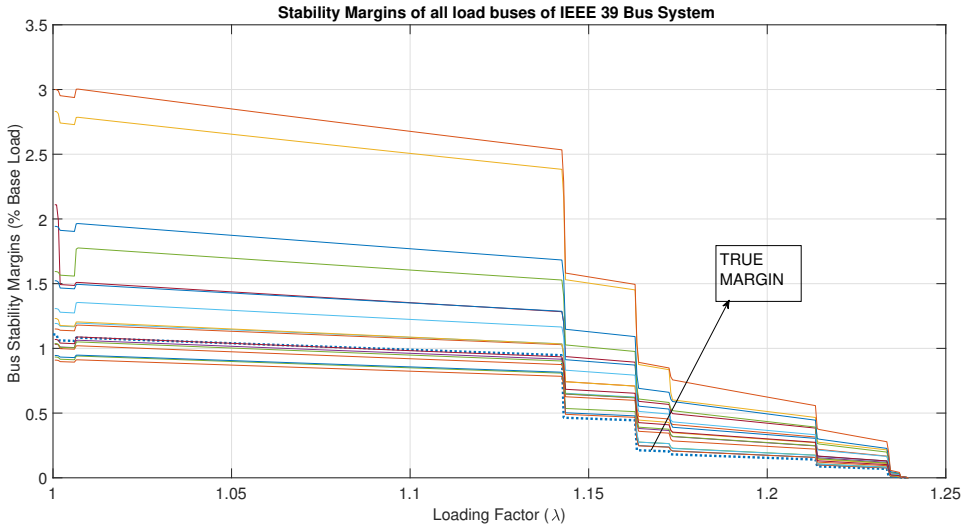

Figure 3.9: Power Margin Estimates for IEEE 39 Bus Test System with $PV-PQ$ transitions

The sharp drops in the power margin plots are enforced by the generators hitting their reactive limits. The power margins experience a dramatic decline during the $PV-PQ$ transitions of the generators, which effectively drag the system to the collapse. Figure 3.10 gives the power margins when the reactive limits of the generators are set to infinity.

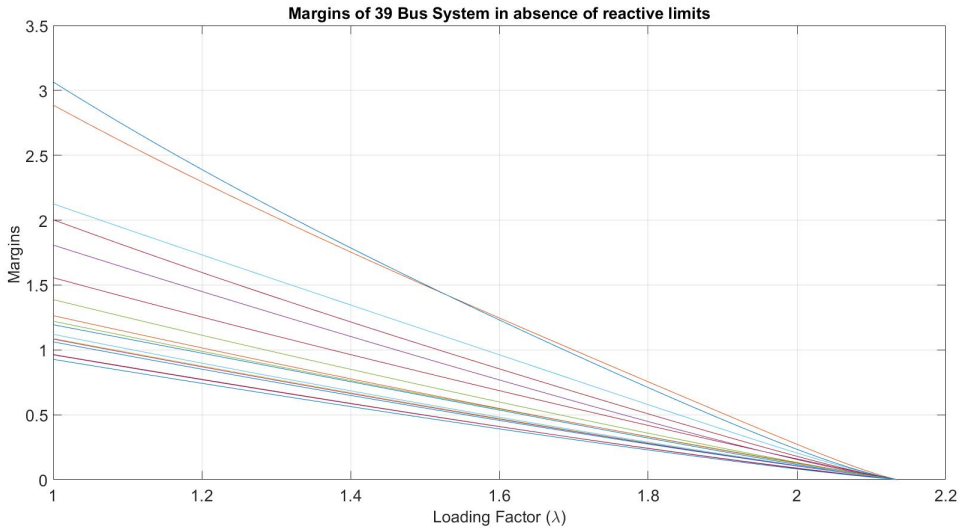

Figure 3.10: Power Margin Estimates for IEEE 39 Bus Test System with No reactive Limits

Figure 3.11 represents the estimated complex power margins in regions close to the sta-

bility limit.

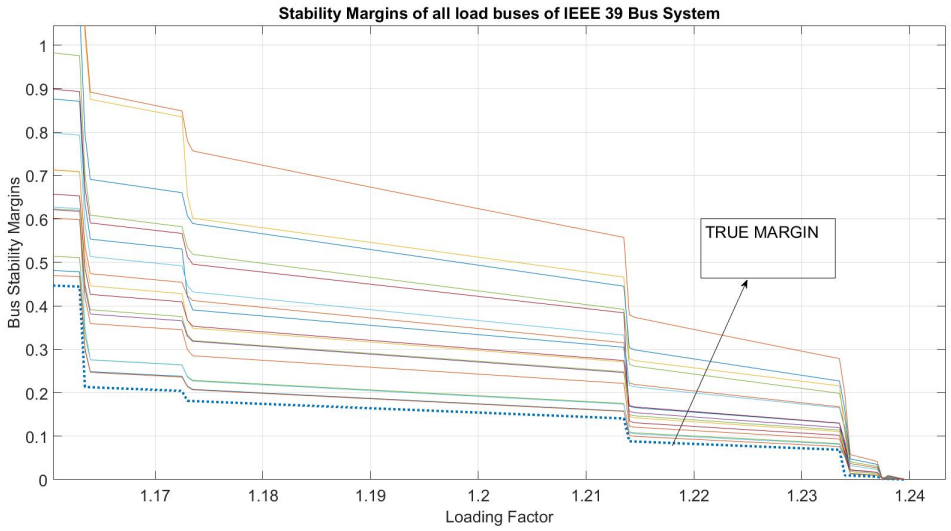

Figure 3.11: Power Margin Estimates for IEEE 39 Bus Test System close to collapse

The power margin represents the estimated available power at *each bus*. For a system wide comparison across all buses, the power margin needs to be mapped in terms of the loading factor, λ , using the definition,

$$\lambda_k = \frac{S_{j,k}}{S_{j,0}} \tag{3.44}$$

Where beginitemize $S_{j,k}$= Complex power load at Bus j, at instant k.

$S_{j,0}$= Complex power load at Bus j, at base load.

If M_P represents the mapped the power margin in terms of system loading, then

$$M_p = \lambda_{max} - \lambda_k \tag{3.45}$$

$$M_p = \frac{S_{j,max}}{S_{j,0}} - \frac{S_{j,k}}{S_{j,0}} \tag{3.46}$$

$$M_p = \frac{\Delta S}{S_{j,0}} \tag{3.47}$$

The dashed line (in blue) in figure 3.9 represents the true power margin of the system,

and we can observe that all the margin estimates of different buses do not coincide with the true margin. Most of the margin estimates overshoot the true margin, and the spread becomes tighter as the stability limit is reached. This indicates that the margins produced by the buses seem to agree more as the system approaches collapse, but never truly coincide with the true margin of the system. In order to come up with a reliable estimate of the power margin which is as close as possible to the true margin, the outputs of the different VIP sensors must be fused in a meaningful manner, so that the system has one accurate power margin estimate. This effort translates the problem of identifying the true margin of the system in to a problem of sensor fusion. Although there are several algorithms which tackle the problem of sensor fusion, the one that has been utilized in this research effort is the Dempster-Shafer Sensor Fusion. Various statistical properties of the margin estimates have also been studied, and have been presented in this text, the Dempster-Shafer combination seems to be a more meaningful approach to achieve the objective of true margin identification. The basics of the Dempster-Shafer theory have been briefly discussed in this text, in the next section, to give the reader an idea about the theory and its ramifications in the field of sensor fusion.

3.2.3 Power and Impedance Margin-Comparison

In order to compare performance of the margins on the 39 bus system, we have divided the loading factor ranges up into seven regions between PV-PQ transitions in which the results are relatively stable. These regions are illustrated in figure 3.12 and defined in table 3.1.

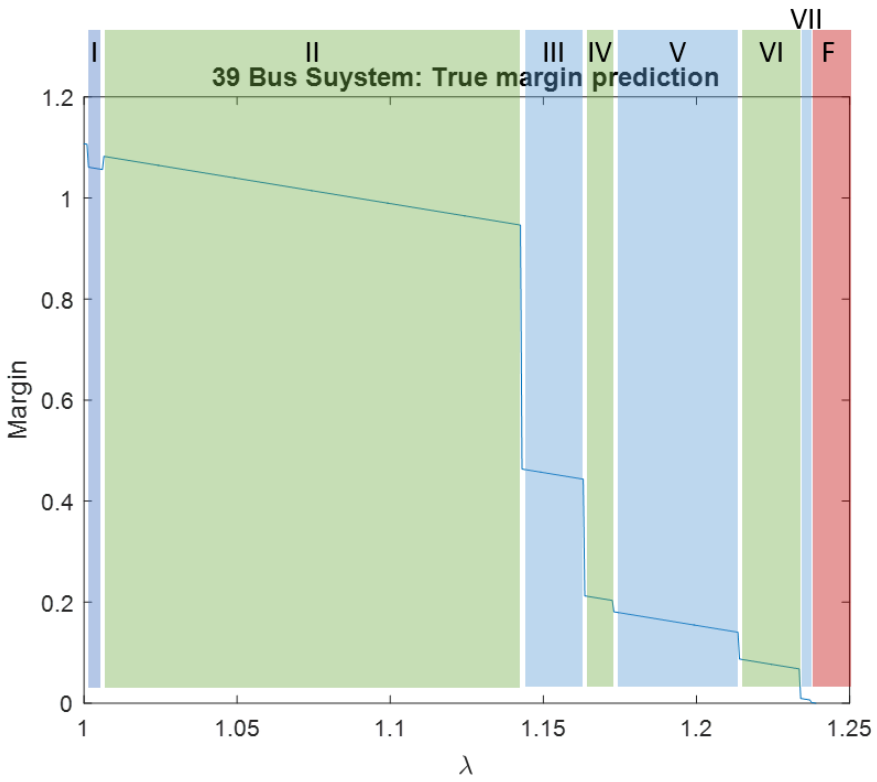

Figure 3.12: Regions between PV-PQ transitions for IEEE-39 Bus System

Table 3.1: Regions between PV-PQ transitions in the 39 bus system

Region	Loading Factor Range	Step range ($\Delta Lf = 0.005$)
I	1.0025-1.0060	5-12
II	1.0070-1.1425	14-285
III	1.1440-1.1630	288-326
IV	1.1645-1.1725	329-345
V	1.1740-1.2135	348-427
VI	1.2150-1.2335	430-467
VII	1.2350-1.2370	470-474
Failure	≥1.2380	≥474

As an evaluation criterion, we can evaluate the mean-squared error (MSE) for each margin estimation methods, averaged throughout each region.

Let $\epsilon_{j,k}$ be the error in any given margin estimate $M_{est,j,k}$ at some bus j at some loading factor λ_k defined by $\epsilon_{j,k} = |\hat{M} - M_{est,j,k}|$ where $\hat{M}$ is the projected true margin. Then the MSE

is given by

$$MSE = \frac{1}{N} \sum_{\substack{\forall j \\ k \in R}} \epsilon_{j,k}^2$$

Where R is the set of measurements in the given region. The results are shown in table 3.2.

Table 3.2: MSE for each region from power and impedance estimation methods

Region	I	II	III	IV	V	VI	VII
M_Z	0.6244	0.1769	0.0065	0.0048	0.0022	0.00112	$4.5e^{-}05$
M_P	0.0241	0.0179	0.0017	0.011	$4.6e^{-04}$	$8.8e^{-05}$	$1.36e^{-05}$

Apart from being more accurate, the power margin method is preferred because of the following reasons.

1. At certain key region, when the system loading increases and nears voltage collapse, the power margin provides a more accurate estimate of the true margin.

2. The power margin estimates tend to fall both above and below the true margin for all regions. Therefore if it is possible to assign weights to the measurements, the true margin could be estimated through a weighted average or through selection of the optimal measurement bus. While the impedance margin results tend to be more tightly clustered, in most regions the estimates fall either entirely above or entirely below the true margin, rendering the proposed true margin estimation methods invalid.

3. The power margin provides a more intuitive measure of how close the system is to failure by defining the margin in terms of an observable parameter, viz. power delivered to a bus.

3.2.4 Quadratic Forecast of V-I Characteristics

A linear forecast, however is not able to capture the non linearity of the V-I curve, especially close to the critical point. Figure 3.13 shows the V-I characteristics of Bus 7 of IEEE 39 Bus

System and the associated linear fit and quadratic fit.

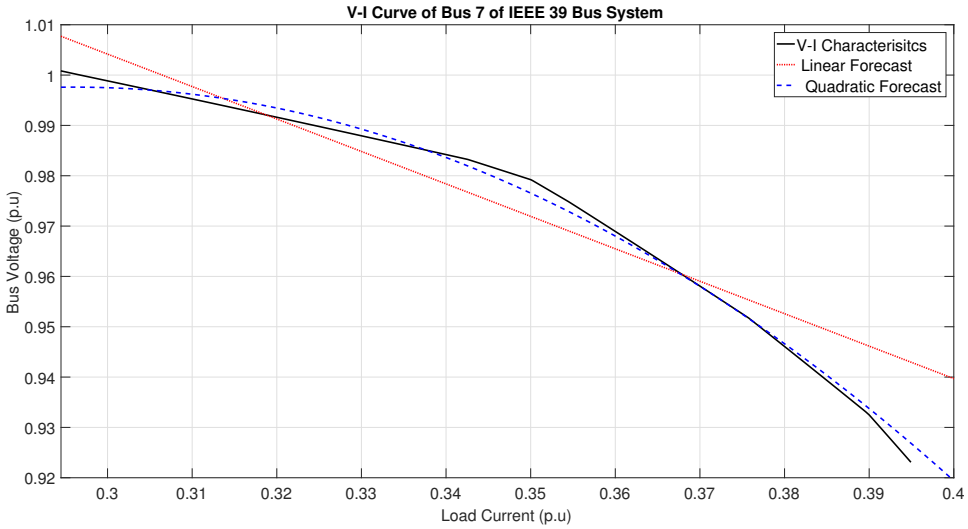

Figure 3.13: V-I Characteristics of Bus 7 of IEEE 39 Bus System and associated fitted functions

It is clear that close to the collapse point, there is a significant departure of the estimated linearly fitted function from the real characteristics. The figure also shows a quadratic fit of the characteristics which captures much more information about the VI curve than a linear fitted function. The next section will further elaborate on fitting the V-I characteristics. A quadratic forecast of the V-I characteristics of a load bus can also be used to estimate the proximity to voltage collapse. As the V-I characteristics tend to get increasingly non linear, a polynomial of suitable degree can be used to fit the measurements samples of voltage and current phasors. The procedure to estimate the stability margin from a V-I characteristics is given in the appendix. Figure 3.13 plots the shape of the V-I curve and by looking at the figure it is clear that a quadratic forecast should perform better especially when the system is close to collapse point. Extrapolation by a higher order polynomial may prove to be a better fit but at the same time it might pose a considerable computational burden on the system. Furthermore higher order polynomials tend to be oscillatory in nature which may affect the quality of the extrapolation especially at instants which coincide with the PV-PQ transitions. At these discontinuities the polynomial may get badly scaled which can lead to unrealistic results. A quadratic polynomial

fitting is preferred because of the improved accuracy over a linear forecast while posing a mild computational burden. A huge computational requirement of higher order polynomials does not justify the marginal increase in the accuracy. Moreover higher order polynomials also need large data windows so as to be able to make an estimate of the margin which suggests that the margin estimation has to be delayed till the estimator collects the required number of measurement samples. In voltage collapse scenarios this requirement may not be acceptable as a continuous monitoring of margin is very important for triggering emergency controls.

For a PQ load, the V-I characteristics is a nonlinear curve and a quadratic fitting has been realized to capture these characteristics. In general, voltage at any load bus can be expressed in terms of a polynomial function of the load current, as

$$V_L = f(I_L) \tag{3.48}$$

$$V_L = P_n(I_L) = a_0 I_L^0 + a_1 I_L + a_2 I_L^2 + ... + a_n I_L^n = \sum_{j=0}^{n} a_j I_L^j \tag{3.49}$$

If the length of the data samples is M, i.e, the number of samples of voltage and current phasors, then for fitting a polynomial of order n, the condition

$$n < M \tag{3.50}$$

has to be satisfied.

In this work the order of the polynomial is 2 (n=2), so essentially we are trying to fit a parabola to the incoming samples of the current and voltage phasors. Without loss of generality, we can express our objective function as

$$E = \min \sum_{i=1}^{M} [V_{L,k} - P(I_{L,k})]^2 \tag{3.51}$$

For a quadratic fitting polynomial the value of M can be taken as 3, which satisfies the condition

3.50. Hence from 3.49 we can write for the voltage at any arbitrary loading level $'k'$,

$$V_{Lk} = a_0 + a_1 I_{L,k} + a_2 I_{L,k}^2 \tag{3.52}$$

Since we are trying to minimize the sum of squares of the distances between the actual value of voltage and the expected value, we need to take partial derivatives with respect to each parameter and make them equal to 0,

$$\frac{\partial E}{\partial a_j} = 0, j = 0, 1, 2..n \tag{3.53}$$

Since M=2 for a quadratic fit, the use of equation 3.53 leads to the following algebraic expression

$$\begin{bmatrix} 1 & I_{L,k} & I_{L,k}^2 \\ 1 & I_{L,k+1} & I_{L,k+2}^2 \\ 1 & I_{L,k+2} & I_{L,k+2}^2 \end{bmatrix} \begin{bmatrix} a_0 \\ a_1 \\ a_2 \end{bmatrix} = \begin{bmatrix} V_{L,k} \\ V_{L,k+1} \\ V_{L,k+2} \end{bmatrix} \tag{3.54}$$

Equation 3.54 can be further solved to get the fitting parameters a_0, a_1 and a_2. Once the fitting parameters are obtained we can write for the power

$$S_k = V_{L,k} I_{L,k} \tag{3.55}$$

$$S_k = (a_0 + a_1 I_{L,k} + a_2 I_{L,k}^2) I_{L,k} \tag{3.56}$$

Knowing that at the critical point, $\frac{dS}{dI} = 0$, we can write for $I_{L,max}$,

$$a_0 + a_1 I_{L,max} + 3 a_2 I_{L,max}^2 = 0 \tag{3.57}$$

Equation 3.57 can be used to find the estimated maximum current at the critical point, which can be further used to derive an estimate of S_{max}. Margin can be trivially derived from this

point. Figure 3.14 plots the stability margins of all the load buses of IEEE 39 Bus System using quadratic curve fitting of V-I characteristics of load buses.

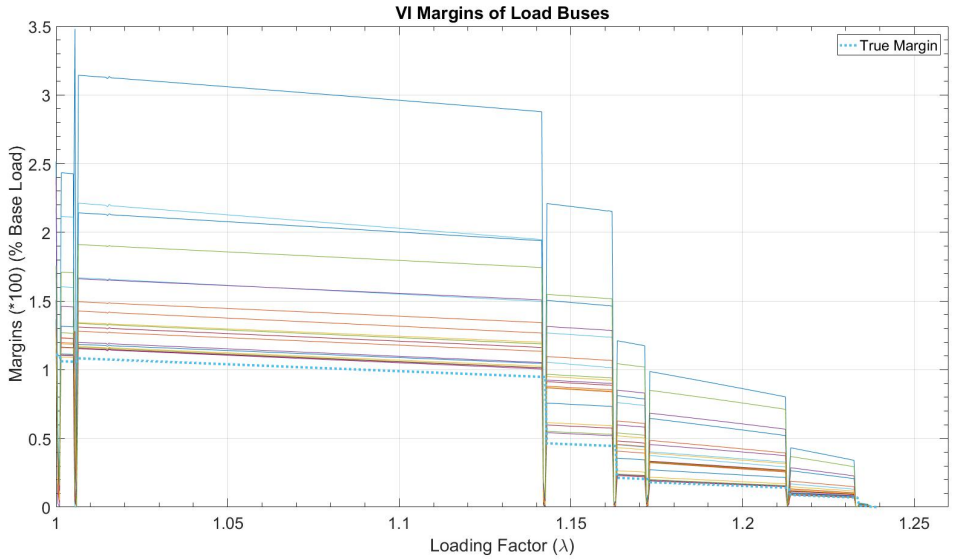

Figure 3.14: Distribution of Power Margin Estimates of IEEE 39 Bus System derived from a Quadratic forecast V-I Characteristics of load buses

Since this method precludes the estimation of the Thevenin parameters the results obtained are better than the previous methods. Table 3.3 lists the mean square error in different regions for Bus 7 of the IEEE 39 Bus system. These number can be compared with 3.3 and it becomes clear that margin derived from V-I characteristics is better.

Table 3.3: MSE for each region from power and impedance estimation methods

Region	I	II	III	IV	V	VI	VII
M_{VI}	0.0709	0.0441	0.0013	$2.9e^{-05}$	$4.17e^{-}05$	$5.8e^{-}05$	$1.2e^{-}05$
M_P	0.0241	0.0179	0.0017	0.011	$4.6e^{-04}$	$8.8e^{-05}$	$1.36e^{-05}$

3.3 Algorithm for True Power Margin Calculation

In order to have a methodology to compare various margin estimation methods, it's important to establish a baseline or reference margin that be used as an evaluation criteria. Such a metric would obviously not be accessible in a physical VIP implementation, but we can take

advantage of the simulation to shed light on the performance of different margin estimation methods.

3.3.1 Continuation Power Flow

The Matpower package includes a Continuation Power Flow (CPF) algorithm that, starting from a base scenario, uses continuation or branch tracing methods to determine steady state stability limits. The algorithm employs a predictor-corrector method to track voltage profiles at each bus as power increases. The program can be used to find the saddle-node bifurcation point and establish a baseline maximum load factorv (fig 3.15).

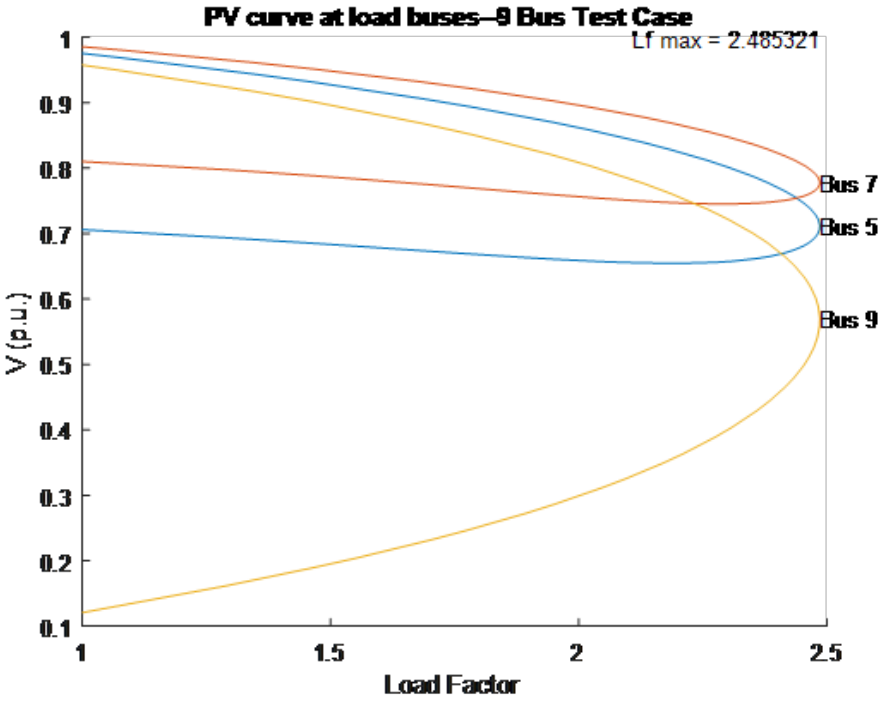

Figure 3.15: PV curves resulting from CPF

The CPF algorithm implementation in Matpower has one shortcoming that hampers its usefulness to our study: it does not take into account PV-PQ transitions that occur when generator buses hit their reactive power limits. Even when a solution to the base case would include a PV-PQ transition for a solution, the CPF algorithm's implementation of the power flow solver

ignores generator reactive limits.

3.3.2 Binary Search Method

Due to this limitation an alternate approach is needed to find system power margins when generator reactive limits are in effect.

The heart of this algorithm is a binary search function or half-interval search function. This function works by incrementing the power supply and demand in the base case until the solution fails to converge. One the first failure is encountered, the step size is halved and the power is stepped back. If a convergence is found, the step size is halved and the power is stepped forward. If the solution once again fails to converge, the step size is halved and the power is stepped backwards. This continues until the step size is smaller than the desired tolerance and the solution converges. (fig. 3.16)

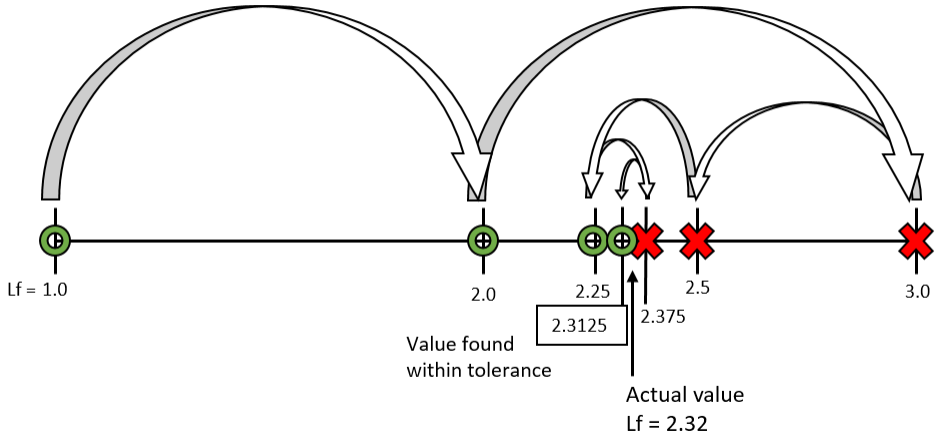

Figure 3.16: λ_c search algorithm

We can verify the algorithm's results by comparing the results without generator Q-limits enforced to the output of the CPF algorithm.

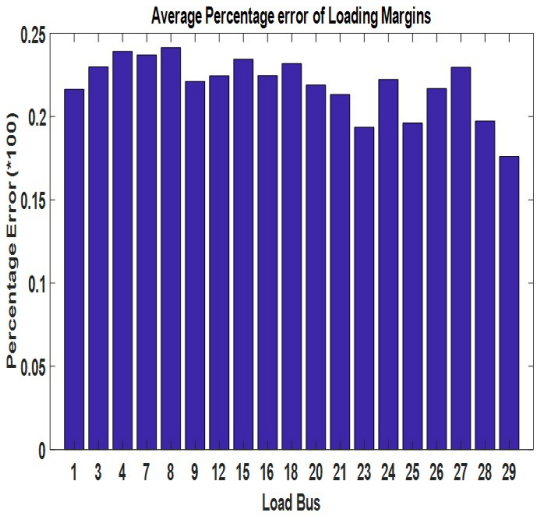

Figure 3.17: Z extrapolation Method

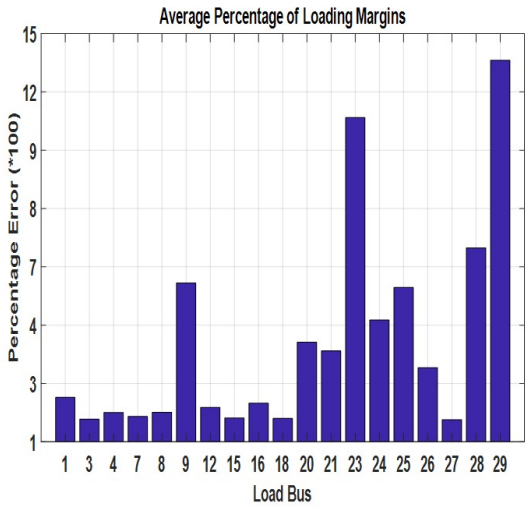

Figure 3.18: Thevenin Equivalent Method

Table 3.4: Comparison of results

	9-Bus	39-Bus
CPF	2.485321	2.135527
search algorithm	2.4852	2.1356

3.4 Comparison of Margin Estimation Techniques

This section goes over a comparative study of the margin estimation techniques developed so far in the previous sections. The comparative study is carried on the IEEE 39 bus system as well as IEEE 118 bus system. Both the standard systems are subjected to a small disturbance and the longer term voltage stability is analyzed. The small disturbance is simulated as a gradual load increase across all PQ buses and the system margins are evaluated at every PQ location at every loading instant. For the IEEE 39 bus systems the average percentage error between the VIP derived margin and the true margin is calculated from base load up until the critical load. Figures 3.17, 3.18 and 3.19 plot the results of the simulations.

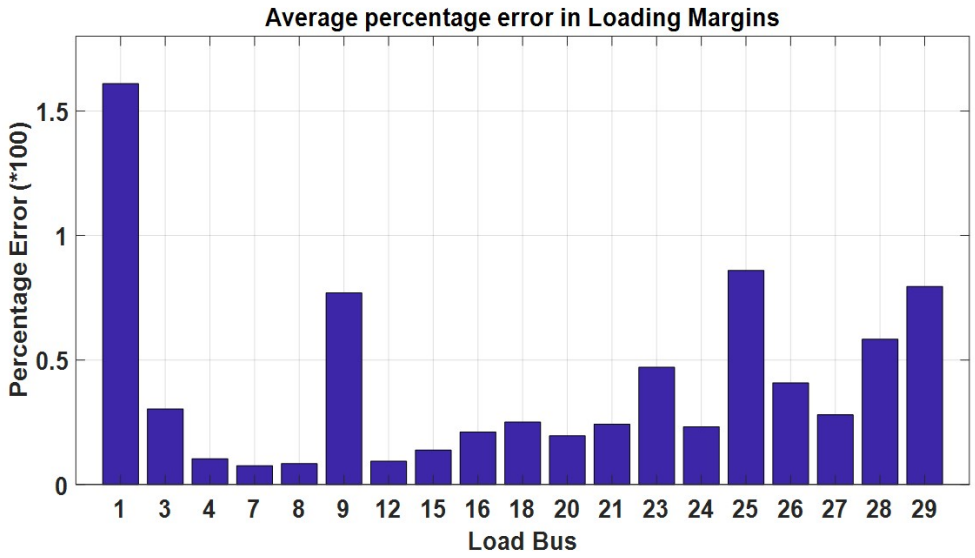

Figure 3.19: Quadratic curve fitting of V-I characteristics

IEEE-118 bus system is subjected to a proportional load increase at all PQ buses and the loading margins are estimated. Fig. 3.20 plots the average error distribution of margin errors (Maximum Margin Error- Minimum Margin Error) for IEEE-118 bus system, close to critical load, from $\lambda = 1.84$ to $\lambda = 2.109$, which is the critical loading factor for this system. Since the Z extrapolation method is based on the impedance trajectories, the spread of the Thevenin impedances as seen from different buses will determine the spread of margins and hence the spread of errors. Since the spread of Thevenin Impedances as seen by different buses is tight, the estimated critical loading factors obtained by extrapolating the impedance trajectories are confined to a narrow range.

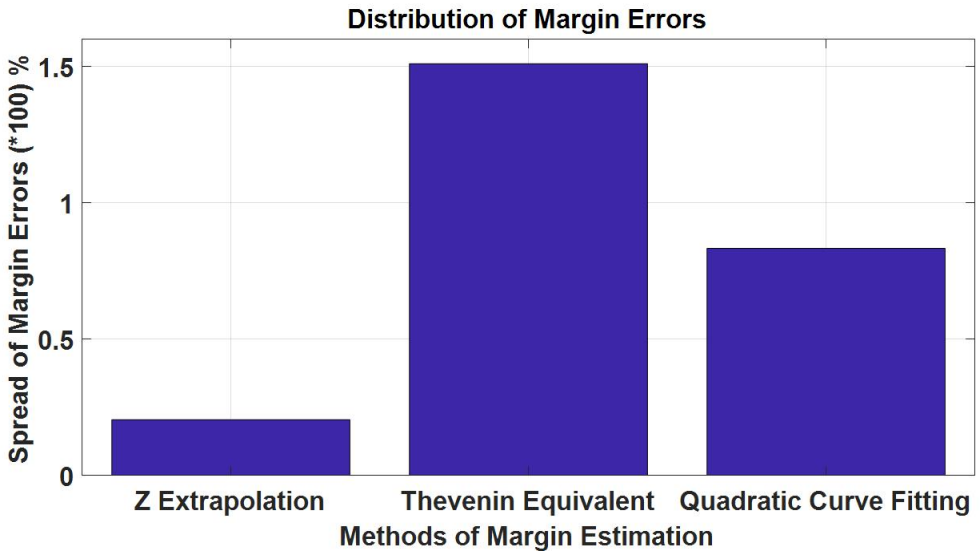

Figure 3.20: Average Error Distribution across all PQ buses

However, the tighter spread of errors does not necessarily guarantee high accuracy of individual margins. The individual margins could be highly inaccurate even if the spread of errors is tight.The most accurate VIP location is not fixed across the network but rather varies as the system conditions change. Various factors have been observed to affect the accuracy spectrum of VIP derived margins. Some of them include generators reaching reactive limits, equipment outages like loss of a line or a generator and disturbances such as load variations. It thus becomes necessary to reevaluate the margins following events which change the system operating point.The spread of errors between the VIP margins and the true margin is small in case of the Z extrapolation method, followed by the quadratic curve fitting method and is the largest in case of the Thevenin Equivalent method as shown in 3.20.

4. ACCURACY ASSESSMENT OF VIP DERIVED MARGINS

4.1 Distribution of VIP derived Margins

[1] As the system size increases it is possible to obtain a large number of VIP margin estimates corresponding to every PQ bus in the system. Each individual estimate of the VIP margin is associated with a distinct measure of accuracy, which is dependent on system loading and other conditions, such as the status of over-excitation limiters. This results in a wide spectrum of margin estimates of varying accuracy, which naturally begets the question - which margins to trust more and which estimates should be ignored. The results of a number of simulations performed on a wide variety of systems seem to indicate that only a small percentage of VIP derived margins are close to the true system margin. The majority of the margin estimates are characterized by less accuracy and hence more uncertainty. To shed some light on to the accuracy distribution of the VIP margins, IEEE-118 bus system model is used to present some results.Due to the difference in the Thévenin equivalents as observed from different locations VIP derived margins tend to have locationaly dependent accuracy.

The locations in the power network which experience less changes in the Thévenin equivalent as the system is progressively stressed through a load multiplier,λ , tend to have more accurate measure of margin than other locations. This distribution of margins necessitates the proper identification of those VIP points in a network which are more resilient to the changing system conditions. As the system conditions change, the accuracy spectrum also shifts with new VIP points taking precedence in terms of accuracy and replacing the previous VIP estimates. Thus it is essential to keep track of the accurate estimates continuously as the loading parameter is varied to the critical point. The PV-PQ transitions induce discontinuities and cause a shift in the accuracy spectrum of VIP margins. Generally, in the absence of any PV-PQ transitions

[1] Part of the data reported in this chapter is reprinted with permission from "Locational Accuracy of VIP Indices for Voltage Collapse Margin Estimation-Begovic, Miroslav, et al. (2018)-Proceedings of the 51st Hawaii International Conference on System Sciences| 2018"

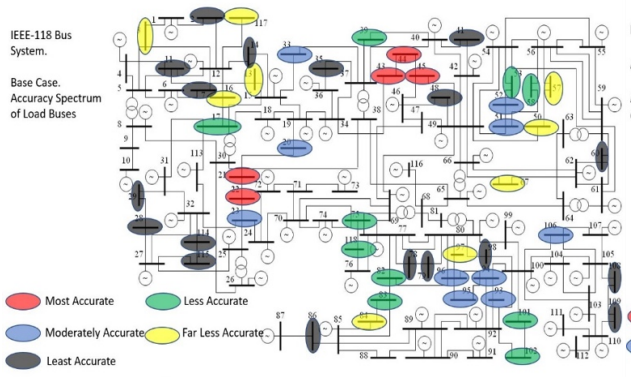

Figure 4.1: Base Load

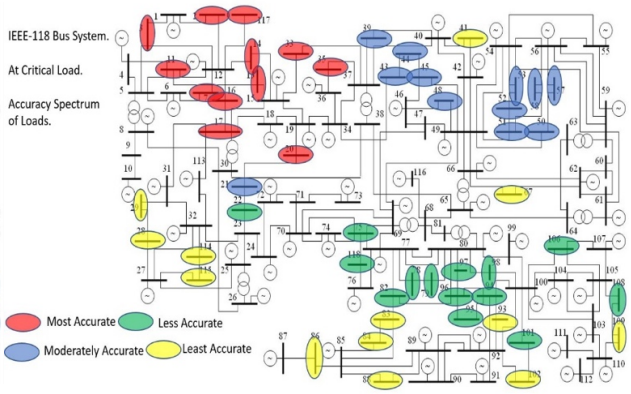

Figure 4.2: Critical Load

the accuracy of the VIP margins does not vary very much. Thus, it is essential to monitor the generator reserves to account for changes after any impending PV-PQ transition that would affect the ac curacies of the VIP estimates. As the system loading is increased, the accuracy of the VIP margins changes mildly and at instants where PV-PQ transitions take place the shift in the accurate locations is drastic.

As the system loading is increased, the accuracy of the VIP margins changes mildly and at instants where PV-PQ transitions take place the shift in the accurate locations is drastic. Figure 4.2 shows a snapshot of the accuracy spectrum of IEEE 118 bus close to the critical point. It is interesting to note the changes that take place as the system is increasingly stressed to the critical point. The most significant of changes to consider is the emergence of well-defined groups of VIP points near the critical point. This further leads credence to the idea of being able to identify or filter the most accurate estimates and combine them into a single system wide margin. If such a VIP-derived fused margin is found, it would meet the criteria of simplicity and swiftness while at the same time lowering the inaccuracy of the individual VIP estimates.
In addition to system loading, the accuracy of VIP margins also depends on system conditions, which include system topology, parameters of different components of the system. Since the system topology remains constant in a given situation, system loading is the primary factor in a given system which determines the accuracy spectrum of VIP locations. Further, it is possible to obtain a different distribution of the VIP locations in terms of their accuracy under a different

set of PV-PQ transitions It has been observed that when different sets of generators are allowed to reach their reactive limits, it alters the set of VIP locations in terms of both accuracy of margins and voltage sensitivity of loads.

A certain VIP location which is accurate under a particular set of system conditions and at some particular system loading, could turn out to be completely inaccurate under a different set of conditions or even at a different system loading. Since it is practically impossible to expect a consistent accuracy pattern across all the VIP locations, it is becomes necessary to monitor some of the locally measurable properties of the VIP locations, which change in synchronism with the changes in the accuracies of VIP locations, as system loading or system condition or both change. Any such property could provide an opportunity to generate more accurate margin estimates. Figure 4.3 shows the accuracy spectrum of VIP locations under a different set of PV-PQ transitions than the one shown in Figure 4.2.

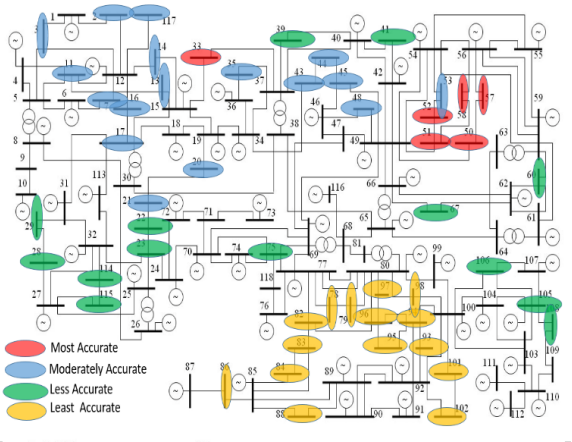

Figure 4.3: Accuracy Spectrum of VIP Locations in IEEE 118 bus under a changed set of PV-PQ transitions close to critical load, $\lambda = 1.903$

4.2 Effect of System Conditions on Margin Accuracy

The inaccuracies inherent in the Thévenin parameter identification, due to the nonlinear characteristic of the system, are reflected in the VIP margins in the form of a distribution around the true system margin. The assumption of constancy of the Thévenin equivalent makes it possible

to use the present estimated values of the Thévenin equivalent in order to yield a measure of the power injected at a bus at the critical loading factor. The assumption of constancy works well within a sampling window of sufficiently short length. When spread over the entire loading space, which may include an arbitrary number of PV-PQ transitions, system parameters tend to gradually drift from their initial values. This small but a gradual drift in the system parameters offsets the estimation of the true maximum power. Depending on the drift experienced by the VIP locations, the accuracy of VIP margins changes. A wide variety of changes in the external system conditions can lead to large changes in the parameters of the Thévenin model.

Apart from system loading, which is normally the dominant factor in determining the VIP margins, factors such as the status of OELs of generators also greatly impacts the values and changes of VIP margins. In addition, contingencies like line outages also lead to a change in the estimated margins at loads and thus creating a different distribution of VIP margins. In view of these observations, it becomes very difficult to predict a particular VIP location in order to reveal the information about available system margin. Whenever any generator reaches the reactive limit, it represents a changed system condition, making it necessary to reevaluate the accuracy ranking of the VIPs. Similarly, line outages cause a change in system topology, which negatively impacts the available system margin and changes the order of the accurate VIP locations. In this work, VIP margin accuracy is assessed by manually altering the reactive limits of the generators, thus creating a distinct pattern of PV-PQ transitions.

4.2.1 Generator Reactive Limits

The standard IEEE 9 bus system as shown in Figure 4.4 is studied under a different a set of generator reactive limits and the related impact on the VIP derived margins. The standard 9 bus system is equipped with three generators, including the slack bus, and three loads to which one more load is added for the purposes of having redundant measurements. Three different cases are created, which correspond to any one of the generators reaching its limit or both generators reaching their respective limits. The load on Bus 8 is varied proportionally in the three cases

along with the generator reactive limits, to create a distinct loading profile for each case, which allows the possibility of different PV-PQ transitions. It is to be expected that when two generators, with the exception of the swing bus, are allowed to reach their limits, the impact on the system margin and the accuracy spectrum of VIPs will be significant as opposed to only one generator reaching the limit. For the sake of simplifying the analysis, different loading factor regions are created.

Since the system behavior remains almost unchanging between two successive PV-PQ transitions, it is important to evaluate the margins in such regions, separated by consecutive PV-PQ transitions. A generator switching from PV mode to PQ mode signifies a precipitous decline of the reactive reserves of the system, while also presenting an extra burden to the system. In the absence of any emergency controls or reactive compensation at buses, PV-PQ transitions can effectively drag the system into collapse. However, it has also been observed that generators can switch from PQ to PV mode, which signifies an increase in the reactive reserves of the system. Such switches have been observed to have an effect of increased margin available in the network. Under any such transitions, the accuracy of a VIP margin depends on the accuracy of estimation of $S_{j,max}$ or $P_{j,max}$. Load buses, which are able to estimate them as close as possible to their true values, are naturally associated with better accuracy in their margin estimation.

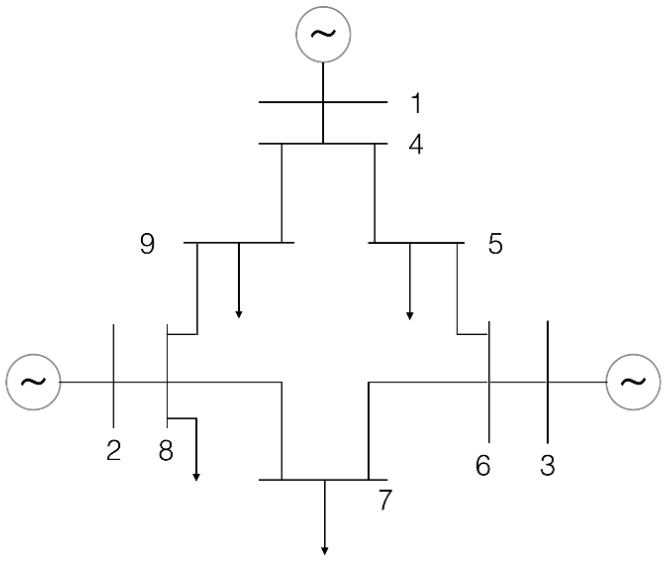

Figure 4.4: IEEE 9 Bus System

In Figure 4.4, bus 1 is the slack bus while buses 2 and 3 are voltage-controlled buses. The first case is created by manipulating the reactive limits of the generators in such a way that allows only generator-2 to reach its limit, thus changing from a PV (voltage-controlled) bus to a PQ bus. Table 4.1 lists the data for this case and the associated accuracy ranking of VIP locations. The loading factor ranges for region -I and region II are from $\lambda \approx 1 - 1.68$ and $\lambda \approx 1.68 - 1.89$ respectively.

Table 4.1: Generator Data and Accuracy Ranking of VIP Locations

Generators	Q-Limit (MVAR)	Accuracy Ranking of VIP Locations	
		Region-I	Region-II
Gen-1 (Slack)	400	Bus-9	Bus-8
Gen-2	100	Bus-5	Bus-9
Gen-3	300	Bus-7	Bus-7
		Bus-8	Bus-5

Figure 4.5 shows the estimates of the margins for the case when only generator-2 reaches the reactive limit. significant change in the accuracy spectrum results when generator at bus 2 reaches the limit. Before the PV-PQ transition, the VIP margin of Bus 8 is characterized by highest inaccuracy. The switching of generator 2 also has a huge impact on the system margin. The available margin then undergoes a drastic change and drops by more than 50 %. The critical

loading factor of the system is $\lambda \approx 1.869$. In the second case, the generator at bus 3 is allowed to reach its reactive limit and switch from PV mode to PQ mode, while the generator at bus 2 stay in PV mode. Table 4.2 lists the data for this case and the associated VIP margin accuracy ranking. The loading factor ranges for regions -I and II are from $\lambda \approx 1-1.65$ and $\lambda \approx 1.65-2.161$ respectively.

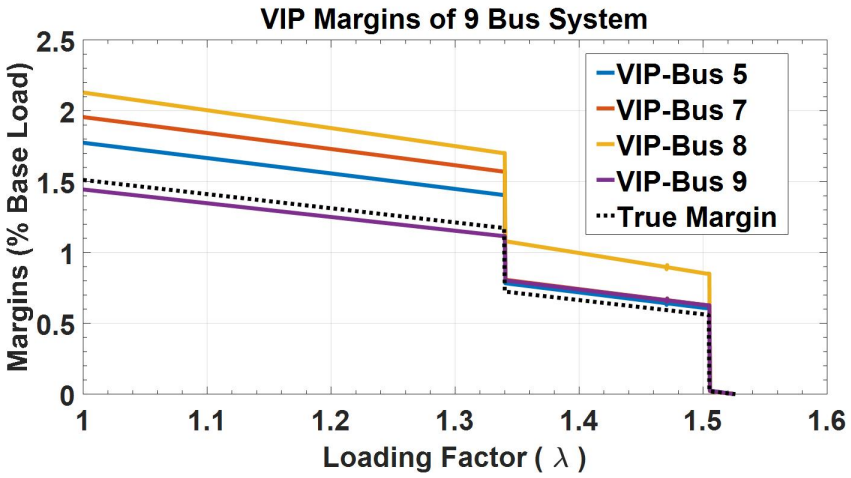

Figure 4.5: VIP Margin distribution under Generator 2 limit violation

Table 4.2: Generator Data and Accuracy Ranking of VIP Locations

Generators	Q-Limit (MVAR)	Accuracy Ranking of VIP Locations	
		Region-I	Region-II
Gen-1 (Slack)	500	Bus-7	Bus-9
Gen-2	355	Bus-5	Bus-7
Gen-3	50	Bus-9	Bus-5
		Bus-8	Bus-8

Figure 4.6 plots the VIP margins when only generator-3 is allowed to reach the reactive limit. Figures 4.5 and 4.6 can be compared and the differences in the VIP margins are apparent.The VIP margins of figure 6 show a markedly different distribution around the true margin with different accuracy ranking as is shown in Table 4.2. The critical loading factor in this case turns out to be $\lambda_c \approx 2.161$. The apparent increase in the system critical loading factor can be attributed to the increase in the reactive reserves of the system. By allowing a different generator to reach the reactive limit, a different spread of VIP margins was obtained. In reality, generators

have fixed reactive limits, which are independent of system loading, however this experiment reveals the margin tracking capability of the VIP algorithm, as well as its locational dependence of accuracy of margin estimates. In the third and final case, both generators are allowed to reach their respective reactive limits and a different distribution of the VIP derived margins is obtained. Table 4.3 lists the data for this case.

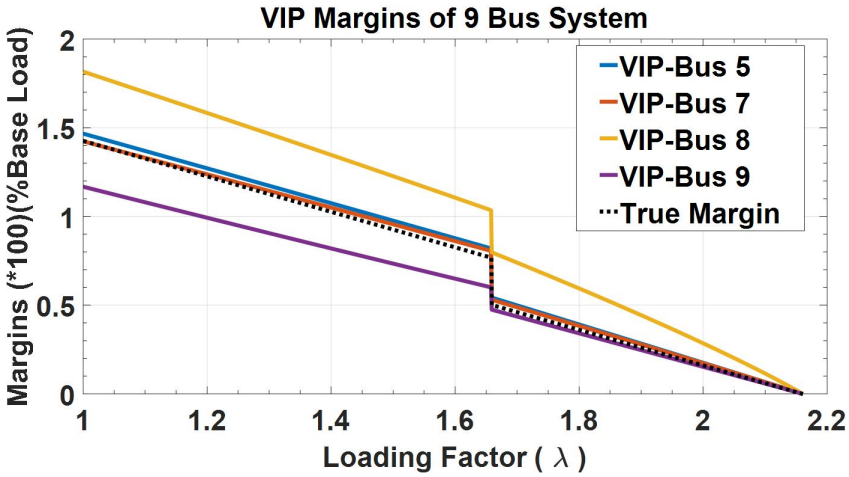

Figure 4.6: VIP Margin distribution under Generator 3 limit violation

As both generators are allowed to reach their respective limits in this example, the system approaches instability faster, and voltage collapse occurs at a system loading factor of $\lambda_c \approx 1.26$. This also changes the pattern of margin spread around the true margin and the new accuracy rankings are listed in Table 4.3. Since the impact on margins is significant, it becomes necessary to study some of the easily measurable electrical properties of the buses, which change in accordance with the change in the VIP margins as system operating point moves through different conditions.Any such property should have the feature of being easily measurable at every system loading factor and should be able to reflect the changes in the VIP margins with a significant amount of fidelity. It could then provide an easy access in to the changes that happen to the bus margins, under events of contingencies or any future PV-PQ transitions or even under heavily stressed conditions. By monitoring such a property, the accuracy of the VIPs could be easily established with a higher degree of certainty. Figure 4.7 shows the VIP margins when both generators are allowed to reach their limits. Note the difference in the spread of VIPs

around the true margin. The loading factor ranges for regions -I, II and III are from $\lambda \approx 1 - 1.14$, $\lambda \approx 1.14 - 1.15$ and $\lambda \approx 1.15 - 1.26$ respectively.

Table 4.3: Generator Data and Accuracy Ranking of VIP Locations

Generators	Q-Limit (MVAR)	Accuracy Ranking of VIP Locations		
		Region-I	Region-II	Region-III
Gen-1 (Slack)	400	Bus-7	Bus-8	Bus-7
Gen-2	75	Bus-5	Bus-9	Bus-8
Gen-3	20	Bus-9	Bus-7	Bus-9
		Bus-8	Bus-5	Bus-5

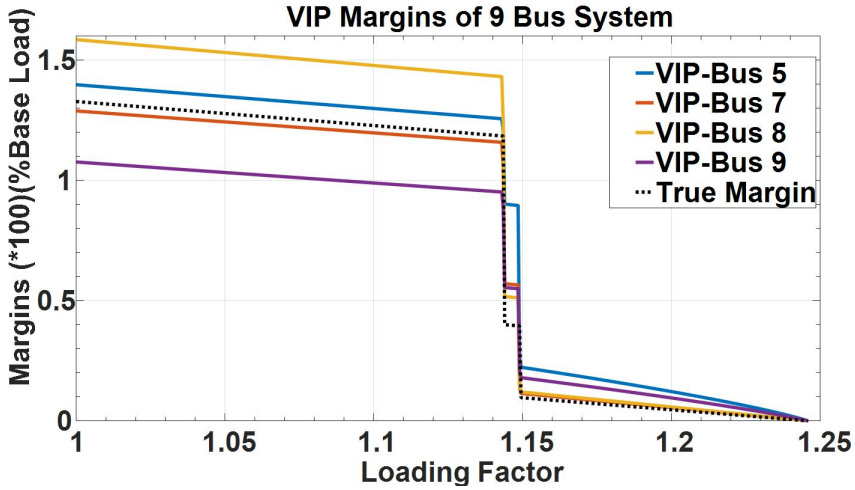

Figure 4.7: VIP Margin distribution under all Reactive Limit Violations

4.2.2 Effect of Transmission Line Outages

Transmission line outages have a similar effect on VIP security margins. Any outage radically shifts the distribution of the margins while simultaneously also disturbing the accuracy profile of the margins. IEEE 9 bus system is used to study the impact of the line outages. The line connecting buses 4 and 5 is taken out and the system is simulated under the effect of increased loading. The transmission line 4-5 is one of the more heavily loaded lines and the effect on the margin is significant. In the simulation, the line outage causes one of the generators to violate its reactive limit and hence drive the system into collapse. Table 4.4 lists the accuracy ranking of the VIPs during the outage.

Table 4.4: Accuracy Ranking of VIP Locations

Rank	Accuracy Ranking of VIP Locations		
	Pre-Outage	Post Outage	After Limit Violation
I	Bus-9	Bus-5	Bus-5
II	Bus-5	Bus-7	Bus-7
III	Bus-7	Bus-9	Bus-8
IV	Bus- 8	Bus-8	Bus-9

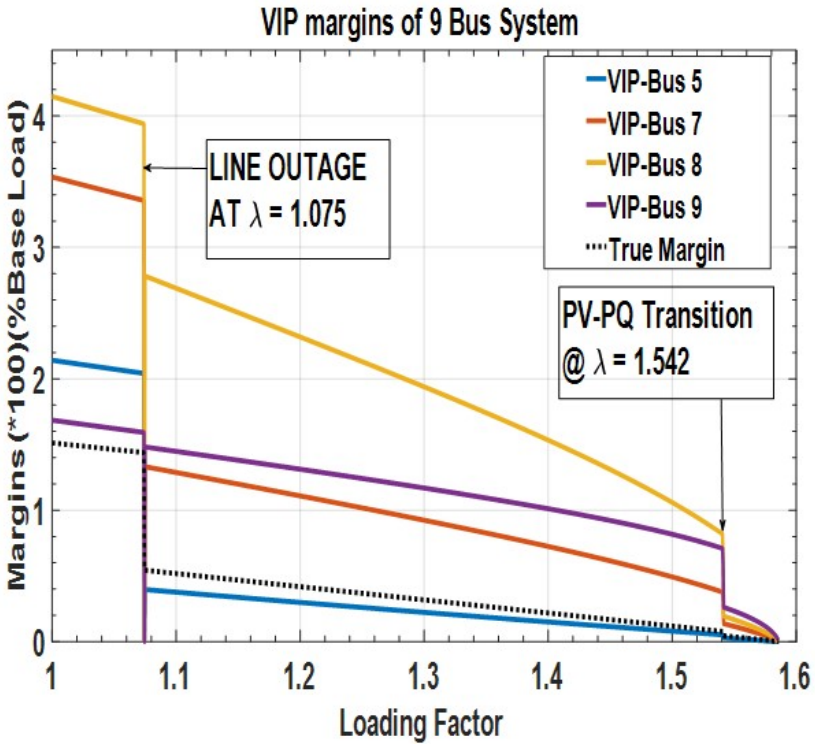

Figure 4.8: VIP Margin distribution under Line Outage (4-5)

4.3 Characterization of VIP Margins

The vulnerability of the VIP margins to the changing system conditions necessitates some form of locational characterization of such margins. Any electrical property that undergoes similar changes in commensurate with the changes in the margin accuracy could provide an easy access in to the accuracy spectrum of VIP margins and hence can be used to assign degrees of confidence to particular margin estimates. However, due the increasing nonlinearity of the

system and the difficulties associated with extrapolating the Thévenin parameters near the critical point, a one-on-one linear correspondence between the VIP margin accuracy and any such electrical property may or may not exist. The limitations imposed by the nonlinearity of the system can be overcome by exploiting the redundancy of data that is available in a VIP network. In this sense the multiplicity of data becomes an asset which if manipulated in a meaningful manner, can be used to offset the liability; which is the in deterministic nature of the VIP algorithm. In order to achieve this objective a couple of measurable electrical properties were tested.

4.3.1 Short Circuit Current Study

The first property that was explored to have any correlation with the accuracy of the VIP margins is the short circuit current magnitude. The short circuit study is performed on the IEEE 39 bus system. with faults occurring independently on each node and the short circuit current was calculated. The assumptions made in this study are

1. The fault was assumed to take place on phase A of the line, so the results have been obtained accordingly.

2. The mutual coupling between the lines was ignored, which means the sequence impedances (positive,negative and zero), are the same.

To calculate the fault current, the primitive impedance matrix is inverted to get the primitive admittance matrix and by making use of the node incidence matrix, a sequence admittance matrix is obtained which can then be inverted to get the sequence impedance matrix. From the sequence impedance matrix, fault current is easily calculated, since we know the three phase faults will only have the positive sequence fault currents t. In the abc frame the magnitude of the fault is same in all the phases but the phasor angle is different which can be calculated accordingly. The short circuit currents are tested for correlation with the accuracy of the margin estimates. The plot of the margin estimates is divided into different regions for analysis pur-

Table 4.5: Loading Factor Range of Different Regions.

Region	Loading Factor Range	Step range ($\Delta f = 0.005$)
I	1.0020-1.0060	1-13
II	1.0065-1.1425	14-286
III	1.1435-1.1630	288-327
IV	1.1640-1.1725	329-346
V	1.1735-1.2135	348-428
VI	1.2145-1.2335	430-468
VII	1.2345-1.2370	470-475
Failure	≥ 1.2375	≥ 476

poses and correlation is tested in each region by some loading factor in the region. Table 4.5 lists the loading factor range of different regions. The regions represent the system characteristics in between the PV-PQ transitions.

Each region is bounded by a $PV-PQ$ transition and each region is associated with the range of loading factors. The correlation is tested in each region at some loading factors. The error is defined by calculating the Chebyshev Distance between the margin estimates of each individual bus and the true margin of the system. Figures 4.9 and 4.10 plot the correlation between the VIP margin accuracy (which is quantified in terms of the distance from the true margin) and the magnitude of the short circuit bus at the corresponding VIP location. From the plots there seems to be little or no correlation at all between the accuracy of the VIP margins and the magnitudes of short circuit currents. The correlation figures however do roughly allude to the observation that locations with higher short circuit current could also possess a higher accuracy in the margin prediction. That is as far as we can go with the short circuit current study and no definitive statements can be made to further support this view. Owing to these observations and also the fact that the short circuit currents are topology dependent, and will change when the topology of the network changes, because of the loss of some lines or generator outages, the characterization of VIP margins on the basis of short circuit study is not recommended.

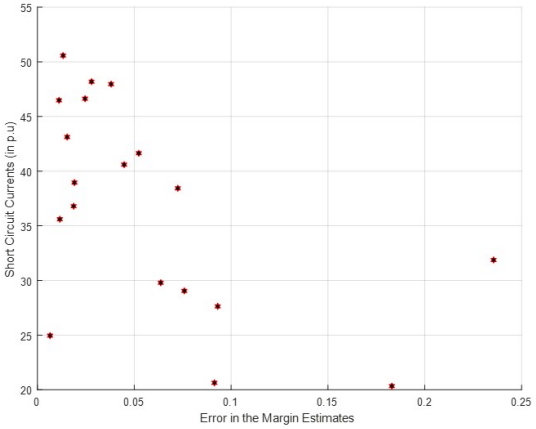

Figure 4.9: Base Load

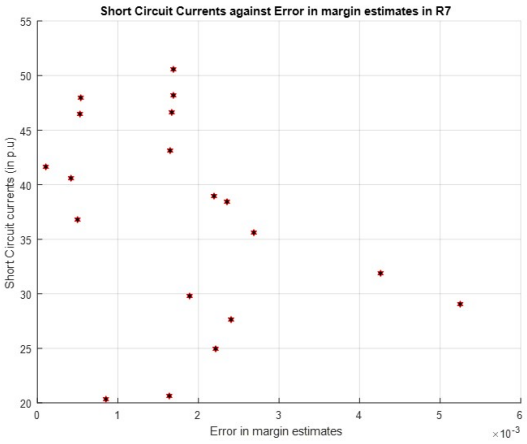

Figure 4.10: Critical Load

4.3.2 Local Measure of Voltage Sensitivity

To allow for the locational characterization of the VIP margins, a sensitivity metric is proposed for monitoring the local sensitivity of VIP locations with respect to the change in the local load. The sensitivity metric is defined as

$$K_j^{\lambda_k} = \frac{\delta V_j^{\lambda_k}}{\delta S_j^{\lambda_k}} = \frac{\frac{V_j^{\lambda_k} - V_j^{\lambda_{k-1}}}{V_j^{\lambda_k}}}{\frac{S_j^{\lambda_k} - S_j^{\lambda_{k-1}}}{S_j^{\lambda_k}}} \tag{4.1}$$

Where $K_j^{\lambda_k}$ is the measure of the sensitivity metric at bus j at system loading λ_k while $\frac{\delta V_j^{\lambda_k}}{\delta S_j^{\lambda_k}}$ refers to the ratio of percentage change in the voltage at bus j with respect to the percentage change in the complex load at bus j„ between two consecutive instants of system loading. The percentage change in the voltage and in the local load is used for normalization, because different VIP locations have different amounts of loads present on them. Local sensitivity of VIP locations can be easily determined, and the computation can be performed for every loading factor. This has the benefits of being able to assign confidence degrees to the individual VIP margins as the system is uniformly stressed from base load until collapse. The use of the con-

fidence degrees can be further exploited to yield a meaningful data fusion of the VIP margins. Since each VIP margin carries some degree of uncertainty, a fusion of a bunch of margins can effectively reduce the entropy of the individual margins and can possibly yield a better estimate of the system margin. Of course, in order for data fusion to produce meaningful results, more accurate VIP locations need to identified and isolated from the less accurate VIP locations. This process of elimination of the less accurate margins needs to be performed at every instant of system loading. The robustness of the sensitivity metric to filter out the more accurate margin estimates is contingent on the accuracy with which the Thevenin parameters are estimated.

As already stated, the fundamental source of inaccuracy in the VIP algorithm is the inclusion of the loads (nonlinear) into a system equivalent. Such characterization of loads can render the assumption of near-constancy of the Thévenin equivalent invalid, which in turn will have adverse effects on the estimated margins. In a wide variety of experiments that have been performed, the local sensitivity of the VIP margins at different locations, as given by equation 4.1, has shown a consistent correlation with the accuracy of VIP margins. Often assuming the shape of a decreasing exponential function, the VIP locations that are characterized by higher values of the sensitivity metric turn out to be more accurate than VIP locations with low values of the sensitivity metric. Furthermore, as we move towards the higher end of the sensitivity spectrum, the number of such locations decreases, indicating that a significant number of the locations are characterized by low sensitivity measures which agrees with the behavior of accuracy spectrum of the VIP margins.

Several systems were tested for the correlation between the VIP accuracy and the sensitivity metric as defined in equation 4.1. Figures 4.11 and 4.12 demonstrate the correlation in case of IEEE 118 bus system at the base load which corresponds to $\lambda_k = 1$ and the critical load, $\lambda_k = 2.109$ times the base load.

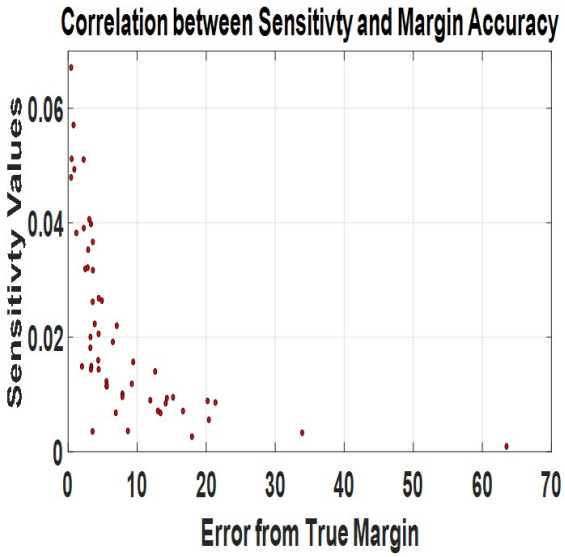

Figure 4.11: Base Load

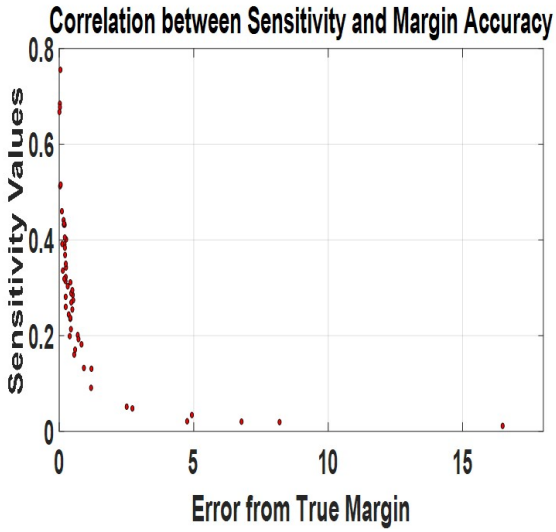

Figure 4.12: Critical Load

To further lend support to this argument, figures 4.13 and 4.14 demonstrate the correlation as tested on the 1354 bus PEGASE system.

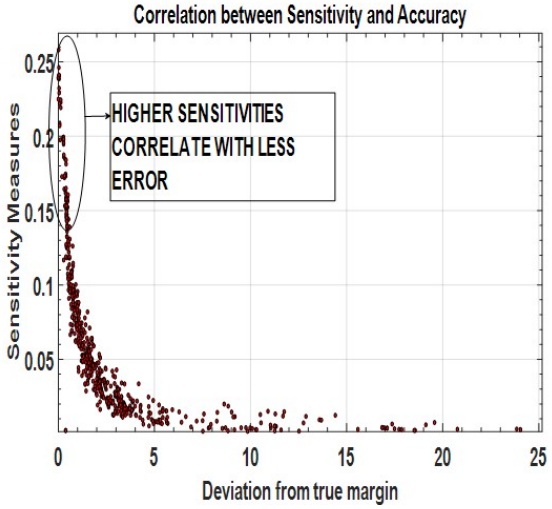

Figure 4.13: Base Load

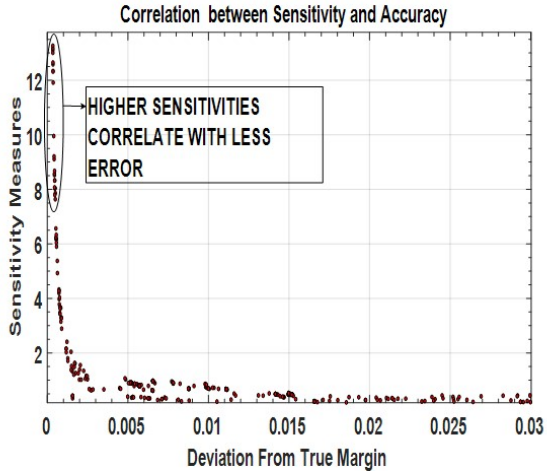

Figure 4.14: Critical Load

It can thus be concluded that as the system is progressively stressed, the correlation between the VIP accuracy and the VIP sensitivity grows stronger. At the base load the spread is over a wider region but is distributed over a narrow region near the critical load. This suggests that as the system moves closer to the collapse, the accurate VIP locations tend to get more sen-

sitive. This observation can be exploited at every instant of system loading and the accurate VIP locations can be identified throughout the network.

4.4 Elimination of inaccurate estimates based on Sensitivity Metric

The IEEE-118 Bus System is subjected in this simulation to a series of different tests for studying the spectrum of VIP margins, the changes caused by different system conditions and for validating the effectiveness of the sensitivity metric in its ability to identify the most accurate VIP locations. A total of 100 test cases have been created, each with a unique combination of the generators reaching the respective reactive limits. By allowing a different combination of generators to reach the reactive limits, enough diversity is created in the system in order to empirically test the validity of the sensitivity metric. Each case is characterized by a unique PV curve with distinct instants of PV-PQ transitions. A combination of five such generators is taken in each case and their reactive limits are altered to ensure that they reach their limits. Since the IEEE-118 Bus System has 54 thermal units, a huge number of combinations is possible depending on the sample size taken. To limit the number of combinations and make it more manageable, a sample of five generators is taken. It has been observed that a sample of five generators creates sufficient diversity in the spectrum of PV-PQ transitions. In a similar fashion different sets of PV-PQ transitions are simulated and the impact on the VIP margins is analyzed. The process of drawing combination is done in the following manner:

1. The standard IEEE-118 Bus case is simulated, without any modifications, under a proportional load increase.

2. The generator that do not reach their reactive limits at the critical load are identified. Such generators are 24, 25, 26, 27, 31, 40, 42, 61, 66, 69, 72, 73, 87, 89, 90, 91, 107, 111, 112, 113, 116.

3. Combinations of five generators are drawn out of the set of generators that do not reach their reactive limits by making use of $n!/(n-k)!k!$, where n is the number of generators

in PV mode at the critical load and k is the sample size, which in this case is 5.

4. The sample size could be adjusted, increased or decreased, depending on the number of combinations sought. However, a large sample size may result in numerical problems in the power flow solutions, because of forcing a large number of generators to switch at once, and a sample size of less than five may not generate sufficiently diverse combinations.

5. A sample size of five results in 20349 combinations, out of which 100 very diverse combinations are selected. The 100 combinations that are selected are the combinations of generators which lie in the vicinity of heavy loads (Buses 66-118).

By simulating a particular combination of generators to reach the reactive limits, a unique set of PV-PQ transitions is obtained. It is important to note that in each case, in addition to the generators which are forced to switch, other generators will also reach their limits as system loading is varied. Every new combination presents a changed system condition with a distinct PV curve. The most accurate VIP location is tracked in each case. As different generators switch from PV mode to PQ mode, the critical VIP locations travel across the system and the accuracy spectrum changes with every new PV-PQ transition. Figure 9 shows some of the common VIP locations that are most accurate across 100 test cases. It is clear from Figure 9 that there is no single location that is the most accurate across all the test cases. In fact, the most accurate location keeps on changing and moves across the entire system under a changing set of PV-PQ transitions. IEEE-118 bus system has a total of 53 possible VIP locations.

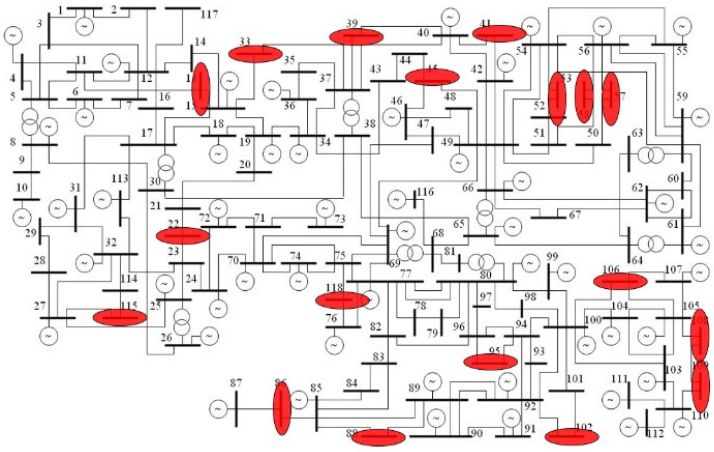

Figure 4.15: Movement of the most critical VIP location

The sensitivity metric is employed for measuring the local sensitivities of the VIP locations and the sensitivity bounds of top 5%, top 10%, top 20%, top 30%, top 40% , top 50% and top 60% are created and the correlation with similar bounds of accuracy is studied. The 5% sensitivity bound includes the top 5% most sensitive VIP locations and so on. As the sensitivity thresholds are increased, thus encapsulating more buses, the corresponding correlation with a similarly increased accuracy threshold is verified. This is important for two reasons. First, increasing the bounds and studying the correlation for each bound would shed light on the optimum size of the sensitivity threshold and second, such an analysis could be helpful in revealing the number of outliers that appear in each threshold.

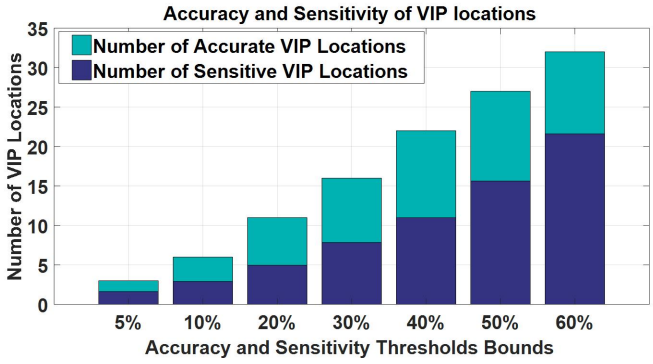

Figure 4.16: Correlation between most accurate VIP location and most sensitive VIP location.

To further illustrate the effectiveness of the sensitivity metric in identifying the more accurate VIP locations, Figures 4.17,4.18, 4.19 and 4.20 plot the margin distribution with and without the sensitivity metric. For the IEEE 39 Bus system a sensitivity bound of 20% is chosen and for the 1354 PEGASE system, a sensitivity bound of 5% is chosen to illustrate the performance of the metric.

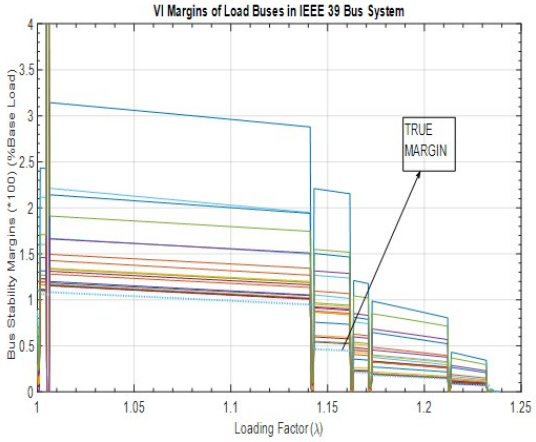

Figure 4.17: All VIP Estimates

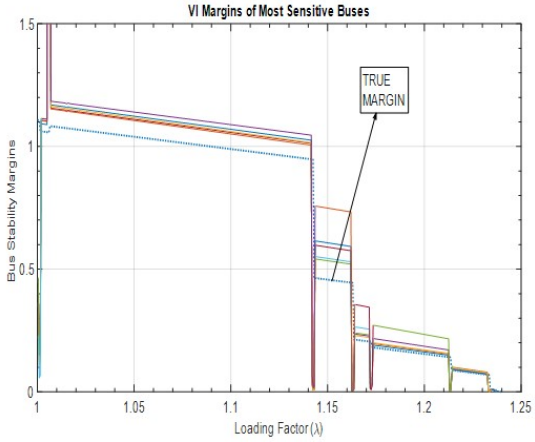

Figure 4.18: Most Sensitive VIP Estimates

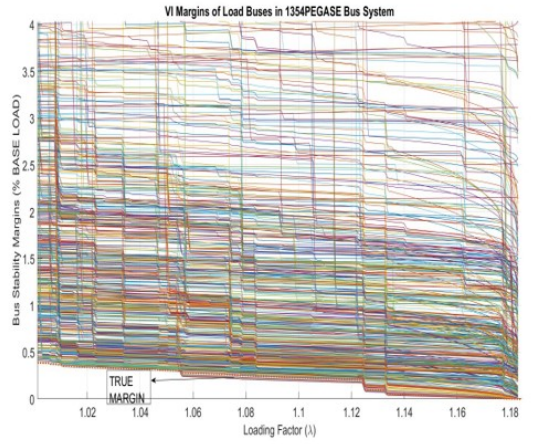

Figure 4.19: All VIP Estimates

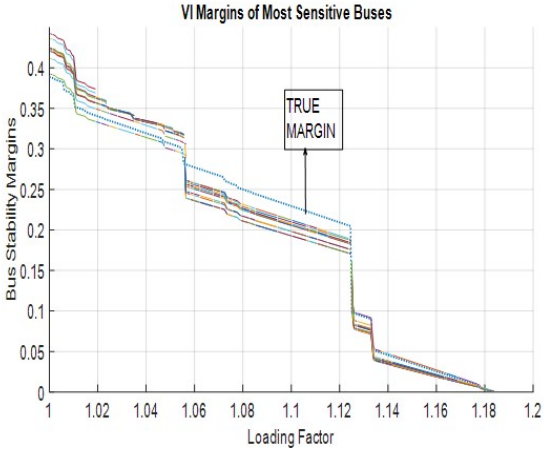

Figure 4.20: Most Sensitive VIP Estimates

The performance of the sensitivity metric has been discussed in this section. The effectiveness of the metric in successfully eliminating the highly inaccurate estimates of the security margin has been demonstrated on a variety of systems. The next logical step is to perform a meaningful fusion or combination of the retained estimates of the security margin in order to

arrive at a singular measure of the system wide margin. The directions and methodology for the data combination will be addressed in the next chapter.

4.5 Generator Sensitivities

In the preceding sections we developed a sensitivity metric in order to identify the most critical loads which turned out to be fairly accurate in replicating the true margin of the system. In this section we will try and develop a similar sensitivity metric for the generators. The generators are the energy sources in any system and play a critical role in maintaining voltage stability. However just like the loads in a system generators vary in their relative importance in maintaining the voltage stability. The sensitivity metric will allow us to map out the most important generators which could be then monitored more closely so as to prevent their outage. The sensitivity metric is defined as

$$K_{QG} = \frac{\triangle Q_{g,i}}{\sum_{j\in[PQ]} \triangle Q_{d,j}} \frac{MVAR}{MVAR} \tag{4.2}$$

Where

$\triangle Q_{g,i}$= Change in reactive output of generator i

$\sum \triangle Q_{d,j}$= Change in the overall system reactive load. PQ is the set of load buses.

As the system is stressed the response of the generators is not uniform. Different generators respond the the new load differently so it becomes necessary to quantify their response by a metric which could be used to gauge their effectiveness in supplying the increased load demand. So in essence the metric used here captures the urgency of the response of generators in maintaining voltage stability. Generator which exhibit a high value of this metric tend to more important and more responsive in maintaining stable voltages than the others. The sensitivities of the generators can be plotted by using equation 4.2 . It is important to note that the data required to calculate the metric is readily available in the control center and no additional

equipment or computational resource is needed to evaluate the sensitivity metric. Figure 4.21 plots the sensitivities of the generators for the New England system.

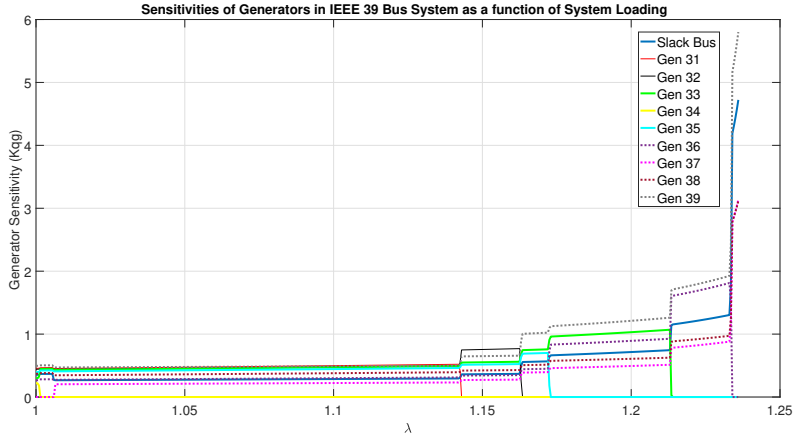

Figure 4.21: Generator Sensitivities of IEEE 39 Bus System

The response of the generators tends to get increasingly nonlinear as the system approaches the collapse point. This is because of the onset of the non linearity close to the collapse. Since the loads are modelled as constant power in transmission system the line currents increase with the system loading which further increases the losses and that leads to more voltage drop. The losses in the system increase in the nonlinear fashion and the reactive output of the generators becomes nonlinear to compensate for the increased losses in the system. Some of the curves can be seen dropping to zero at certain loading levels. These correspond to the individual generators hitting their reactive limit. Figures 4.22 and 4.23 plot the generator sensitivities for IEEE 57 and 118 bus system respectively.

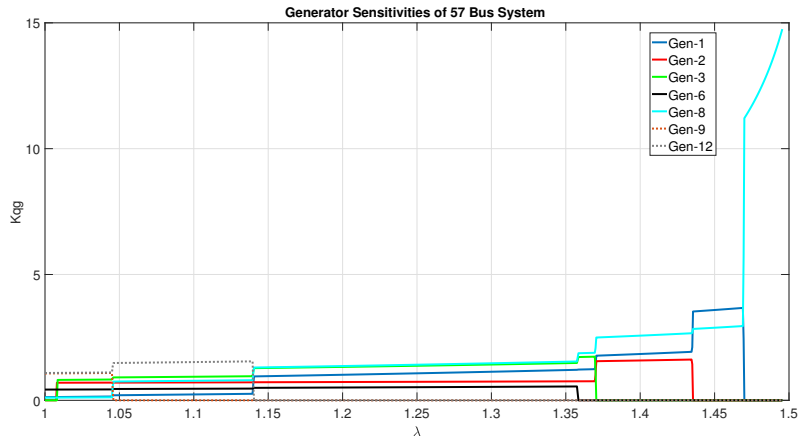

Figure 4.22: Generator Sensitivities of IEEE 57 Bus System

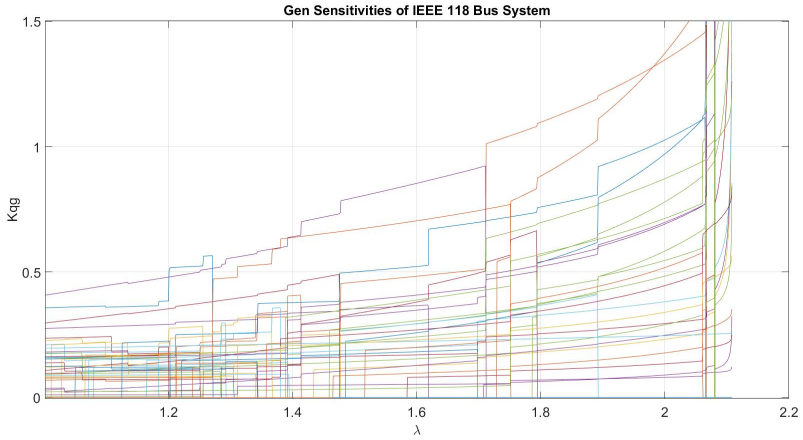

Figure 4.23: Generator Sensitivities of IEEE 118 Bus System

Figure 4.23 has been slightly zoomed in to notice the individual sensitivities. The importance of monitoring the generator sensitivities can be more appreciated by simulating the generator outages and observing its impact on the stability margin and the critical loading level. Figure 4.24 simulates the loss of generators in IEEE 57 Bus System. A random operating point is chosen and in the vicinity of the operating point, generators are ranked in terms of their sensitivity. In the figure the loss of most sensitive, second most sensitive and the least sensitive generator is simulated.

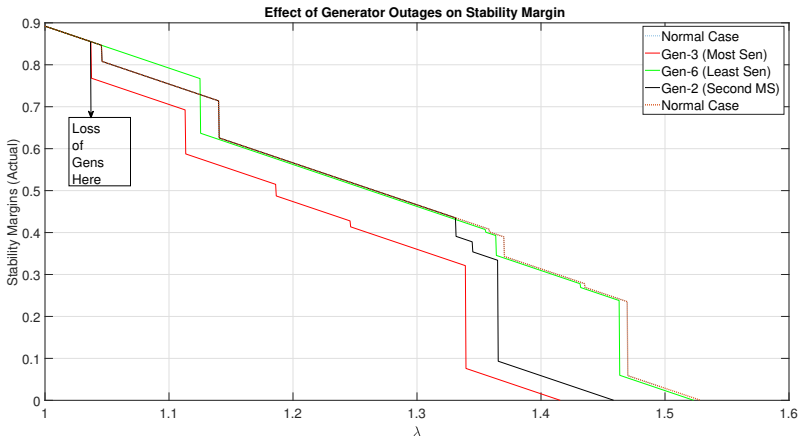

Figure 4.24: Impact of Generator Outages in IEEE 57 System

Generator outages happen at a loading level of 1.035 approximately. The red curve represents the stability margin in the event of the loss of the most sensitive generator, while the black curve represents the stability margin in the event of the loss of the second most sensitive generator. The green curve is the representation of the stability margin when the least sensitive generator is lost. For comparison purposes the stability margin pertaining to the normal case (no generator outages) is also plotted. It can be deduced that the loss of the most sensitive generator has the most damaging impact on the system stability margin, reducing the margin by about 10% and decreasing the critical loading factor by about 13%; 1.415 from 1.528 in the normal case , followed by the second most sensitive generator, reducing the margin by about 5 % and decreasing the critical loading factor to 1.458 from the normal value of 1.528 while the least sensitive generator has a minimal impact on the stability margin. This observation can be further validated more on a larger system like the IEEE 118 Bus system. In figure 4.25 the generator outages are simulated at a loading level of approximately 1.38 and the respective impacts on the system margin are tabulated in 4.6.

Table 4.6: Impact of Generator Outages on the System Margin and Critical Loading Factor

Loss of Gen	Sensitivity Measure (near OP)	Drop in Margin	New CLF	Decrease in CLF
Gen 80	Most Sensitive	≈ 80%	1.832	≈ 13%
Gen 8	Very High Sensitivity	≈ 15%	1.84	≈ 12.5%
Gen 49	High Sensitivity	≈ 35%	1.919	≈ 9%
Gen 59	Moderate Sensitivity	≈ 5%	1.92	≈ 8.8%
Gen 116	Very Low Sensitivity	≈ 0.5%	2.091	≈ 0.85%
Gen 87	Least Sensitive	0	2.1085	≈ 0.02%

CLF: Critical Loading Factor

OP: Operating Point

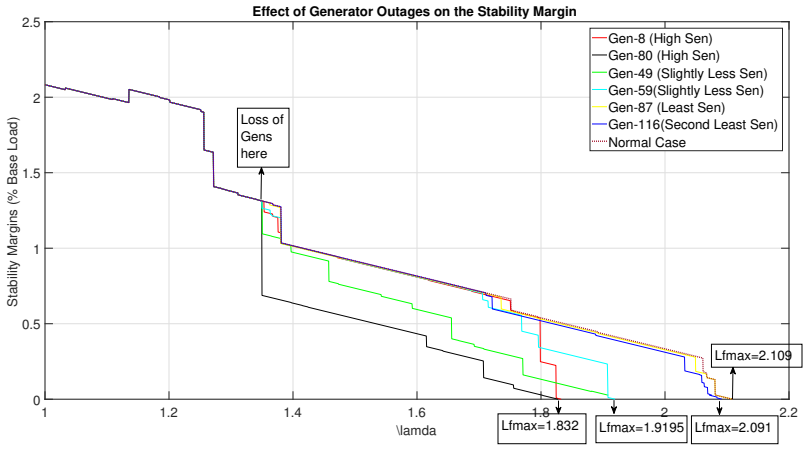

Figure 4.25: Impact of Generator Outages in IEEE 118 System

Figure 4.26 plots the same results for a different operating point, one that is close to the collapse point. In this scenario generator outages happen at a loading level of approximately 1.785.

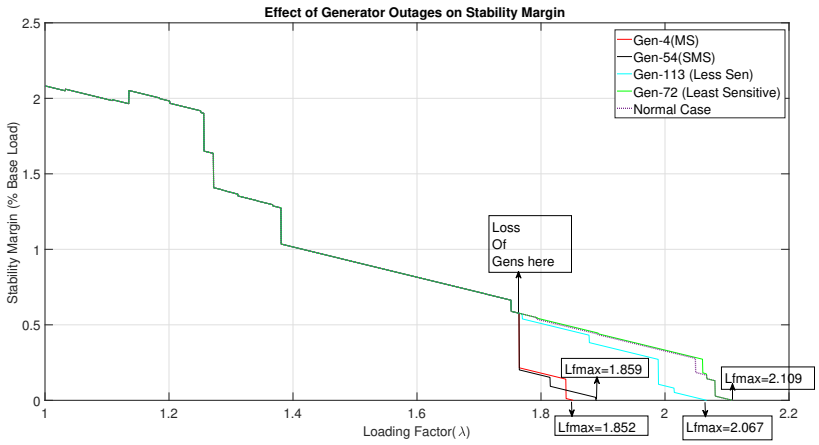

Figure 4.26: Impact of Generator Outages in IEEE 118 System close to collapse

Once again a same pattern is observed with the most sensitive generator causing the most damage to the system margin and the critical loading factor than the less sensitive generators. The outage of Generator 4 causes the system to collapse at a loading factor of 1.852 as opposed to the 2.109 which is the critical loading level in the normal case without any outages. In fact as soon as the generator 4 is lost, the entire system collapses very fast. This can be compared with the outage of generator 72 which has almost no impact on the critical loading factor of the system. This simply means that less power can be transferred with the outage of generator 4 than with the outage of generator 72.

5. DATA COMBINATION

5.1 Introduction

As stated very early in this work the motivation behind characterizing the VIP margins of the system, is to synthesize a more accurate description of the true security margin in the absence of almost all system information. In Chapter 2, VIP margins of a power systems were constructed based on the voltage and current phasors at the load buses. The estimates thus obtained were tested in terms of their accuracy and a certain correlation with the respective sensitivities was established in Chapter 3. It was shown that by monitoring the more sensitive locations in a power system, it is possible to locate the VIP estimates which hover very close to the true system margin. Such available VIP estimates are the subject of investigation for this chapter. It is expected that under the application of some meaningful data combination/fusion process, the resulting the VIP estimates could potentially yield a much more specific and highly accurate description of the true margin of the system. Such a meaningful data combination is realized by making use of Dempster-Shafer Evidential Reasoning.

Dempster-Shafer framework is an alternate to the conventional theory of probability to represent the uncertainty. A mojor departure from the traditional probability theory lies in the fact that the D-S framework allows for the allocation of confidence measure or probability mass to sets or interval rather than just individual hypothesis which precludes any assumption about the individual components of a set. This increases the versatility of the D-S framework, making it more useful at a higher level of abstraction and a good risk assessment tool in engineering applications where precise measurements are not possible or knowledge is obtained from expert elicitation. D-S framework allows for the modelling of conflict in the combination of evidence obtained from different sources.

5.1.1 Dempster-Shafer Evidential Theory

Sensor fusion is an evolving technology that uses multiple data sources in a similar way that humans' cognitive processes make deductions based on observations about the environment [92]. Since information from one sensor might be incomplete or inaccurate, sensor fusion is an attempt to take the advantage of the multiplicity of data. Applications are widespread ranging from medical imaging, target tracking and identification, and robotics [93].

Arthur Dempster introduced the notion of upper and lower probabilities [94]which were then refined and recast by Glen Shafer into a Mathematical Theory of Evidence [95]. In the later years, the Dempster Shafer model witnessed more changes and refinements. One of the key ideas of the DST involves the allocation of belief to the absence of preference. In the DST model the *hypothesis* represents a possible system state or a possible answer to a given problem and the set of all hypothesis (singletons) are contained within the *frame of discernment* Ω. The hypothesis are unique and mutually exclusive. The set of all the subsets of the frame of discernment, 2^{Ω}, may contain a single hypothesis or a conjunction of hypothesis. The individual hypothesis are supported by pieces of evidence which could be system properties or events which lend credence to specific hypothesis or a conjunction of hypothesis. In the DST framework the evidence and the hypothesis share a one to one relationship which prohibits the possibility of having different pieces of evidence in support of one hypothesis. The relationship between the pieces of evidence and the resulting hypothesis is cemented by a statement from the data source.

In the context of our application, the data sources are the VIP points scattered in a power system and the voltage sensitivity measures are the pieces of evidence in support of a particular hypothesis. The frame of discernment contains the retained VIP estimates of the margins which make up the hypothesis. By means of a data source we define a formal mapping of

$$m : 2^{\Omega} \rightarrow [0,1] \tag{5.1}$$

which assigns an evidential weight to $A \subseteq \Omega$. The set A could be a single hypothesis or a conjunction of hypothesis. The function m used to assign evidential weights or confidence measures to a set of hypothesis is referred to as Basic Probability Assignment and must fulfill

$$\sum_{A \subseteq \Omega} m(A) = 1 \tag{5.2}$$

Equation 5.2 normalizes all statements from a single data source in order to ensure that no data source is given unfair preference. And finally it is assumed that

$$m(\emptyset) = 0 \tag{5.3}$$

Equations 5.1,5.2 and 5.3 [96] define the rules that govern the assignment of probability assignments to the hypothesis. An important distinction between the probability distribution function and the basic assignment is that while the probability functions are defined on Ω the basic assignment is defined on 2^{Ω}. The basic assignment is also associated with three additional properties which serve to further distinguish it from the the probability function. For the basic assignment it is not mandatory that

1. $m(\Omega) = 1$

2. $m(A) \leq m(B) if A \subset B$

3. A relationship should exist between $m(A)$ and $m(\neg A)$

From the basic assignment it is possible to construct other evidential functions such a belief and plausability functions. The belief function represents the total belief assigned to a set of hypothesis while the Plausability is the measure of total confidence not assigned to the negation of Belief. [95]

DS theory relies on a BPAs to rate the amount of belief a sensor can contribute to the optimal hypothesis selection. Even if a sensor ascribes low BPA to an observation, the observation can still turn out to be the best hypothesis if the sensor ascribes high BPA to its uncertainty (or if it is outvoted by its peers).

The BPA assigment of set A can be referred to as the probability mass of A and written $m(A)$. It defines a mapping of each set within the power set, $\mathbb{P}$, (the set of all subsets of the range of hypotheses) to a value between 0 and 1. The value that is assigned to $m(A)$ is the support for the evidence of only the set A and *does not include the BPA of any subsets of A*.

For any subset of the power set, the Belief and Plausibility functions define the lower and upper bounds of the probability interval. Indeed these functions were initially referred to by Dempster as the upper and lower probabilities in his seminal work on the topic [94]. This lower bound, Belief (Bel) is defined a the sum of all BPAs of the subsets of some set of interest. If A is the set of interest and B represents its subsets, then

$$Bel(A) = \sum_{B|B \subset A} m(B) \tag{5.4}$$

The upper bound of the probability interval, Plausibility (Pl) is the sum of all BPAs of the sets that intersect the set of interest. Using the same notation, of A and B, Pl can be formally written as

$$Pl(A) = \sum_{B|B \cup A \neq \emptyset} m(B) \tag{5.5}$$

Plausibility can also be defined by the complimentary relationship,

$$Pl(A) = 1 - Bel(\bar{A}) \tag{5.6}$$

5.1.2 Combination of Evidence

The combination rule as put forward by Dempster and later by Shafer allows for the combination of evidence from multiple sources. The combination rule is associative in nature which means that the order of combination of evidence is irrelevant. The output of the combination rule can be used to calculate the Belief and Plausability functions for each hypothesis. The hypothesis with the least interval of uncertainty is accepted as the most plausable explanation for the event in question.

The general form for the combination of evidence from two sensors which assign BPAs m_1 and m_2 onto a set of propositions A and B, respectively. The combined set of evidence, $m_{12}(C)$ is the sum of the product of the BPAs of compatible (intersecting) propositions: $C|A \cap B = C$. The sum is multiplied by a normalizing factor which is calculated from the sum of incompatible proposition fusions which result in BPAs assigigned to the empty set.

$$m-_{12}(C) = K \sum_{A \cap B = C} m_1(A) m_2(B) \tag{5.7}$$

where

$$K = \frac{1}{1 - \sum_{A \cup B = \emptyset} m_1(A) m_1(B)} \tag{5.8}$$

A fusion of evidence example is given in the next section.

5.2 Dempster-Shafer Combination Implementation

Each sensor assigns a BPA to itself and its set of neighbors. Since the BPAs of a set must add up to 1, the leftover BPA is assigned to the union of all sets, θ, which can be interpreted as the

measure of uncertainty.

5.2.1 Four Bus System

In this section we will study the data combination on a simple 4 bus system which consists of two VIP measuring points. The four bus system considered considered for the example is shown in the figure 5.1

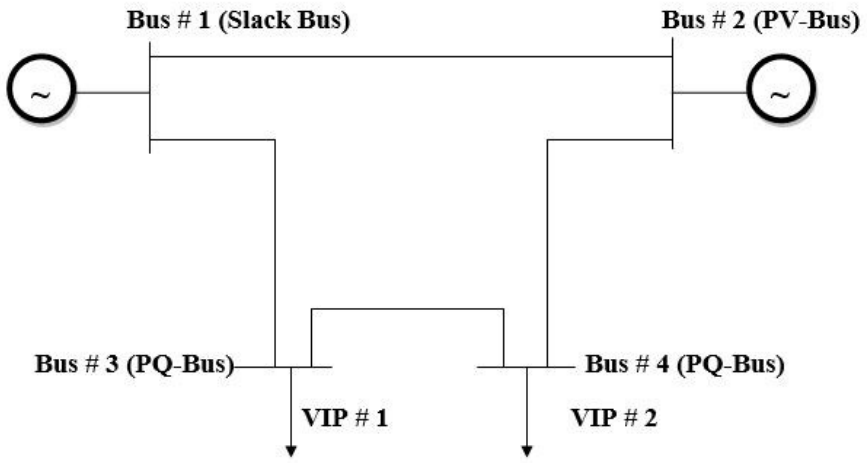

Figure 5.1: A Simple 4 Bus System with two VIP points

The system consists of a slack bus , a PV bus and two PQ buses at which the VIP algorithm can be executed. The final objective is to come up with an accurate description of the system margin to failure by utilizing only the phasor measurements at the PQ buses. By making use of the techniques presented in chapter 2, the VIP security margins are estimated at each loading interval at load buses 3 and 4. This results in a stream of data points as a function of the loading variable. For the purposes of the combination of the VIP margin data, the frame of discernment for the problem needs to be established first. Since we have only two possible VIP points in the system, the frame of discernment would consist of two possible hypothesis for the system

margin.

$$\Omega = M_1, M_2 \tag{5.9}$$

In equation 5.9 M_1 and M_2 refer to the margin to failure as estimated at buses 3 and 4 for a particular loading scenario. The power set of the frame of discernment would be

$$2^{\Omega} = \emptyset, M_1, M_2, M_1 \cup M_2 \tag{5.10}$$

In this example the data sources are the VIP sensors and the hypothesis are estimated margins. Now we have established the frame of discernment and the power set, the next set entails the assignment of basic probability or evidential weights to the subsets of the power set. In this work, BPA assignment is performed on the basis of sensitivity of bus voltage to the change in the local load at the bus. For the purposes of illustration, the BPA measures would be assumed to be some arbitrary number for now. In the later sections, the assignment of basic probability measures would be explored more in some detail. Let A and B represent the set of hypothesis assigned to the VIP data source 1($Bus-3$) and 2$Bus-4$. Table 5.1 lists the statements from the data sources on the set of hypothesis (subsets of the power set).

Table 5.1: Initial probability assignments

VIP Source 1	2^{Ω}	VIP Source-2
$m(A_1) = 0.1$	M_1	$m(B_1) = 0.4$
$m(A_2) = 0.3$	M_2	$m(B_2) = 0.5$
$m(A_3) = 0.6$	$M_1 \cup M_2$	$m(B_3) = 0.1$

By definition, mass assigned to the empty set is zero ($m(\emptyset) = 0$). Table 5.2 illustrates the combination rule. The normalization factor is the one minus the sum of the masses of the hypothesis which product an empty set, i.e the hypothesis which do not intersect.

Table 5.2: Combination of Hypothesis

$\cap$	A_1	A_2	A_3
B_1	M_1	$\emptyset$	M_1
B_2	$\emptyset$	M_2	M_2
B_3	M_1	M_2	$M_1 \cup M_2$

To proceed further we can write for hypothesis M_1

$Z_1 = A_1 \cap B_1 = M_1 = m(A_1).m(B_1) = 0.1 \times 0.4 = 0.04$

$Z_2 = A_1 \cap B_3 = M_1 = m(A_1).m(B_3) = 0.1 \times 0.1 = 0.01$

$Z_3 = A_3 \cap B_1 = M_1 = m(A_3).m(B_1) = 0.6 \times 0.4 = 0.24$

For hypothesis M_2

$Z_4 = A_2 \cap B_2 = M_2 = m(A_2).m(B_2) = 0.3 \times 0.5 = 0.15$

$Z_5 = A_2 \cap B_3 = M_2 = m(A_2).m(B_3) = 0.3 \times 0.1 = 0.03$

$Z_6 = A_3 \cap B_2 = M_2 = m(A_3).m(B_2) = 0.6 \times 0.5 = 0.30$

For hypothesis M_3

$Z_7 = A_3 \cap B_3 = M_1 \cup M_2 = m(A_3).m(B_3) = 0.6 \times 0.1 = 0.06$

The normalizing factor is calculated from the masses of the hypothesis that result in null intersection. The normalizing factor is given by

$$K = 1 - (A_1 \cap B_2 + A_2 \cap B_1) = 1 - (0.05 + 0.12) = 0.83 \tag{5.11}$$

At this point we invoke the Dempster's rule to combine the basic assignments.

$\overline{m}(M_1) = \frac{0.04+0.01+0.24}{0.83} = 0.349$

$\overline{m}(M_2) = \frac{0.15+0.003+0.30}{0.83} = 0.578$

$\overline{m}(M_1 \cup M_2) = \frac{0.06}{0.83} = 0.0722$

This procedure is repeated at every loading factor with a different mass assignment to ob-

tain the fused mass for each hypothesis. The belief and plausibility functions are not calculated since in the context of our work the objective is to combine the individual hypothesis rather than choosing a particular hypothesis or a conjunction of hypothesis as a possible answer. The final combined/fused margin is given by

$$M_F = \sum_j M_j \overline{m}(j) \tag{5.12}$$

In 5.12, $j \in PQ$. set of buses, M_j is the estimated stability margin obtained at bus j while $\overline{m}(j)$ is the combined/fused BPA obtained from the Dempster's Combination rule and M_F is the combined or fused stability margin. In a way, the final result appears to be a weighted sum of individual margins, with weights obtained by combining the initial BPAs in accordance with the Dempster's rule. This process is repeatable and can be performed whenever there is a change in the system loading. A different system loading profile will give rise to a different bus voltage sensitivity profile. As it has been mentioned and will be seen in more detail in the next chapter, the voltage sensitivity profile of the loads can be construed as a measure of the accuracy of individual bus margins. This enables the transformation of the sensitivity values to probability assignments, necessary to initiate the fusion process.

In this example the power set has a small cardinality, since the test system has only two VIP locations. In large systems, however with a large number of VIP locations the cardinality of the power set can grow exponentially to staggering numbers. In addition to the large cardinality of the power set, such systems also bring the problem of allocation of BPAs to a conjunction of hypothesis. Such BPA allocation could be impossible in systems with thousands of VIP locations. Therefore in order to reduce the level of complexity in large systems at the cost of a less robust implementation, some modifications are made to the Dempster Shafer model.

1. Each data source (VIP sensor), assigns a BPA measure to its estimate while assuming absolute ignorance about other VIP estimates.

2. The BPA measures assigned to a conjunction of the hypothesis (e.g, $M_1 \cup M_2$) is zero.

These modification significantly reduce the level of complexity encountered in large test systems. Although, these changes have an impact on the robustness of the algorithm, but as will be seen in later chapters, the effect on the accuracy of the algorithm is not significant.

6.1 Mapping of voltage sensitivities to BPA assignment

[1] In this section, we will try to look at the transformation of the bus voltage sensitivity values which are obtained by monitoring the changes in the bus voltage magnitude as a function of the local load. It is possible the predicate the assignment of BPAs on some other easily measurable property, provided the property chosen shows a highly meaningful correlation with the accuracy of the stability margin. The assignment of the BPAs in Dempster Shafer theory is left open ended. The primary goal is to able to reflect as accurately as possible the accuracy of the individual hypothesis. To that end, any mathematical function which captures accurately the physical response of the individual sensors is acceptable. For the purposes of this work, the mapping of the voltage sensitivities to their corresponding BPA measures is done by making use of 6.1

$$m_{(VIP-n)\lambda_k} = \frac{K_{\lambda_k}}{K_{\lambda_k} + a_{\lambda_k}}; a_{\lambda_k} > 0, \forall \lambda_k \tag{6.1}$$

In 6.1, $m_{(VIP-n)\lambda_k}$ refers to the BPA assignment value to the n^{th} VIP estimate at a loading factor of λ_k, K_{λ_k} is the local bus voltage sensitivity magnitude of the n^{th} VIP estimate at a loading factor of λ_k and a_{λ_k} is the scaling factor or the tuning factor. This factor can be adjusted to better map the accuracy profile of the VIP distribution in to the corresponding weights or BPAs. The choice of the function used in 6.1 is irrelevant as long as it satisfies the conditions 5.1, 5.2 and 5.3 laid out in Chapter 4. Equation 6.1 is chosen as such for its simplicity in implementation and the ease that it offers in adjusting the BPA values in accordance with the estimated values of the VIP margins.

[1] Part of the data reported in this chapter is reprinted with permission from "Locational Accuracy of VIP Indices for Voltage Collapse Margin Estimation-Begovic, Miroslav, et al. (2018)-Proceedings of the 51st Hawaii International Conference on System Sciences| 2018"

Several inferences can be made for the scaling factor a_{λ_k}. In order to have a meaningful mapping of the sensitivity values to the BPA assignment, it can be deduced that

1. The scaling factor should be positive for every loading factor. This property would satisfy 5.1 thus ensuring $m_{(VIP-n)\lambda_k} \in (0,1)$.

2. In a chosen set of VIP locations which are retained for fusion, the mass or the BPA ascribed to the least sensitive VIP location should be the lowest. Conversely the BPA assigned to the most sensitive VIP location in a chosen set of VIPs should be the highest. In other words, for the least sensitive bus, $a_{\lambda_k} > K_{(min),\lambda_k}$, where, $K_{(min),\lambda_k}$ is the sensitivity value of the least sensitive VIP location. Similarly for the most sensitive VIP location, $a_{\lambda_k} < K_{(max),\lambda_k}$. The values of the scaling factors for all the other potential candidates will fall in between automatically.

For these reasons, the value of the scaling factor is chosen to be

$$a_{\lambda_k} = |K_{(max),\lambda_k} - K_{(min),\lambda_k}| \tag{6.2}$$

In 6.2, $K_{(max),\lambda_k}$ and $K_{(min),\lambda_k}$ refer to the bus voltage sensitivity magnitudes of the most sensitive VIP location and the least sensitive VIP location of the chosen set of VIP locations at the loading factor λ_k. It is interesting to note that the scaling factor is a function of the loading factor λ_k and varies as the system loading profile changes. Such a definition of the scaling factor ensures the right assignment of the BPA measures which properly reflect the corresponding the bus voltage sensitivity magnitudes. Such an assignment has been worked out on a number of test systems and the results have been found consistent with what one should expect. As an example Figures 6.1 and 6.2 show the mapping of the sensitivity values to the corresponding BPA assignment for IEEE 9 Bus System at base load.

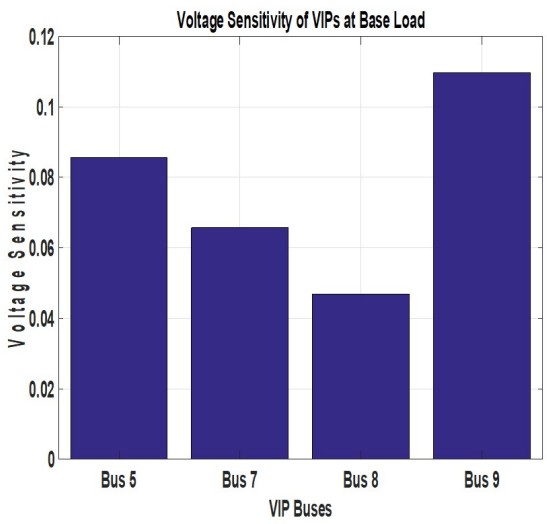

Figure 6.1: Voltage Sensitivity at Base Load

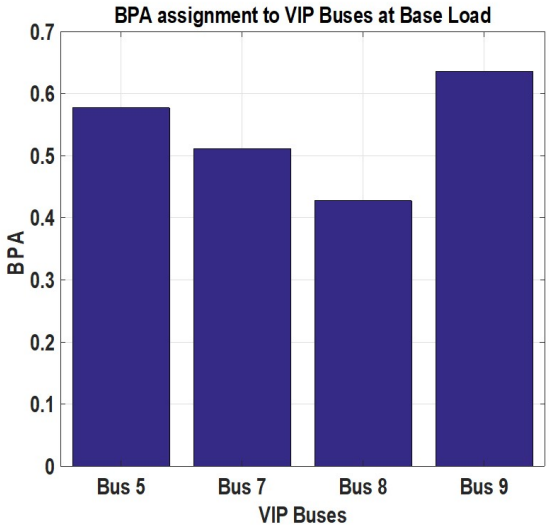

Figure 6.2: BPA assignment at Base Load

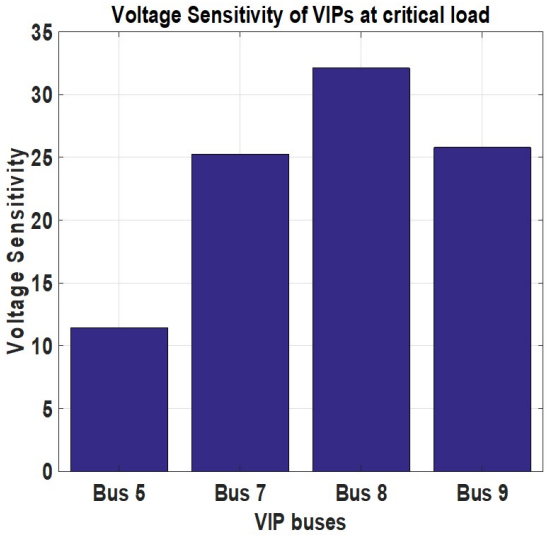

Figure 6.3: Voltage Sensitivity at Critical Load

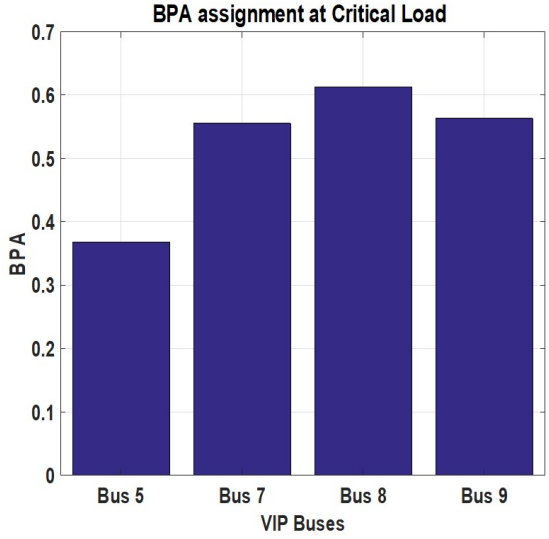

Figure 6.4: BPA assignment at Critical Load

Figures 6.3 and 6.4 serve to illustrate the same mapping when the system is sufficiently close to the collapse. This represents a highly stressed system condition and the mapping of the sensitivity values is rendered accurately in terms of the BPAs assignment to the individual VIP locations.

As mentioned earlier, the process of BPA assignment can be done as a function of the system loading factor. Equation 6.1 expresses the loading factor dependence of the BPAs. Since

the BPAs assigned are expressed in terms of the bus voltage sensitivities, which are itself the function of the total bus load, the resulting weight measures also share a relationship with the changing load profile. This quality is important as it enables the calculation of the overall system margin at every loading step. Figure 6.5 illustrates the relationship of the assigned BPAs and the system loading as tested on the IEEE 9 bus system.

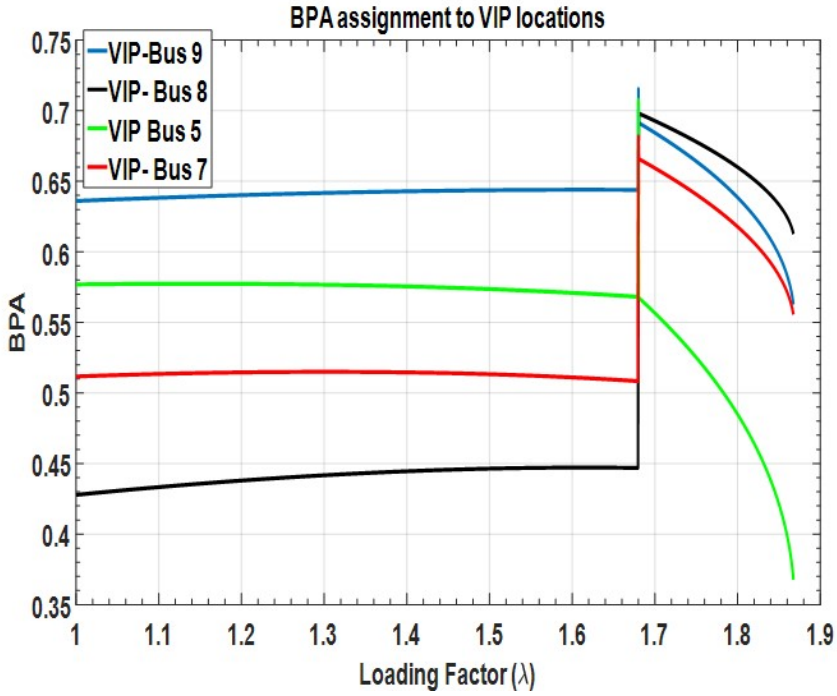

Figure 6.5: BPA assignment as a function of Loading Factor

6.2 Results of VIP data Combination

In the previous chapter, an example was presented on the application of the Dempster Combination rule on a system with two VIP measuring locations. Although in the said example, the BPAs assigned to the VIP margins were arbitrary, the fundamental principle of combining the individual BPAs or weights remains the same. In case of stressed power systems, the only changing variable in the fusion process is the BPA itself. In section 5.1, the calculation of the BPA under a changing system loading has been shown.

The principles laid out in the preceding chapters are now put to use. A wide variety of test

systems are used to illustrate the estimation of the VIP margins as per the methods outlines in Chapter 2. Such distributions of the VIP margins are then subjected to the sensitivity tests to filter out the most accurate margins. The most accurate VIP margins thus obtained are used as the input to the data combination algorithm in order to obtain the fused or updated weights (also read BPAs). A weighted average of the remaining margins is then taken to yield the over all system security margin. Taking the IEEE 9 bus system as an example, figures 6.6 and 6.7 plot the VIP margin distribution from base load to the critical loading of the system and the overall fused margin of the system respectively. To aid in comparison, the system true margin obtained by running repeated load flow program is also plotted in both figures.

The true system margin represents the actual security margin left in terms of percentage of the base load. This work is predicated on the assumption that the driving force of the instability is the long term load restoration mechanism by constant power loads. As such, this work is focused on the small disturbance (in the form of uniform load increase) longer term voltage stability where the maximum power deliverable is limited by the action of over excitation limiters (OELs). In this context, the true security margin of the system is evaluated by running a series of load flow programs while enforcing the generator reactive limits. As the system load is gradually increased, the critical loading factor of the system is evaluated every time a generator reaches its respective limit. The true margin can be trivially derived after the critical loading factor is known.

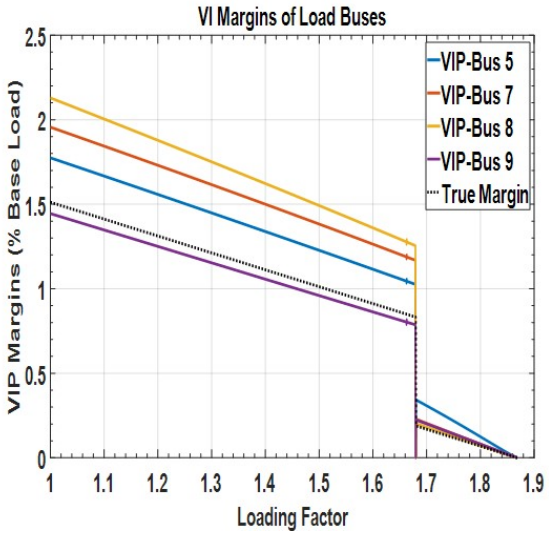

Figure 6.6: VIP margin distribution

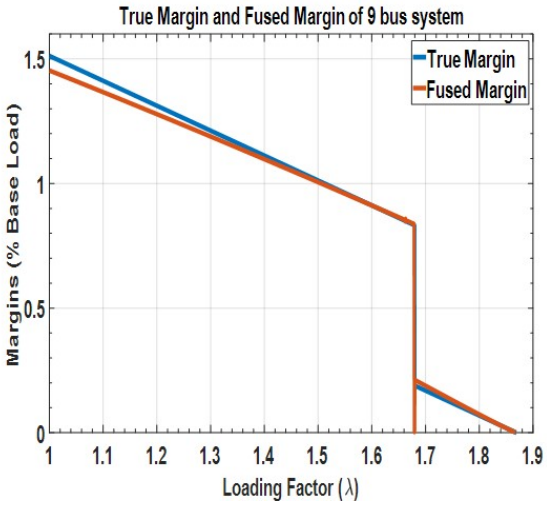

Figure 6.7: Overall combined system margin

The increased accuracy of the combined margin is evident. The VIP margins are evaluated by using a quadratic forecast of the voltage and current phasors which are then subjected to the data fusion algorithm to yield the overall system margin as shown in figure 6.7. The sensitivity factor is not invoked here because of the scarcity of the available VIP measuring locations. However, in large systems it is imperative make use of the VIP sensitivities in order to isolate the more accurate ones than less accurate ones. At this point it would be interesting to observes the effect of the wrong BPA assignment to the VIP estimates. The *"wrong"* BPA assignment refers to the incorrect assignment of the weights to the problem hypothesis. As mentioned before, based on the correlation between the accuracy of the VIP estimate and the corresponding VIP sensitivity, it is expected that a more sensitive VIP location must also be more accurate in its representation of the overall system margin. This fact has been used in the assignment of the BPAs to the VIP locations. More precisely, the BPAs have been assigned in the decreasing order of the voltage sensitivities, which means that the VIP location with the highest sensitivity has been assigned the highest BPA and so on. If the assignment order is reversed such that the lowest VIP location is assigned the highest BPA, it is seen that such an assignment scheme actually causes an increased error in the overall system margin and the true margin. Figure 6.8 plots the overall systemn fused margin when the BPA assignment is reversed.

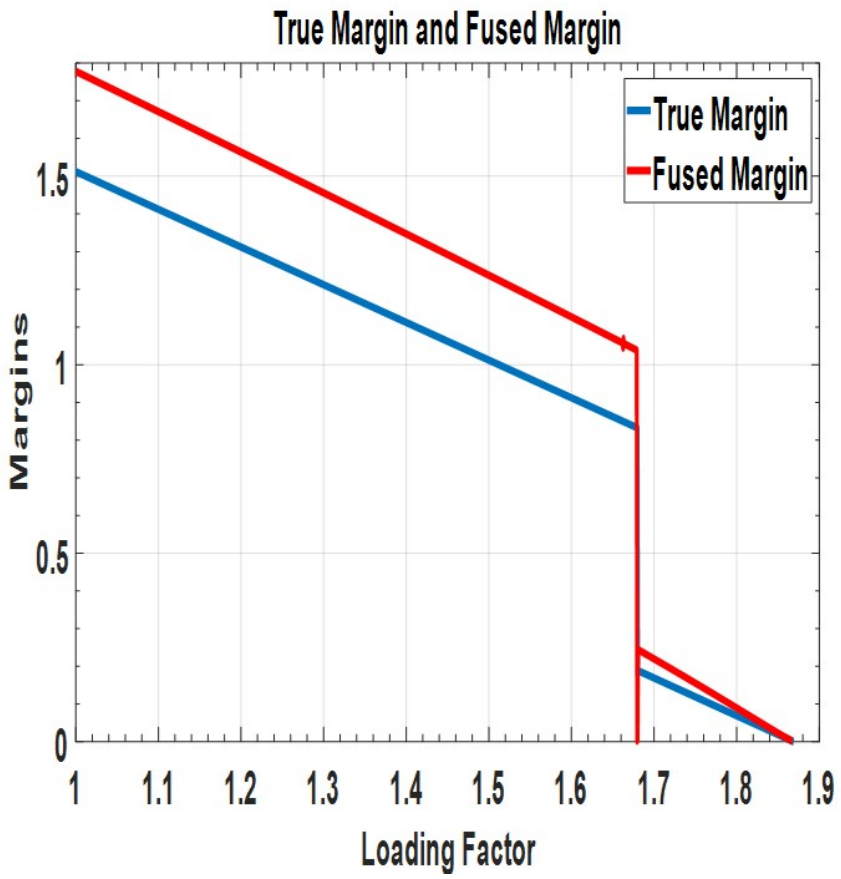

Figure 6.8: Overall System Margin with reversed BPA assignment

Table 6.1 lists the information content in the final fused margin of figure 6.7.

Table 6.1: Information content of Final Fused Margin of IEEE 9 bus system

VIP	Percentage in Final Fused Margin
Bus 8	≈ 28 %
Bus 9	≈ 22 %
Bus 7	≈ 21 %
Bus 5	≈ 10 %

As mentioned before, the scaling to large systems can't be done unless the VIP margin distributions are scrutinized for accuracy. In chapter 3, the effectiveness of the sensitivity factor was illustrated by creating roughly 100 test cases, each with a unique signature of the PV-PQ transitions. In this section, that experiment is taken a step further and the effectiveness of the fusion algorithm is illustrated on those test cases. More specifically, different sensitivity bounds

are created and the VIP locations in such chosen bounds are selected for data combination. The results of different bounds are then compared. In other words, this experiment effectively tries to measure the reduction of the envelope of error as observed in the raw VIP margin distributions, filtered VIP margin distribution and the final overall fused margin.

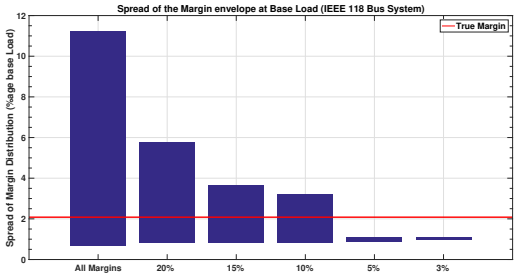

Figure 6.9: Base Load

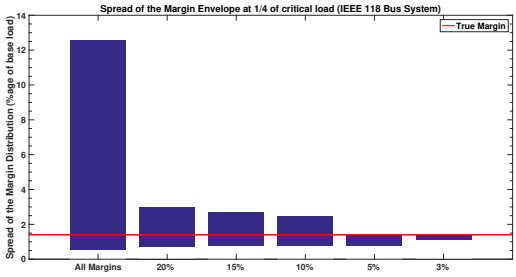

Figure 6.10: $\frac{1}{4}\lambda_{crit}$

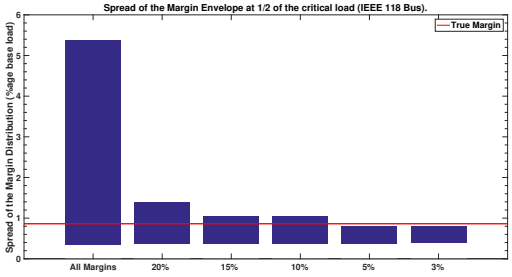

Figure 6.11: $\frac{1}{2}\lambda_{crit}$

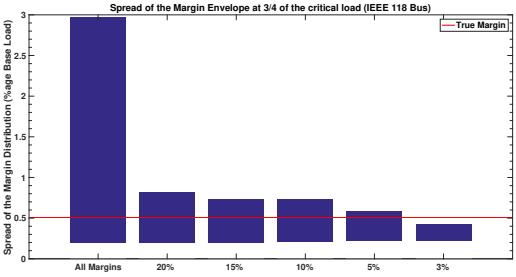

Figure 6.12: $\frac{3}{4}\lambda_{crit}$

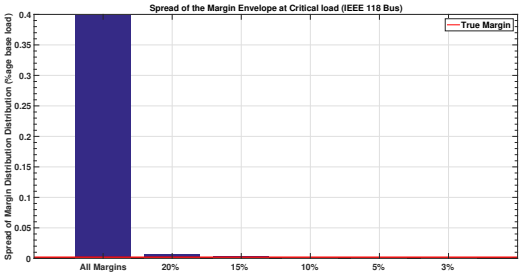

Figure 6.13: λ_{crit}

At this point, it is important to consider the utility of the sensitivity factor and also establish a reasonable sensitivity bound on the number of VIP locations that must be closely monitored to yield the closest representation of the true security margin of the system. Figures 6.9,

6.10,6.11,6.12 and 6.13 essentially try to answer the question," How many VIP locations must be considered for data fusion"?. These figures plot the spread of the margin distribution at various chosen loading scenarios. In the figures, λ_{crit} refers to the critical loading factor of the system. It is clear that by monitoring the sensitivities of the VIP locations, a significant reduction in the spread of the margins is possible, and hence by extension in the error of VIP margins.In figure 6.9, when the entire VIP distribution is taken into account, it can be seen that the values range from approximately 0.65 to roughly 11.5, where as the true margin of the system sits at around 2.08. If instead of the entire VIP distribution, only top 20 % of the VIPs are monitored, it is clear the spread in this case ranges from 0.81 to 5.76 times the base load. Similarly as the sensitivity bound is made smaller (or more strict), more reduction in the error of VIP margins is possible.However, it can be noticed that very small sensitivity bounds, like top 3 % or the top 5%, do not encapsulate the true margin of the system at base load.

Choosing such bounds may lead to a very tight spread of the VIP margins but at the same time might also lead to increased errors. For this reason, there exists a trade off between the size of the sensitivity bound and the value of the true margin. Since the data fusion algorithm essentially works as a weighted average of the individual VIP margins, with the weights being updated by Dempster's Combination rule, it becomes necessary that the selected sensitivity bound should contain the true margin of the system. Further, as the system is stressed, the VIP margins tend to get more accurate and are squished together, which explains the reduction in the spread of VIP margins at higher loading. It is clear from figure 6.12, that the true margin is contained in every sensitivity bound, except the 3% bound. Since the 5% bound results in the tightest spread around the true margin, this bound should be chosen for data fusion at this system loading. Based on all the data, it is reasonable to suggest that a 5% to 10% sensitivity bound should result in the least error in the final fused margin. Again in continuation to the experiment that was carried out in Chapter 3, the actions of the over-excitation limiters on the generators are manually altered to create different cases each with a unique set of such transitions. The results of the these experiments are presented in figures 6.14, 6.15 and 6.16.

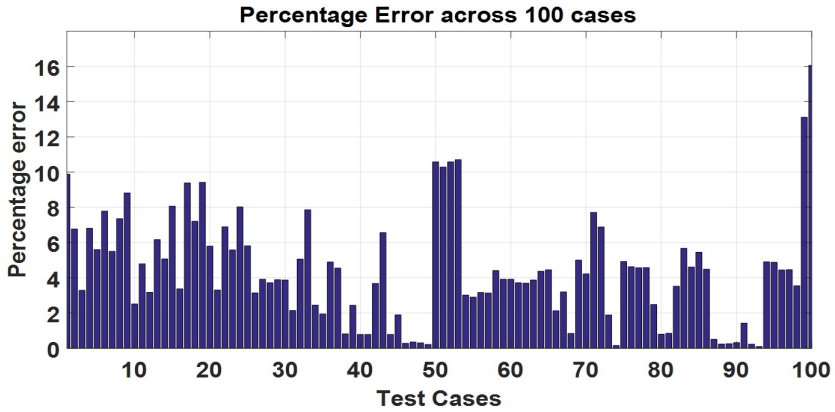

Figure 6.14: Error between True Margin and Fused Margin with 5% sensitivity bound

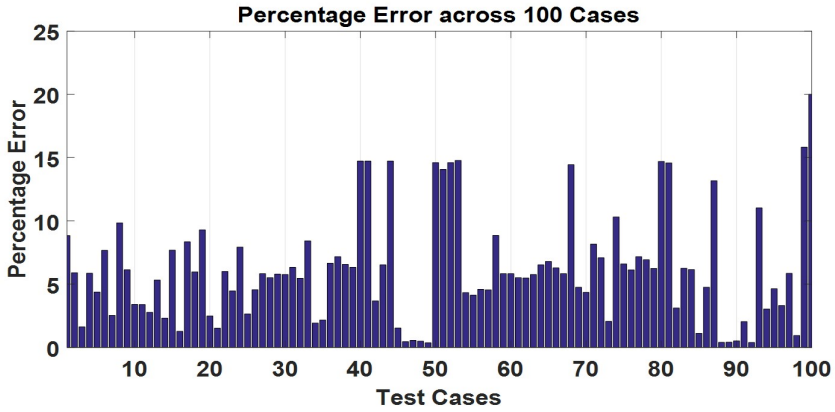

Figure 6.15: Error between True Margin and Fused Margin with 10% sensitivity bound

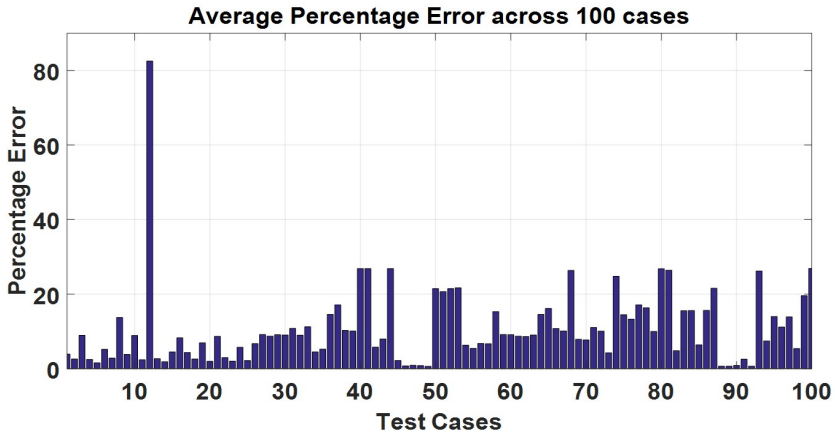

Figure 6.16: Error between True Margin and Fused Margin with 20% sensitivity bound

Figures 6.14,6.15 and 6.16 essentially try to demonstrate the spread of the errors between the true margin and the final fused margin of the system, while considering various sensitivity

bounds. The errors presented for each test case are representative of the system state when the margin has dropped below 30%. It is clear that increasing the sensitivity bound leads to the accumulation of more errors as can be seen from 6.16, while a 5% sensitivity bounds leads to the minimum error which is consistent with the previous results in figure 6.12, where it was seen that a 5% sensitivity bound is the most efficient bound at this system loading. In view of these results, it can argued that as the system is progressively stressed, a 5% sensitivity bound on the VIPs works best close to the critical loading and a 10%b bound seems more efficient towards the base load. Of course, this arrangement depends on the method used to estimate the VIP margins. In this method, the VIP margins are estimated by extrapolating the Thevenin Parameters ($\overline{E}_{Th}, \overline{Z}_{Th}$), in order to estimate the maximum deliverable power. If a quadratic curve fitting method were to be used, it is expected that the results might turn out to be slightly different. That will be considered in a future work. Figure 6.17 plots the averaged out error for the 100 test cases for each sensitivity bound.

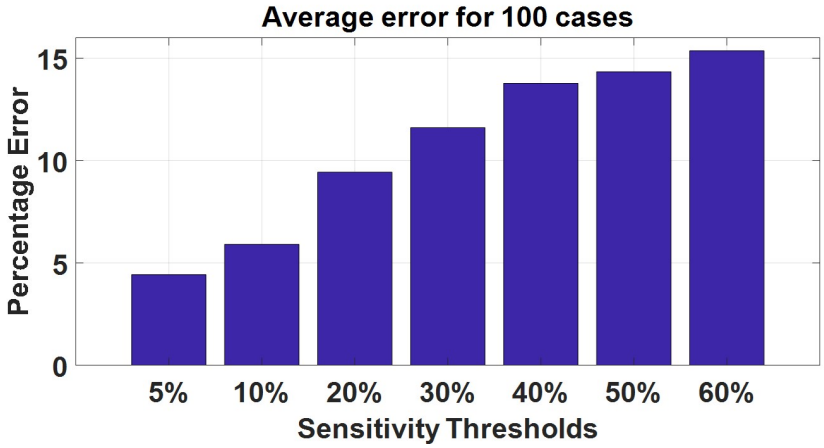

Figure 6.17: Average Error across 100 cases for different sensitivity thresholds

Based on Figure 6.17, it could be said that during highly stressed conditions if the VIP margins of the top 5% load buses are monitored and considered for data fusion, that would bring our estimate closer to within 5% of the actual system margin. This is very encouraging considering the fact that this analysis is performed in the absence of almost all system information. For illustration purposes, figures 6.18, 6.19,6.20 and 6.21, plot the true margin and the fused mar-

gin of IEEE 39 Bus System, IEEE 118 Bus System, 1354 PEGASE system and 2869 bus PEGASE system.

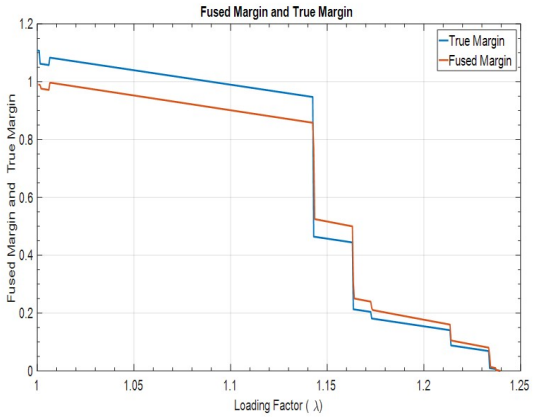

Figure 6.18: IEEE 39 Bus System

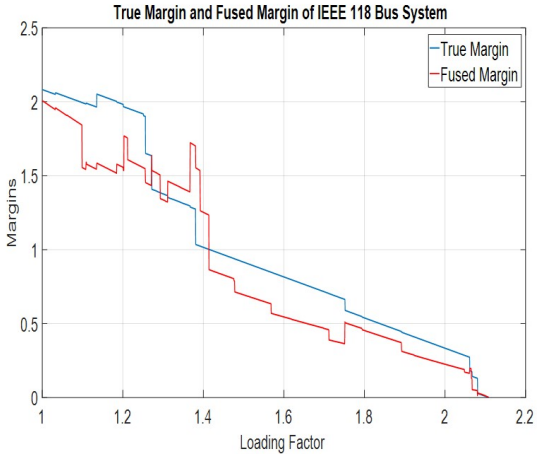

Figure 6.19: IEEE 118 Bus System

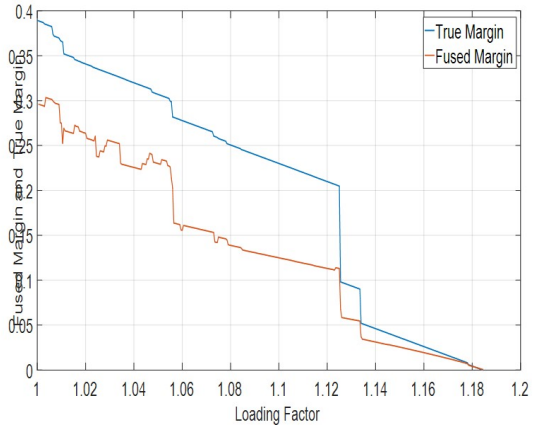

Figure 6.20: 1354 PEGASE System

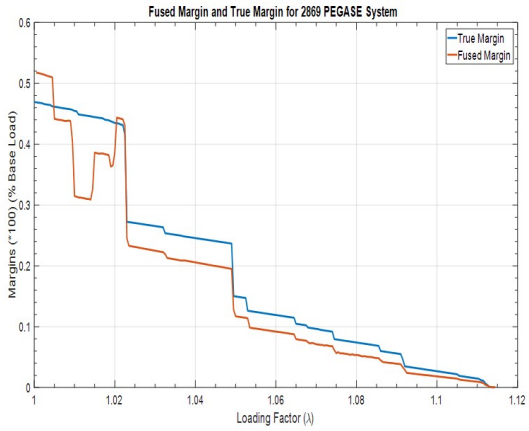

Figure 6.21: 2869 PEGASE System

The VIP margins used for data combination in these figures were derived from the S_{max} method based on the estimation of $\overline{E}_{Th}$ and $\overline{Z}_{Th}$, and the sensitivity thresholds chosen for illustration are 10%, 10%, 5% and 1% respectively.

7. SUMMARY AND CONCLUSIONS

The phenomenon of voltage collapse in electric power systems has received a considerable amount of attention in the last decade. Both steady state and dynamic behavior have been studied, although very few protection and control schemes have been implemented. The ultimate objective of this research project is to further investigate the voltage collapse phenomenon in the longer term under the influence of small disturbances and develop protection and control schemes for mitigating such undesirable events in modern electric grids. In doing so, the research work in this project builds on an earlier work in the area of Voltage Instability Prediction (VIP) for monitoring the proximity of a large power grid to a possible voltage collapse scenario. Voltage collapse, and hence an electric blackout, is a response of the electric grid to the violations of several constraints that limit a large scale power grid's ability to transfer electric energy from the source to the consumers. A voltage collapse is characterized by the slow decline of the bus voltages across a network up until a certain threshold before falling off precipitously. A famous example of an electric blackout or a power outage that happened in the last decade is the Northeast blackout of 2003 which affected an estimated total of 55 million people in the Northeastern and Midwestern United States and parts of Ontario on August 14, 2003. As a result of a computer bug in the General Electric's Unix based Energy management system the control alarms which monitor the status of power flow along transmission lines were stalled for more than an hour. The failure to redistribute the power flow resulted in the overloaded transmission lines hitting the unpruned foliage thus triggering a race condition. This led to a cascading event with the decline of the bus voltages in the northeastern grid, culminating in a massive blackout. In addition to the economic losses the blackout also contributed to almost 100 deaths.

7.1 Conclusions

The work done in this research aims to estimate the proximity of a large power grid to such a possible voltage collapse event in real time and in the absence of almost all system information. In doing so the algorithm trades the speed and resilience of using the local measurements for the complexity of calculating accurately the stability margins of large nonlinear systems. A stability margin is a measure of closeness to a possible voltage collapse event and the VIP algorithm estimates this margin by measuring only the voltage and current phasors at a load bus. Such a measure of margin evaluated at a single node in a power network is not necessarily the true representation of the actual system margin because of the heuristic nature of the algorithm. However, since a given power network encompasses a large of number such nodes, the VIP algorithm can be executed at each such node and a measure of system margin is obtained. Since the method relies only on the local measurements, thus bypassing all the immense complexities involved in estimating the bifurcations in large nonlinear systems, such multiplicity of data turns out to be an asset which if exploited in a meaningful manner can reveal a lot of information about the system state.

The primary objective of this work is to address the glaring disparity found in VIP-derived stability margins and to provide a platform that would allow the consolidation of such disparate measures of the system margin. At the same time it is desired that any such method need not necessarily add more complexity to the basic VIP algorithm while also attempt to bridge the gap between the true security margin and the resulting estimate of the same margin. As has been mentioned before this work focuses on the small disturbance, long term voltage stability issue, where the disturbance is simulated by gradual and uniform load increase and the driving mechanism of instability is the load power restoration by constant power loads while the maximum power that the transmission system can deliver is limited by the action of Over Excitation Limiters.

To accomplish this task, several methods were explored with varying degrees of accuracy and complexity. Some ideas like the 'Bus Voltage Coherency (elaborated more in the Appendix) need to be investigated further. Based on the preliminary studies this method has shown potential and could provide an interesting solution to the problem at hand. Furthermore, the use of super-bus analysis could further enhance the capabilities of the coherency technique. In addition to tackling the dimensionality problems in large systems, such a technique, could in principle lead to robust estimation of the system margin. However, the amount of complexity that such a method can possibly bring to the equation remains to be investigated. This work, however focuses more on the method of the local sensitivity measures, explored in detail in Chapter 3, which enables the characterization of the VIP derived security margins. The method of local sensitivity measures relies on the local bus voltage phasors and the local load growth pattern at a bus, quantities which are readily available and don't require any specialized equipment or an algorithm to extract. In chapter 3, the clustering of the most sensitive VIP locations around the true security margin was demonstrated on a number of test systems. The effect of generator switching and line outages on the VIP margin distribution was studied in Chapter 3. For the IEEE 118 bus system a vast number of test cases were created by allowing different generators to switch from PV-PQ and the robustness of the algorithm was tested. The results presented in the chapter 3 for the IEEE 118 bus indicate that given any random system condition the probability of identifying most accurate buses in critical regions is always more than 80%. More emphasis has been give to the critical regions (A region defines a range of loading factors), which are close to the collapse point as it is there that we want to identify the closest buses, the most. Similar results were obtained for large systems like the IEEE 300 Bus, 1354 PEGASE and the 2869 PEGASE Systems.

Such characterization of the VIP derived margins, however, relies heavily on the accuracy of the estimated Thevenin parameters. In this work, the parameters of the Thevenin model are evaluated based on the sampling of two measurements sets of voltage and the current phasors at two different yet closely spaced loading (or, time) events. This method, although very sim-

ple to implement and quite robust for small systems, does introduce errors in the estimation of the Thevenin Equivalent. The fundamental flaw in this method lies in the inclusion of all other loads, which can be nonlinear and dynamic, in to a system equivalence with the implicit assumption that the system equivalence stays constant between two sets of measurement samples. A lot of research work has gone in to the estimation of the Thevein model parameters but each method comes with an increased cost of computation. It would be germane to add here that a more robust estimation of the Thevenin Equivalent will invariably improve the precision and the efficiency of the sensitivity factor to distinguish the more accurate VIP margins from the less accurate estimates.

The fusion/combination of individual VIP estimates has been realized using Dempster Shafer evidential reasoning. Chapter 4 elucidates some of the fundamentals of the theory. A simple example of a 4 bus system with 2 VIP locations is presented.The results of the data combination are presented in the final chapter.In theory, the Dempster Shafer model could be implemented in a variety of ways with varied levels of complexity. In this work, the implementation of DS fusion is kept very simple to prevent any elaborate changes in the present infrastructure. In the current implementation, each sensor assigns a confidence measure to its own estimate and has no opinion on the estimates of other buses. This way no further communication is required between the sensors to be able to assign the BPA measures. It is also possible to lean towards different statistical methods of fusion, particularly the Least Median of Squares. LMS has been known to be quite robust to the presence of bad data with a breakdown value of 50%. Other potential of methods of data fusion will be explored in future and in conjunction with the super-bus analysis more progress is possible.

Tables 7.1 and 7.2 summarize the results obtained with different IEEE test cases using estimated Thevenin parameters method as well as the quadratic forecast of V-I characteristics of a load bus. Although in effect, both the methods, i.e one which makes explicit use of estimated Thevenin Parameters and the other based on the forecast of V-I characteristics, are based on the approximating the system via a system equivalence, the method based on V-I curve fitting

precludes the estimation of the changing system parameters which explain its higher accuracy in many cases. A definitive argument on the accuracy of algorithms is difficult to make because of the inherent inaccuracies associated with the VIP modelling and considering the fact that the entire analysis is done in the absence of almost all system information. The performance of the algorithm as tested on a wide a variety of systems and under different conditions has proven to be quite robust. The ability to continuously track the most accurate locations in a large power network in real-time without resorting to full system analysis can prove to be very helpful in triggering a wide variety of emergency controls. The simplicity and the ease of implementation of this algorithm make it a very attractive candidate for further research.

Table 7.1: Margin Estimation based on Thevenin Parameters

Test System	Sensitivity Bound Chosen	Percentage Error close to Collapse (Margin<= 30%)
9 Bus	100%	6.5
39 Bus	25%	2.142
118 Bus	15%	6.65
300 Bus	5%	3.28
1354 PEGASE	2%	6.4
2869 PEGASE	<1%	2.6331

Table 7.2: Margin Estimation based on Quadratic Forecast of V-I Characteristics

Test System	Most Sensitive Buses	Percentage Error close to Collapse (Margin<= 30%)
9 Bus	100%	0.8953
39 Bus	25%	1.454
118 Bus	15%	2.422
300 Bus	5%	4.364
1354 PEGASE	2%	1.2
2869 PEGASE	<1%	1.52

7.2 Further Study

While a number of aspects of the VIP-derived margins have been demystified in this work, there still persist some unanswered questions about the versatility of such margins. Of particular significance is the performance of VIP margins under conditions of uneven system loading and

under different equipment outages. There is also a need to extend this work under the operation of load tap changer devices, the action of which is a driving force for long term voltage instability.

The Demspter-Shafer data fusion method presents some intensive computational challenges, many of which have been combated by making use of some simplifying assumptions. However, at the same time the use of such assumptions impacts the robustness of the fusion algorithm. To overcome some of the computational challenges of the D-S framework, it is essential to explore several other compatible data fusion methods. Some statistical estimation methods, like the Least Median of Squares, does seem to hold promise and could offer a consolidation platform with probably higher accuracy and less computational effort. The search for a better and a more robust data fusion algorithm will be considered in future.

Bibliography

[1] K. T. Vu, D. E. Julian, J. O. Gjerde, and M. M. Saha, "Applications and methods for voltage instability predictor (vip)," Jun. 19 2001, uS Patent 6,249,719.

[2] M. M. Begovic and A. G. Phadke, "Voltage stability assessment through measurement of a reduced state vector," *IEEE transactions on power systems*, vol. 5, no. 1, pp. 198–203, 1990.

[3] C. Bai, M. Begovic, R. Nuqui, D. Sobajic, and Y. Song, "On voltage stability monitoring with voltage instability predictors," in *2013 IREP Symposium Bulk Power System Dynamics and Control-IX Optimization, Security and Control of the Emerging Power Grid*, 2013.

[4] V. Venikov, V. Stroev, V. I. Idelchick, and V. Tarasov, "Estimation of electrical power system steady-state stability in load flow calculations," *IEEE Transactions on Power Apparatus and Systems*, vol. 94, no. 3, pp. 1034–1041, 1975.

[5] P. A. Lof, T. Smed, G. Andersson, and D. J. Hill, "Fast calculation of a voltage stability index," *IEEE Transactions on Power Systems*, vol. 7, no. 1, pp. 54–64, Feb. 1992.

[6] B. Gao, G. K. Morison, and P. Kundur, "Voltage stability evaluation using modal analysis," *IEEE Transactions on Power Systems*, vol. 7, no. 4, pp. 1529–1542, Nov. 1992.

[7] Y. Tamura, H. Mori, and S. Iwamoto, "Relationship between voltage instability and multiple load flow solutions in electric power systems," *IEEE Transactions on Power Apparatus and Systems*, vol. PAS-102, no. 5, pp. 1115–1125, May 1983.

[8] H. D. Chiang, I. Dobson, R. J. Thomas, J. S. Thorp, and L. Fekih-Ahmed, "On voltage collapse in electric power systems," *IEEE Transactions on Power Systems*, vol. 5, no. 2, pp. 601–611, May 1990.

[9] M. M. Begovic and A. G. Phadke, "Dynamic simulation of voltage collapse," *IEEE Transactions on Power Systems*, vol. 5, no. 4, pp. 1529–1534, Nov. 1990.

[10] H. Kwatny, A. Pasrija, and L. Bahar, "Static bifurcations in electric power networks: Loss of steady-state stability and voltage collapse," *IEEE Transactions on Circuits and Systems*, vol. 33, no. 10, pp. 981–991, Oct. 1986.

[11] C. A. Canizares, F. L. Alvarado, C. L. DeMarco, I. Dobson, and W. F. Long, "Point of collapse methods applied to AC/DC power systems," *IEEE Transactions on Power Systems*, vol. 7, no. 2, pp. 673–683, May 1992.

[12] V. Ajjarapu and B. Lee, "Bifurcation theory and its application to nonlinear dynamical phenomena in an electrical power system," *IEEE Transactions on Power Systems*, vol. 7, no. 1, pp. 424–431, Feb. 1992.

[13] E. Abed and P. Varaiya, "Oscillations in power systems via hopf bifurcation," in *Proc. 20th IEEE Conf. Decision and Control including the Symp. Adaptive Processes*, Dec. 1981, pp. 926–929.

[14] J. Alexander, "Oscillatory solutions of a model system of nonlinear swing equations," *International Journal of Electrical Power & Energy Systems*, vol. 8, no. 3, pp. 130–136, 1986.

[15] C. Rajagopalan, P. W. Sauer, and M. A. Pai, "Analysis of voltage control systems exhibiting hopf bifurcation," in *Proc. 28th IEEE Conf. Decision and Control*, Dec. 1989, pp. 332–335 vol.1.

[16] V. Venkatasubramanian, H. Schattler, and J. Zaborszky, "Voltage dynamics: study of a generator with voltage control, transmission, and matched mw load," *IEEE Transactions on Automatic Control*, vol. 37, no. 11, pp. 1717–1733, Nov. 1992.

[17] H. O. Wang, E. H. Abed, and A. M. A. Hamdan, "Bifurcations, chaos, and crises in voltage collapse of a model power system," *IEEE Transactions on Circuits and Systems I: Fundamental Theory and Applications*, vol. 41, no. 4, pp. 294–302, Apr. 1994.

[18] E. H. Abed, J. C. Alexander, H. Wang, A. M. A. Hamdan, and H. C. Lee, "Dynamic bifurcations in a power system model exhibiting voltage collapse," in *Proc.] 1992 IEEE Int. Symp.*

Circuits and Systems [, vol. 5, May 1992, pp. 2509–2512 vol.5.

[19] H.-D. Chiang, C.-W. Liu, P. P. Varaiya, F. F. Wu, and M. G. Lauby, "Chaos in a simple power system," *IEEE Transactions on Power Systems*, vol. 8, no. 4, pp. 1407–1417, Nov. 1993.

[20] E. H. Abed, A. M. A. Hamdan, H. C. Lee, and A. G. Parlos, "On bifurcations in power system models and voltage collapse," in *Proc. 29th IEEE Conf. Decision and Control*, Dec. 1990, pp. 3014–3015 vol.6.

[21] R. L. Chen and P. P. Varaiya, "Degenerate hopf bifurcations in power systems," *IEEE Transactions on Circuits and Systems*, vol. 35, no. 7, pp. 818–824, Jul. 1988.

[22] A. Mees and L. Chua, "The hopf bifurcation theorem and its applications to nonlinear oscillations in circuits and systems," *IEEE Transactions on Circuits and Systems*, vol. 26, no. 4, pp. 235–254, Apr. 1979.

[23] H. G. Kwatny, X.-M. Yu, and C. Nwankpa, "Local bifurcation analysis of power systems using matlab," in *Proc. Int. Conf. Control Applications*, Sep. 1995, pp. 57–62.

[24] I. Dobson and L. Lu, "New methods for computing a closest saddle node bifurcation and worst case load power margin for voltage collapse," *IEEE Transactions on Power Systems*, vol. 8, no. 3, pp. 905–913, Aug. 1993.

[25] J. Lu, C.-W. Liu, and J. S. Thorp, "New methods for computing a saddle-node bifurcation point for voltage stability analysis," *IEEE Transactions on Power Systems*, vol. 10, no. 2, pp. 978–989, May 1995.

[26] N. Hawkins, G. Shackshaft, and M. Short, "Online algorithms for the avoidance of voltage collapse: reactive power management and voltage collapse margin assessment," in *Power System Monitoring and Control, 1991., Third International Conference on.* IET, 1991, pp. 134–139.

[27] R. P. Klump and T. J. Overbye, "Assessment of transmission system loadability," *IEEE Transactions on Power Systems*, vol. 12, no. 1, pp. 416–423, Feb. 1997.

[28] N. Yorino, S. Harada, and H. Cheng, "A method to approximate a closest loadability limit using multiple load flow solutions," *IEEE Transactions on Power Systems*, vol. 12, no. 1, pp. 424–429, Feb. 1997.

[29] C. R. R. Dornellas, A. M. Oliveira, A. C. G. Melo, S. Granville, J. C. O. Mello, J. O. Soto, and M. T. Schilling, "The effects of local and optimized power flow control logic in the reliability analysis of bulk systems," in *Proc. IEEE Power Engineering Society. 1999 Winter Meeting (Cat. No.99CH36233)*, vol. 1, Jan. 1999, pp. 454–458 vol.1.

[30] G. D. Irisarri, X. Wang, J. Tong, and S. Mokhtari, "Maximum loadability of power systems using interior point nonlinear optimization method," *IEEE Transactions on Power Systems*, vol. 12, no. 1, pp. 162–172, Feb. 1997.

[31] A. Borghetti, R. Caldon, A. Mari, and C. A. Nucci, "On dynamic load models for voltage stability studies," *IEEE Transactions on Power Systems*, vol. 12, no. 1, pp. 293–303, Feb. 1997.

[32] R. J. O'Keefe, R. P. Schulz, and F. B. Bhatt, "Improved representation of generator and load dynamics in the study of voltage limited power system operations," *IEEE Transactions on Power Systems*, vol. 12, no. 1, pp. 304–314, Feb. 1997.

[33] M. Parniani and M. R. Iravani, "Voltage control stability and dynamic interaction phenomena of static var compensators," *IEEE Transactions on Power Systems*, vol. 10, no. 3, pp. 1592–1597, Aug. 1995.

[34] T. V. Cutsem and C. D. Vournas, "Voltage stability analysis in transient and mid-term time scales," *IEEE Transactions on Power Systems*, vol. 11, no. 1, pp. 146–154, Feb. 1996.

[35] J. Barquin, T. Gomez, and F. L. Pagola, "Estimating the loading limit margin taking into account voltage collapse areas," *IEEE Transactions on Power Systems*, vol. 10, no. 4, pp. 1952–1962, Nov. 1995.

[36] B. Lee and V. Ajjarapu, "A piecewise global small-disturbance voltage-stability analysis of structure-preserving power system models," *IEEE Transactions on Power Systems*, vol. 10, no. 4, pp. 1963–1971, Nov. 1995.

[37] I. Kurihara, K. Takahashi, and B. Kermanshahi, "A new method of evaluating system margin under various system constraints," *IEEE Transactions on Power Systems*, vol. 10, no. 4, pp. 1904–1911, Nov. 1995.

[38] K. Vu, M. M. Begovic, D. Novosel, and M. M. Saha, "Use of local measurements to estimate voltage-stability margin," *Power Systems, IEEE Transactions on*, vol. 14, no. 3, pp. 1029–1035, 1999.

[39] S. Corsi and G. N. Taranto, "A real-time voltage instability identification algorithm based on local phasor measurements," *IEEE transactions on power systems*, vol. 23, no. 3, pp. 1271–1279, 2008.

[40] B. Milosevic and M. Begović, "Voltage-stability protection and control using a wide-area network of phasor measurements," *Power Systems, IEEE Transactions on*, vol. 18, no. 1, pp. 121–127, 2003.

[41] W. Xu, I. R. Pordanjani, Y. Wang, and E. Vaahedi, "A network decoupling transform for phasor data based voltage stability analysis and monitoring," *IEEE Transactions on Smart Grid*, vol. 3, no. 1, pp. 261–270, 2012.

[42] M. El-Kateb, S. Abdelkader, and M. Kandil, "Linear indicator for voltage collapse in power systems," *IEE proceedings. Generation, transmission and distribution*, vol. 144, no. 2, pp. 139–146, 1997.

[43] I. Smon, G. Verbic, and F. Gubina, "Local voltage-stability index using tellegen's theorem," *IEEE Transactions on Power Systems*, vol. 21, no. 3, pp. 1267–1275, 2006.

[44] G. Verbic and F. Gubina, "A novel concept for voltage collapse protection based on local phasors," in *Transmission and Distribution Conference and Exhibition 2002: Asia Pacific.*

IEEE/PES, vol. 1. IEEE, 2002, pp. 124–129.

[45] V. Balamourougan, T. Sidhu, and M. Sachdev, "Technique for online prediction of voltage collapse," *IEE Proceedings-Generation, Transmission and Distribution*, vol. 151, no. 4, pp. 453–460, 2004.

[46] M. Haque, "On-line monitoring of maximum permissible loading of a power system within voltage stability limits," *IEE Proceedings-Generation, Transmission and Distribution*, vol. 150, no. 1, pp. 107–112, 2003.

[47] Y. Gong, N. Schulz, and A. Guzman, "Synchrophasor-based real-time voltage stability index," in *2006 IEEE PES Power Systems Conference and Exposition*. IEEE, 2006, pp. 1029–1036.

[48] A. Wiszniewski, "New criteria of voltage stability margin for the purpose of load shedding," *IEEE Transactions on Power Delivery*, vol. 22, no. 3, pp. 1367–1371, 2007.

[49] Y. Wang, W. Li, and J. Lu, "A new node voltage stability index based on local voltage phasors," *Electric Power Systems Research*, vol. 79, no. 1, pp. 265–271, 2009.

[50] T. Van Cutsem and C. Vournas, "Emergency voltage stability controls: an overview," in *Power Engineering Society General Meeting, 2007. IEEE*. IEEE, 2007, pp. 1–10.

[51] M. Haque, "Use of local information to determine the distance to voltage collapse," in *2007 International Power Engineering Conference (IPEC 2007)*. IEEE, 2007, pp. 407–412.

[52] M. Begovic, D. Novosel, and M. Milisavljevic, "Trends in power system protection and control," *Decision Support Systems*, vol. 30, no. 3, pp. 269–278, 2001.

[53] B. Venkatesh, A. Rost, and L. Chang, "Dynamic voltage collapse index: wind generator application," *IEEE transactions on power delivery*, vol. 22, no. 1, pp. 90–94, 2007.

[54] L. Fu, B. C. Pal, and B. J. Cory, "Phasor measurement application for power system voltage stability monitoring," in *Power and Energy Society General Meeting-Conversion and*

Delivery of Electrical Energy in the 21st Century, 2008 IEEE. IEEE, 2008, pp. 1–8.

[55] M. Begovic, D. Novosel, and B. Djokic, "Issues related to the implementation of synchrophasor measurements," in *Hawaii International Conference on System Sciences, Proceedings of the 41st Annual*. IEEE, 2008, pp. 164–164.

[56] R. Diao, K. Sun, V. Vittal, R. J. O'Keefe, M. R. Richardson, N. Bhatt, D. Stradford, and S. K. Sarawgi, "Decision tree-based online voltage security assessment using pmu measurements," *IEEE Transactions on Power Systems*, vol. 24, no. 2, pp. 832–839, 2009.

[57] J. Tang, J. Liu, F. Ponci, and A. Monti, "Adaptive load shedding based on combined frequency and voltage stability assessment using synchrophasor measurements," *IEEE Transactions on power systems*, vol. 28, no. 2, pp. 2035–2047, 2013.

[58] R. Sodhi, S. Srivastava, and S. Singh, "A simple scheme for wide area detection of impending voltage instability," *IEEE Transactions on Smart Grid*, vol. 3, no. 2, pp. 818–827, 2012.

[59] C. D. Vournas and N. G. Sakellaridis, "Tracking maximum loadability conditions in power systems," in *Proc. iREP Symp. - Bulk Power System Dynamics and Control - VII. Revitalizing Operational Reliability*, Aug. 2007, pp. 1–12.

[60] M. Glavic and T. V. Cutsem, "Detecting with pmus the onset of voltage instability caused by a large disturbance," in *Proc. IEEE Power and Energy Society General Meeting - Conversion and Delivery of Electrical Energy in the 21st Century*, Jul. 2008, pp. 1–8.

[61] W. Gu, Q. Wan, and P. Jiang, "Linearized local voltage stability index considering induction motor load," in *Proc. IEEE Power Energy Society General Meeting*, Jul. 2009, pp. 1–5.

[62] B. Genet and J. C. Maun, "Voltage-stability monitoring using wide-area measurement systems," in *Proc. IEEE Lausanne Power Tech*, Jul. 2007, pp. 1712–1717.

[63] M. Liu, B. Zhang, L. Yao, M. Han, H. Sun, and W. Wu, "Pmu based voltage stability analysis for transmission corridors," in *Proc. Third Int. Conf. Electric Utility Deregulation and Restructuring and Power Technologies*, Apr. 2008, pp. 1815–1820.

[64] S. Pérez-Londoño, L. Rodríguez, and G. Olivar, "A simplified voltage stability index (svsi)," *International Journal of Electrical Power & Energy Systems*, vol. 63, pp. 806–813, 2014.

[65] Y. Wang, C. Wang, F. Lin, W. Li, L. Y. Wang, and J. Zhao, "Incorporating generator equivalent model into voltage stability analysis," *IEEE Transactions on Power Systems*, vol. 28, no. 4, pp. 4857–4866, Nov. 2013.

[66] M. Begovic, D. Novosel, B. Milosevic, and M. Kostic, "Impact of distribution efficiency on generation and voltage stability," in *System Sciences, 2000. Proceedings of the 33rd Annual Hawaii International Conference on*. IEEE, 2000, pp. 7–pp.

[67] J. Candelo, N. Caicedo, and F. Castro-Aranda, "Proposal for the solution of voltage stability using coordination of facts devices," in *2006 IEEE/PES Transmission & Distribution Conference and Exposition: Latin America*. IEEE, 2006, pp. 1–6.

[68] S.-J. S. Tsai and K.-H. Wong, "On-line estimation of thevenin equivalent with varying system states," in *Power and Energy Society General Meeting-Conversion and Delivery of Electrical Energy in the 21st Century, 2008 IEEE*. IEEE, 2008, pp. 1–7.

[69] S. Banerjee, C. Chanda, and S. Konar, "Determination of the weakest branch in a radial distribution network using local voltage stability indicator at the proximity of the voltage collapse point," in *Power Systems, 2009. ICPS'09. International Conference on*. IEEE, 2009, pp. 1–4.

[70] S.-J. S. Tsai and K.-H. Wong, "Adaptive undervoltage load shedding relay design using thevenin equivalent estimation," in *Power and Energy Society General Meeting-Conversion and Delivery of Electrical Energy in the 21st Century, 2008 IEEE*. IEEE, 2008, pp. 1–8.

[71] K. Sun, F. Hu, and N. Bhatt, "A new approach for real-time voltage stability monitoring using pmus," in *2014 IEEE Innovative Smart Grid Technologies-Asia (ISGT ASIA)*. IEEE, 2014, pp. 232–237.

[72] T. An, S. Zhou, J. Yu, W. Lu, and Y. Zhang, "Research on illed-conditioned equations in tracking thevenin equivalent parameters with local measurements," in *2006 International Conference on Power System Technology*. IEEE, 2006, pp. 1–4.

[73] M. Glavic, M. Lelic, D. Novosel, E. Heredia, and D. Kosterev, "A simple computation and visualization of voltage stability power margins in real-time," in *Transmission and Distribution Conference and Exposition (T&D), 2012 IEEE PES*. IEEE, 2012, pp. 1–7.

[74] H. Yuan and F. Li, "A comparative study of measurement-based thevenin equivalents identification methods," in *Proc. North American Power Symp. (NAPS)*, Sep. 2014, pp. 1–6.

[75] L. Warland and A. T. Holen, "A voltage instability predictor using local area measurements (vip++)," in *Power Tech Proceedings, 2001 IEEE Porto*, vol. 2. IEEE, 2001, pp. 6–pp.

[76] D. Julian, R. P. Schulz, K. Vu, W. H. Quaintance, N. B. Bhatt, and D. Novosel, "Quantifying proximity to voltage collapse using the voltage instability predictor (vip)," in *Power Engineering Society Summer Meeting, 2000. IEEE*, vol. 2. IEEE, 2000, pp. 931–936.

[77] S. M. Abdelkader and D. J. Morrow, "Online thévenin equivalent determination considering system side changes and measurement errors," *IEEE Transactions on Power Systems*, vol. 30, no. 5, pp. 2716–2725, 2015.

[78] B. Leonardi and V. Ajjarapu, "Development of multilinear regression models for online voltage stability margin estimation," *IEEE Transactions on Power Systems*, vol. 26, no. 1, pp. 374–383, Feb. 2011.

[79] C. Vournas, C. Lambrou, M. Glavic, and T. V. Cutsem, "An integrated autonomous protection system against voltage instability based on load tap changers," in *Proc. IREP Symp. Bulk Power System Dynamics and Control - VIII (IREP)*, Aug. 2010, pp. 1–14.

[80] L. He and C. C. Liu, "Parameter identification with pmus for instability detection in power systems with HVDC integrated offshore wind energy," *IEEE Transactions on Power Systems*, vol. 29, no. 2, pp. 775–784, Mar. 2014.

[81] I. R. Pordanjani, Y. Wang, and W. Xu, "Identification of critical components for voltage stability assessment using channel components transform," *IEEE Transactions on Smart Grid*, vol. 4, no. 2, pp. 1122–1132, Jun. 2013.

[82] H.-Y. Su, Y.-T. Chou, and C.-W. Liu, "Estimation of voltage stability margin using synchrophasors," in *2012 IEEE Power and Energy Society General Meeting*. IEEE, 2012, pp. 1–7.

[83] A. Chebbo, M. Irving, and M. Sterling, "Voltage collapse proximity indicator: behaviour and implications," in *IEE Proceedings C-Generation, Transmission and Distribution*, vol. 139, no. 3. IET, 1992, pp. 241–252.

[84] A. A. El-Keib and X. Ma, "Application of artificial neural networks in voltage stability assessment," *IEEE Transactions on Power Systems*, vol. 10, no. 4, pp. 1890–1896, Nov. 1995.

[85] D. Q. Zhou, U. D. Annakkage, and A. D. Rajapakse, "Online monitoring of voltage stability margin using an artificial neural network," *IEEE Transactions on Power Systems*, vol. 25, no. 3, pp. 1566–1574, 2010.

[86] V. Dinavahi and S. Srivastava, "Ann based voltage stability margin prediction," in *Power Engineering Society Summer Meeting, 2001*, vol. 2. IEEE, 2001, pp. 1275–1280.

[87] S. Kamalasadan, A. Srivastava, and D. Thukaram, "Novel algorithm for online voltage stability assessment based on feed forward neural network," in *2006 IEEE Power Engineering Society General Meeting*. IEEE, 2006, pp. 7–pp.

[88] T. Assis, A. Nunes, and D. Falcao, "Mid and long-term voltage stability assessment using neural networks and quasi-steady-state simulation," in *Power Engineering, 2007 Large Engineering Systems Conference on*. IEEE, 2007, pp. 213–217.

[89] B. Jeyasurya, "Artificial neural networks for on-line voltage stability assessment," in *Power Engineering Society Summer Meeting, 2000. IEEE*, vol. 4. IEEE, 2000, pp. 2014–2018.

[90] A. Efthymiadis and Y.-H. Guo, "Generator reactive power limits and voltage stability," in *Power System Control and Management, Fourth International Conference on (Conf. Publ. No. 421)*. IET, 1996, pp. 196–199.

[91] Y. Song, "Design of secondary voltage and stability controls with multiple control objectives," Ph.D. dissertation, Georgia Institute of Technology, 2009.

[92] D. L. Hall and S. A. McMullen, *Mathematical techniques in multisensor data fusion*. Artech House, 2004.

[93] A. Boudraa, L. Bentabet, F. Salzenstein, and L. Guillon, "Dempster-shafer's basic probability assignment based on fuzzy membership functions," *Electronics Letters on Computer Vision and Image Analysis*, vol. 4, no. 1, pp. 1–9, 2004.

[94] A. P. Dempster, "Upper and lower probabilities induced by a multivalued mapping," *The annals of mathematical statistics*, pp. 325–339, 1967.

[95] G. Shafer, *A mathematical theory of evidence*. Princeton university press Princeton, 1976, vol. 1.

[96] K. Sentz and S. Ferson, *Combination of evidence in Dempster-Shafer theory*. Citeseer, 2002, vol. 4015.

[97] T. Van Cutsem and C. Vournas, *Voltage stability of electric power systems*. Springer Science & Business Media, 1998, vol. 441.

[98] S. Greene, I. Dobson, and F. L. Alvarado, "Sensitivity of the loading margin to voltage collapse with respect to arbitrary parameters," *IEEE Transactions on Power Systems*, vol. 12, no. 1, pp. 262–272, Feb. 1997.

[99] R. D. Zimmerman, C. E. Murillo-Sanchez, and R. J. Thomas, "Matpower: Steady-state operations, planning, and analysis tools for power systems research and education," *IEEE Transactions on Power Systems*, vol. 26, no. 1, pp. 12–19, Feb. 2011.

[100] M. Larsson, P. Korba, and M. Zima, “Implementation and applications of wide-area monitoring systems,” in *Proc. IEEE Power Engineering Society General Meeting*, Jun. 2007, pp. 1–6.

APPENDIX A

ADDITIONAL TOPICS

A.1 Basic Probability Assignment-Minkowski Distance Metric

The Dempster Shafer theory of evidential reasoning requires the assignment of masses(also known as degree of support) to a set of hypothesis. The mass assignment problem in the Dempster Shafer theory is a very open problem and there are no established methods to accomplish this task. Many researchers have relied on the heuristic knowledge about the system, for assigning masses to a set of different hypothesis. In case of fusing the margin estimates of different sensors, the accuracy of the margin estimates can be tested against certain properties of the system, and a correlation can be drawn between the accuracy of margins and a certain system property. If the estimated margins are fairly correlated with some property, that can be a basis for mass assignment. In the DS evidential reasoning a sensor assigns masses to the power set of the frame of discernment. The power set includes all the possible unique combinations of the frame of discernment. For a sensor to be able to assign masses to the elements of the power set, other than it's own, a distance metric called "Minkowski Distance" is used. The Minkowski Distance is a metric in a normed vector space which can be considered as a generalization of both the Euclidian Distance and the Manhattan Distance. The Minkowski Distance of order p between two points is defined as

$$d(i,j) = \left(\sum_{i=1}^{n} |x_i - y_i|^p \right)^{\frac{1}{p}} \tag{A.1}$$

Minkowski Distance is typically used with p being either 1 or 2. The former being the Manhattan distance and the latter is called a Euclidean Distance. In the limiting case of p reaching infinity

we obtain as what is called a Chebyshev Distance.

$$\lim_{p\to\infty}\left(\sum_{i=1}^{n}|x_i-y_i|^p\right)^{\frac{1}{p}}=max|x_i-y_i| \tag{A.2}$$

A distance matrix can be formed using the Chebyshev distance as given by Equation (3.28). Distance (or Similarity) matrix indicates only the pairwise distance or similarity between two objects in Minkowski Space. The distance is symmetric and triangular.

$$\begin{bmatrix} 0 & & & & \\ d(2,1) & 0 & & & \\ \vdots & \vdots & \vdots & \ddots & \vdots \\ d(n,1) & d(n,2) & d(n,3) & \dots & 0 \end{bmatrix}$$

Properties of Distance Matrix:

1. Positivity:

$$d(i,j)>0, \text{if} i\neq j \tag{A.3}$$

$$d(i,j=0), \text{if} i=j \tag{A.4}$$

2. Symmetry:

$$d(i,j)=d(j,i) \tag{A.5}$$

3. Triangle Inequality:

$$d(i,j)\leq d(i,k)+d(k,j) \tag{A.6}$$

For any sensor to assign masses to the elements of the power set of the frame of discern-

ment, which are present in its neighborhood, the mass assignment can be treated as a function of the Minkowski distance of their margin estimates. For a sensor i to assign a mass to a sensor j, the mass assignment can be expressed as

$$P_{i,j} = f(d(i,j)) \tag{A.7}$$

The function "f" has to satisfy two properties

1. The range of the function "f" has to be $(0,1)$, since mass assignment is defined in the open interval $(0,1)$.
2. It should assign a higher mass if $d(i,j)$ is less and a lower mass, if $d(i,j)$ is more. However this also depends on the mass that a sensor assigns to its own estimate.

It should be kept in mind that we did not yet specify mass assignment by a sensor to it's own estimate. The distance metric can be used to give the sensor an idea about the accuracy of margin estimates of other sensors, but in order for a sensor to be able to assign a mass to it's own estimate, we have to find some correlation between the accuracy of the margin estimates and some electrical property of the buses, like sensitivity of voltage to complex power injections, short circuit currents or some other properties.

A.2 Coherency Relation and Clustering

Let $W = 1,2,...,m$ be a set of load nodes of the power system. A coherency relation on W may generally be defined as [2]

$$C = (i,j) | \mu(i,j,\delta,\theta,V,\lambda) < \epsilon \tag{A.8}$$

where $\mu : W^2 \times \Re^{n+2m+p} \rightarrow \Re^k$ is the criterion function for selecting coherent nodes and which is symmetrical with respect to i and j

$$\mu(i, j, \delta, \theta, V, \lambda) = \mu(j, i, \delta, \theta, V, \lambda) \tag{A.9}$$

Vector $\epsilon \in \Re^k$ is the vector of criteria thresholds chosen for a particular coherency relation μ. The choice of μ is irrelevant for the clustering algorithm. The ordered couple $G = (W, C)$ is the unidirected coherency graph. Once the cluster pairs are established, a search has to be conducted for finding the complete graph(clique) of maximum size. The clique problem is a well known problem in graph theory. It is NP-complete which translates into being solvable in time polynomial to the size of the problem on a nondeterministic computer. Figure A.1 shows a graph with 20 nodes after being subjected to the clustering process. The cliques 1,...,5 are found in the respective order of their numbering and are shown within areas by dashed lines.

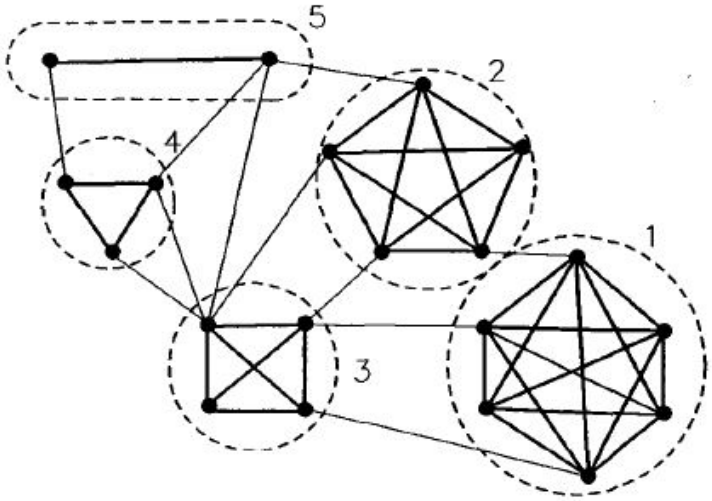

]

Figure A.1: An example of clustering [2]

A.2.1 Coherency Criteria

The coherency criteria adopted in this research effort is the 2-Norm of the Voltage vectors of buses i and j. In a power system where loads are proportionally increasing at all nodes given

by

$$P_{j,k} = \lambda_k P_{j,0} \tag{A.10}$$

$$Q_{j,k} = \lambda_k Q_{j,0} \tag{A.11}$$

where $P_{j,0}$ and $Q_{j,0}$ represent the system base load at Bus j. The coherency relation between the voltage time responses may be obtained by considering the relationship defined by a square matrix C of the form

$$C_{ij} = 1, if \frac{||V_i - V_j||}{|V_i|.|V_j|} \leq \epsilon \tag{A.12}$$

$$0, otherwise \tag{A.13}$$

The matrix, C is a square symmetric matrix whose order is equal to the number of the load buses in the system and entries are binary, $0 and 1$. The C matrix undergoes changes as the loading on the system is increased and as such the clusters keep on changing as the system approaches the stability limit. The matrix gives the cluster pairs, which are then subject to certain transformations. The cluster pairs repeat since the C matrix is symmetric, and hence a transformation is carried which makes the cluster pairs unique.

The cluster pairs are then laid out in a graph, and then the **Bron-Kerbosch algorithm** for searching the maximal cliques, is employed with both pivoting and degeneracy ordering. The algorithm searches for the cliques, all the elements of which mutually satisfy the coherency criteria. The size of the cliques changes with the system loading.

1. Add v to R and remove its non-neighbors from P and X. Then pick another vertex from the new P set and repeat the process. Continue until P is empty.

2. Once P is empty, if X is empty then report the content of R as a new maximal clique (if it's not then R contains a subset of an already found clique).

3. Now backtrack to the last vertex picked and restore P,R and X as they were before the choice, remove the vertex from P and add it to X, then expand the next vertex.

4. If there are no more vertexes in P then backtrack to the superior level.

The objective of using the coherency criteria, as proposed by [2], is to identify the voltage coherent buses in the power network, which can be later used as inputs to the Super node algorithm and can be transformed in to Super Bus. The idea is that if any two buses are voltage coherent they should exhibit the same characteristics and can be combined into a single bus using the equivalent voltage and current. The idea can be extended to many buses which are voltage coherent, which can then be replaced by an equivalent super node.

The criteria threshold is chosen based on the impact of change of the criteria threshold on the sizes of the clusters. Initially the threshold is gradually increased in a uniform fashion and the corresponding change in the cluster sizes is observed. A value for the criteria threshold is chosen at a point where the uniform increase in the threshold results in a small increase in the cluster sizes. For the purpose of our analysis that value of the criteria threshold was found to be $\epsilon = 1.2$.
However the simulations were also run at a $\epsilon = 0.2$, to observe the effects of the small clusters.

A.2.2 Low Selection Threshold

The norm 2 coherency criteria was used on the IEEE 39 bus test system. The cluster pairs were subject to certain transformations, for getting rid of the repeated cluster pairs,since C is a square symmetric matrix, and finding the maximal cliques at each loading factor. The clusters seem to change in size and number as the system loading is increased. Figure illustrates the growth of the cluster pairs as the system loading is increased from the base load to the point of collapse. Cliques are later obtained by implementing the **Bron-Kerbosch algorithm**.

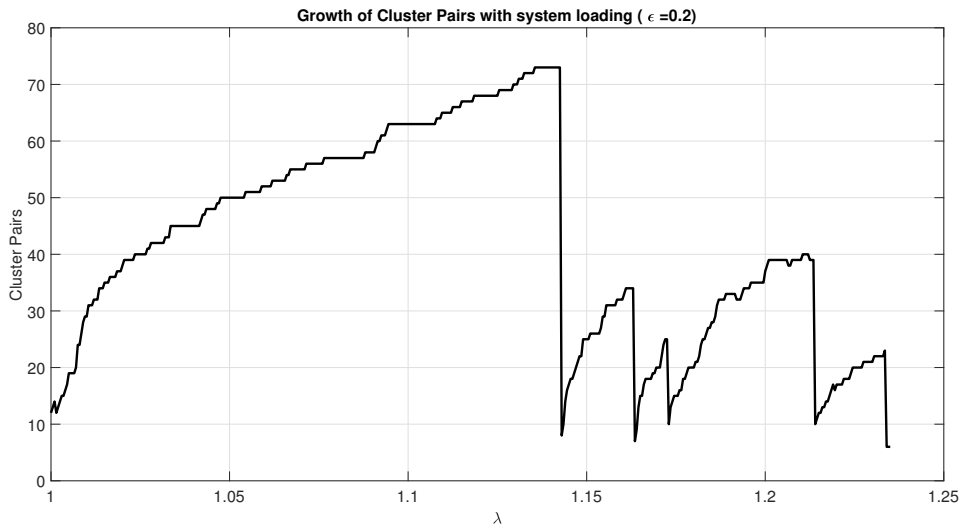

Figure A.2: Growth of Cluster pairs as the system loading is increased

The sizes of the cluster pairs are also presented in the table A.1. The search for the cliques is optimized by splitting a big clique which connects nodes whose electrical paths are linking them through the nodes not belonging to that cluster. This reduces the total number of the cliques obtained, because a majority of the cliques contain nodes which have no electrical connection and hence can not be used as a super node. Also there are cliques which contain buses which have no loads on them which effectively renders them useless for the margin estimation, because an estimate of the Thevenin impedance is only possible when there is a change in the load. When we encounter a bus with no load, which means that $\Delta S_{D,j} = 0; j \notin P,Q$, on this bus, there is no equivalent Thevenin Impedance as seen from this bus, and hence there is no margin estimate for the no load buses. Hence such cliques are disregarded. The cliques which contain load buses which have electrical linkages are chosen to be transformed into super nodes and then their margin estimation as super nodes are studies.

Table A.1: Sizes of cluster pairs

Sample Number	Size of Cluster Pairs
1	[5× 2]
2	[8× 2]
3	[9× 2]
4-6	[10× 2]
7-12	[11× 2]
13-15	[12× 2]
16-19	[13× 2]
20-25	[14× 2]
26-30	[15× 2]
31-32	[16× 2]
33-42	[17× 2]
43-51	[18× 2]
52-53	[19× 2]
54	[20× 2]
55-56	[22× 2]
57-61	[23 × 2]
62-65	[24 × 2]
66-72	[25 × 2]
73	[26 × 2]
74-76	[27 × 2]
77	[28 × 2]
78-79	[29 × 2]
80-98	[30 × 2]
99-118	[31 × 2]
119-130	[32 × 2]
131-139	[33 × 2]
140-146	[34 × 2]
147	[33 × 2]
148-153	[32 × 2]
154-172	[33 × 2]
173-188	[34 × 2]
189-206	[35 × 2]
207-283	[36 × 2]
284-290	[37 × 2]
291-307	[38× 2]
308-319	[39 × 2]
320-331	[40 × 2]
331-373	[41× 2]
374-435	[42 × 2]
436	[41 × 2]
437-465	[42 × 2]
466-467	[41 × 2]
468-472	[40 × 2]

The cluster pairs are laid on a unidirected graph and the maximal cliques are obtained. A MATLAB implementation of the Bron-Kerbosch algorithm is done to find the maximal cliques in the unidirected graph, and the cliques are subjected to the scrutiny process, for getting rid of the inconsequential cliques and for a threshold of $\epsilon = 0.2$, cliques in table A.2 are obtained which are voltage coherent and are electrically connected.

Table A.2: Voltage coherent cliques

Sample Number	Cliques
1 – 6	[16 21], [28 29]
7 – 15	[7 8], [16 21], [28 29]
16 – 19	[3 18], [7 8], [16 21], [28 29]
20 – 25	[3 18], [7 8], [16 21], [28 29]
26 – 54	[1 9], [3 18], [7 8], [16 18 21],[28 29]
55 – 61	[1 9], [3 18], [7 8], [16 18 21], [28 29]
62 – 77	[1 9], [7 8], [3 16 18 21],[28 29]
78 – 465	[1 9], [7 8], [3 16 18 21], [26 28 29]
466 – 479	[7 8], [3 16 18 21], [26 28 29]

In the IEEE 39 bus system, the cliques are circled as shown in figure A.3.

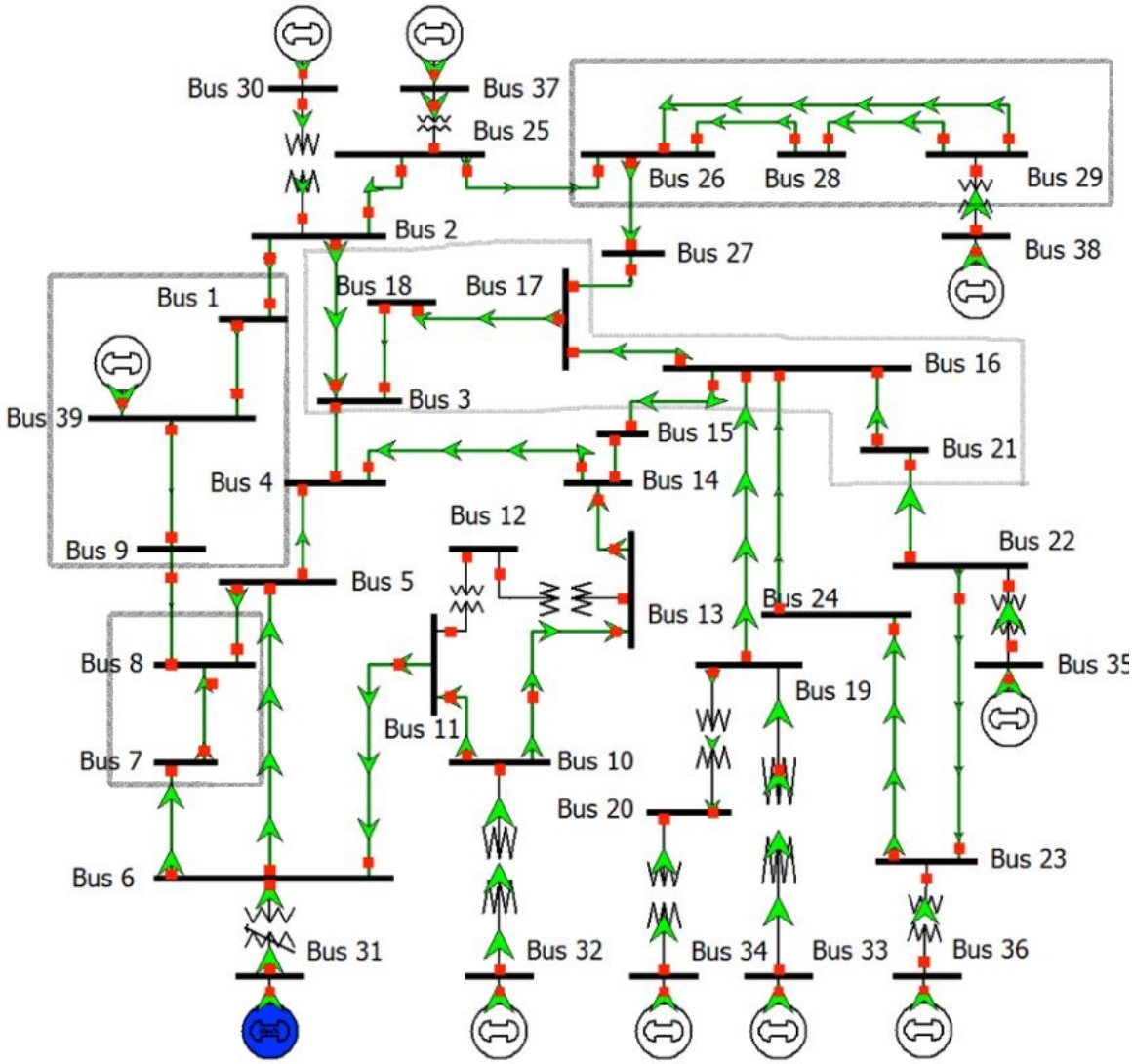

Figure A.3: Coherent Cliques in IEEE 39 Bus system when $\epsilon = 0.2$

Although there are also other smaller cliques, only the ones which persist for the maximum duration are labeled in the Figure . The other cliques are actually the subsets of these big cliques, which merge together as the system loading is increased and form the bigger cliques.

A.2.3 High Selection Threshold

At at threshold criteria of $\epsilon = 1.2$, the cluster pairs increase in number changing rapidly at the beginning, splitting and merging to form bigger cliques until steady state is achieved when the

cluster sizes remain more or less constant. Figure A.4 plots growth of the cluster pairs as the system loading is increased.

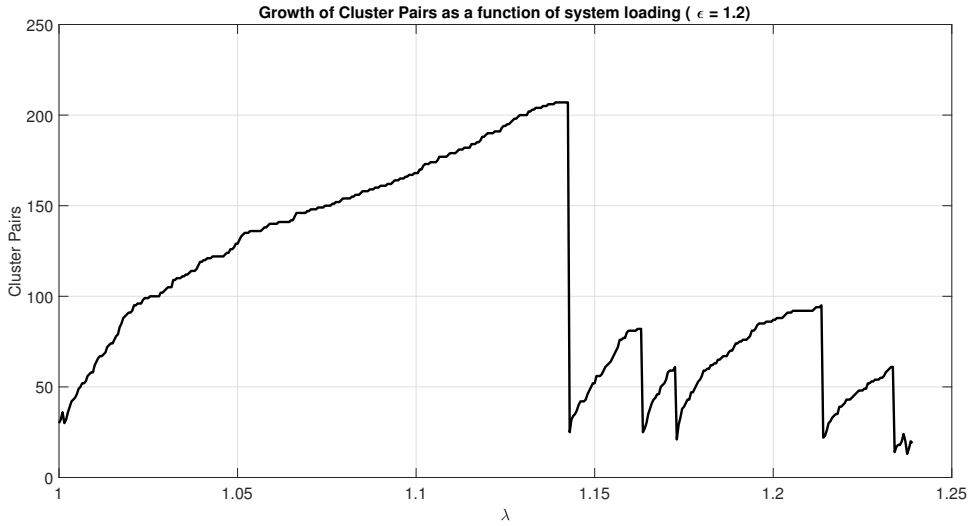

Figure A.4: Growth of Cluster pairs when $\epsilon = 1.2$

It is understandable that the cliques would get bigger in size since the threshold has been relaxed to allow for more pairs to merge together. It can be seen from the growth plots that at a threshold of $\epsilon = 1.2$, the formation of cluster pairs is more chaotic, in the sense their total number is larger and they rapidly split and merge together at the beginning until achieving a steady state in what can be termed as Region 5.

Out of a vast array of cliques, the cliques which seem to persist for a longer time are labeled in the figure A.5.

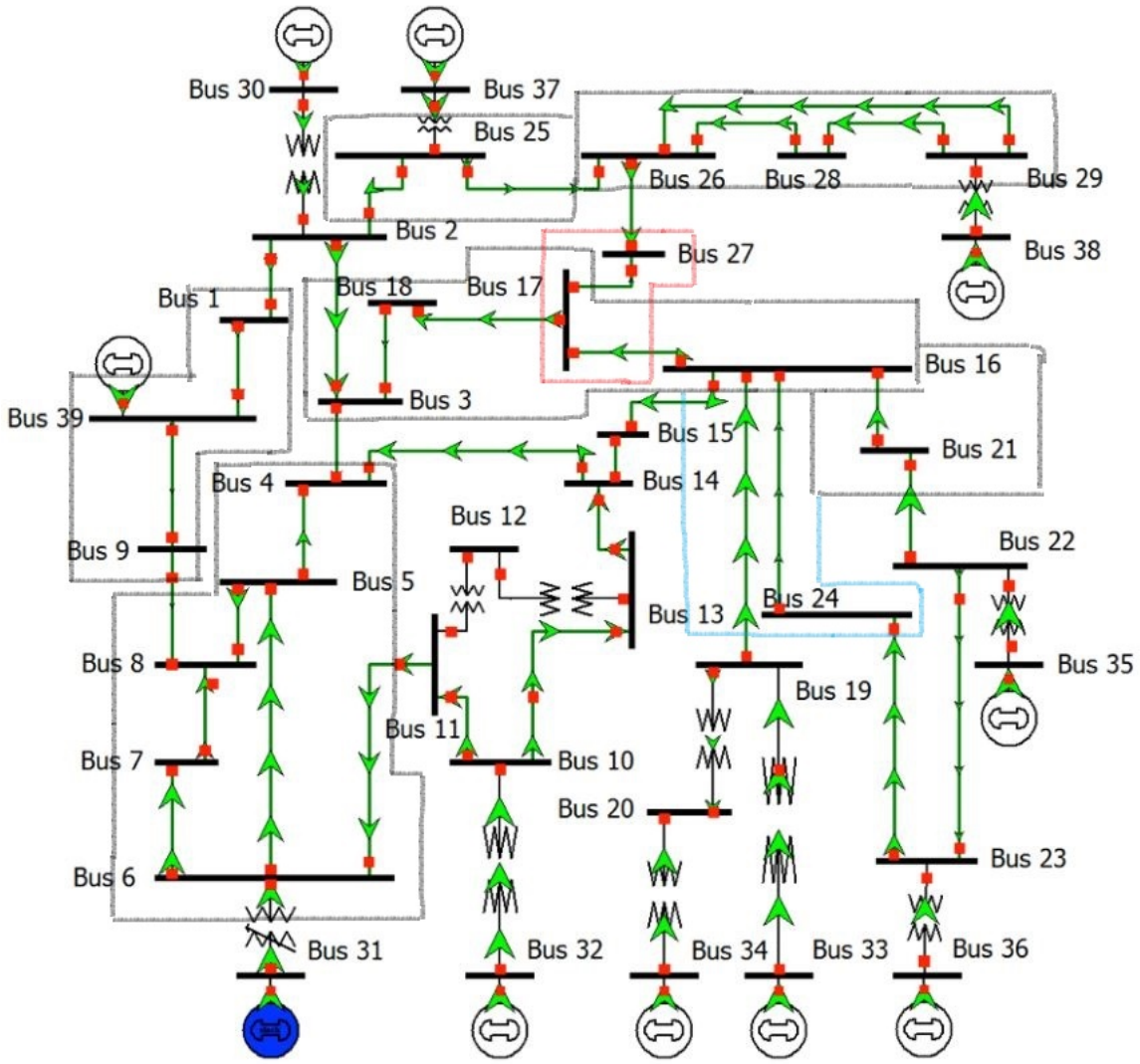

Figure A.5: Coherent cliques when $\epsilon = 1.2$

It is clear that the clique sizes have grown bigger at this value of the threshold than at $\epsilon = 0.2$

APPENDIX B

MODIFICATIONS TO VIP ALGORITHM

B.1 Multi-port Network Model

As pointed out earlier a problem with the VIP algorithm is that the Thevenin equivalent seen from any given bus is not observable.Since VIP has to take at least two consecutive measurements to calculate the Thevenin equivalent, it is important that there is a change in the load. At the same time, other loads in the system change too. Seen from the bus of inception, all changes in the system correspond to a change in the Thevenin equivalent, which invalidate the assumption that the Thevenin equivalent keeps constant during the two measurements.This was pointed by [49] and [75]. As put forward by [49] the fundamental flaw in the VIP lies in the inclusion of other loads in to the system equivalence. The fact that they are nonlinear and dynamic makes it theoretically impossible to represent them as a single Thevenin impedance value. Ideally, if all loads are equipped with PMU, the Thevenin equivalence could be determined based on network information. The feasibility of this approach remains unknown, for this would require high computation complexity and an enormous number of PMUs. By excluding all loads from the equivalent system, leaving the system with only sources, as shown in Figure B.1, a new equivalent system can be constructed where the equivalent impedance is no longer the Thevenin equivalent impedance seen from the bus, but an equivalent impedance dependent solely upon network configuration.Meanwhile, load and generator information will be included in the equivalent voltage thus derived. Instead of monitoring and comparing the load impedance and the Thevenin equivalent impedance, a new indicator can be formulated based on maximum loadability. Assuming all generator buses are equipped with PMUs and the effect of all other loads on the equivalent voltage can be modeled as constant virtual impedance, the equivalent voltage can be accurately calculated with ease.

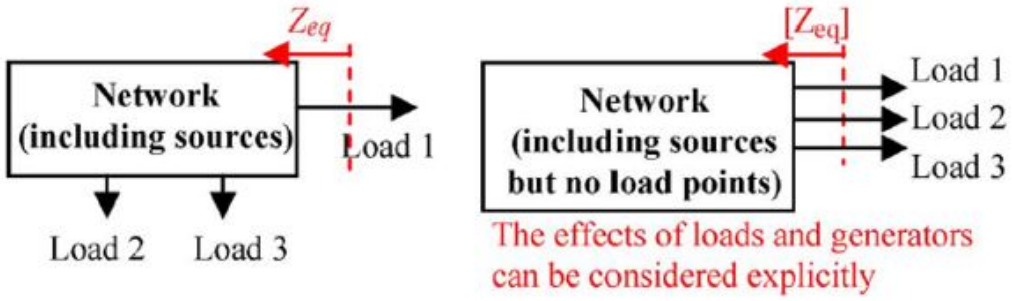

Figure B.1: Thevenin Equivalent including all loads (to the left) and Thevenin Equivalent excluding all loads(to the right)

The figure on the left side of B.1 is called the single-port equivalent system and the figure on the right side of B.1is called the multi-port equivalent system in the paper by Wang et al. The multi-port equivalent system can be further decoupled by bringing all the generators outside of the network as shown in Figure B.2. The transmission network is converted to an equivalent impedance matrix Z_{LL}.

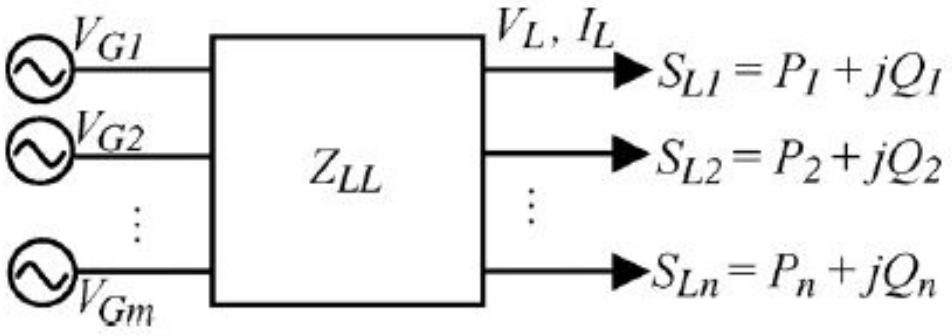

Figure B.2: Multi-port Network Model

Figure B.2 shows that the equivalent impedance is independent of load impedance and equivalent voltage can be estimated given all the generator voltages are known. From the above illustration it can be concluded that by carefully modelling the system and thoughtfully designed PMU placement strategy, a sensor network will bring about a more accurate modeling of the system. The stability margin thus estimated will possibly yield a better reflection of the real scenario which will have a stronger correlation with the bus voltage sensitivities.

As outlined in [49] the multi-port power system can be described as:

$$\begin{bmatrix} -I_L \\ 0 \\ I_G \end{bmatrix} = [Y] \begin{bmatrix} V_L \\ V_T \\ V_G \end{bmatrix} = \begin{bmatrix} Y_{LL} & Y_{LT} & Y_{LG} \\ Y_{TL} & Y_{TT} & Y_{TG} \\ Y_{GL} & Y_{GT} & Y_{GG} \end{bmatrix} \begin{bmatrix} V_L \\ V_T \\ V_G \end{bmatrix} \tag{B.1}$$

where Y matrix is known as the system admittance matrix, V and I stand for the voltage and current vectors, and the subscript L, T and G represent load bus, tie bus and generator bus respectively. Eliminate the tie buses and the above equation can be expressed as follows

$$V_L = KV_G - Z_{LL}I_L \tag{B.2}$$

$$Z_{LL} = (Y_{LL} - Y_{LT}Y_{TT}^{-1}Y_{TL})^{-1} \tag{B.3}$$

$$K = Z_{LL}(Y_{LT}Y_{TT}^{-1}Y_{TG} - Y_{LG}) \tag{B.4}$$

where K is an $n \times m$ matrix obtained from system admittance matrix Y, and Z_{LL} is an $n \times n$ impedance matrix.

For any load bus j, we can obtain

$$V_{Lj} = E_{eqj} - Z_{eqj}I_{Lj} - E_{coupled-j} \tag{B.5}$$

$$Z_{eqj} = Z_{LLjj} \tag{B.6}$$

$$E_{eqj} = [KV_G]_j \tag{B.7}$$

$$E_{coupled-j} = \sum_{i=1, i\neq j}^{n} Z_{LLji}I_{Li} \tag{B.8}$$

where Z_{eqj} is the Thevenin Impedance of the network at bus j without the inclusion of the other loads. The impact of other loads is modelled as a virtual impedance. The virtual impedance is

defined by:

$$Z_{cj} = \frac{E_{couple-j}}{I_{Lj}} \tag{B.9}$$

For the IEEE 39 Bus System the Thevenin Impedances using a multi-port model without the inclusion of the PV-PQ transitions is plotted in B.3

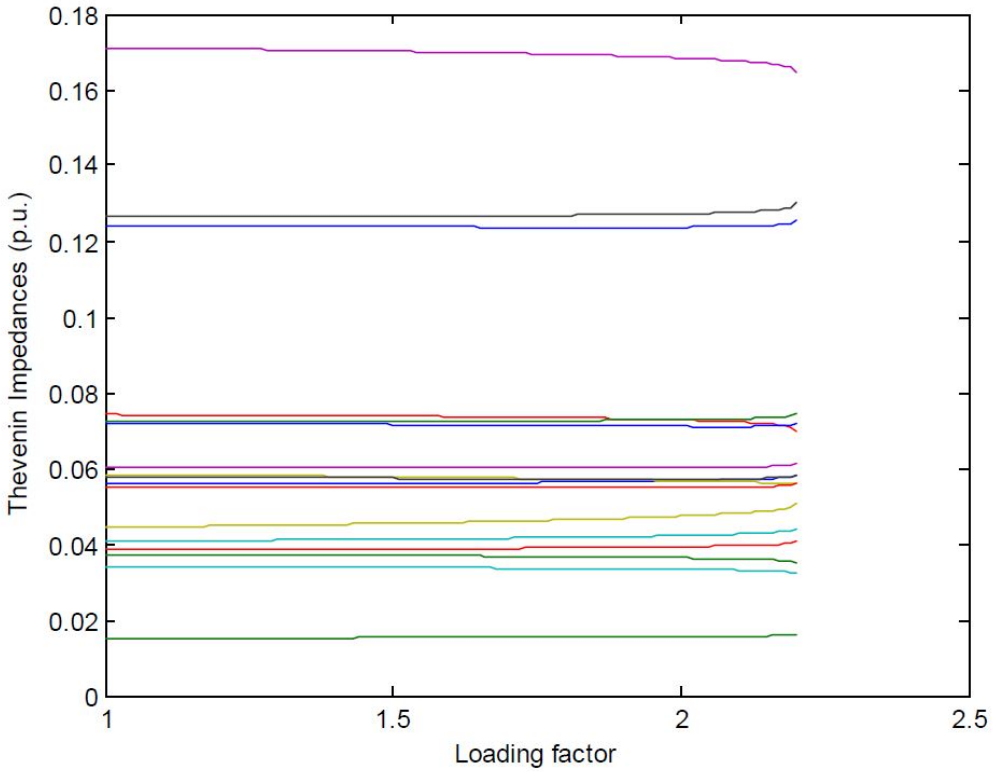

Figure B.3: Thevenin Impedances using a multi-port model

It can inferred from the figure B.3 that the Thevenin Impedances are almost constant at every bus. The virtual impedance which models the effects of other loads stays relatively constant with increasing the physical loads.Figure B.4 plots the Thevenin voltages seen at load buses

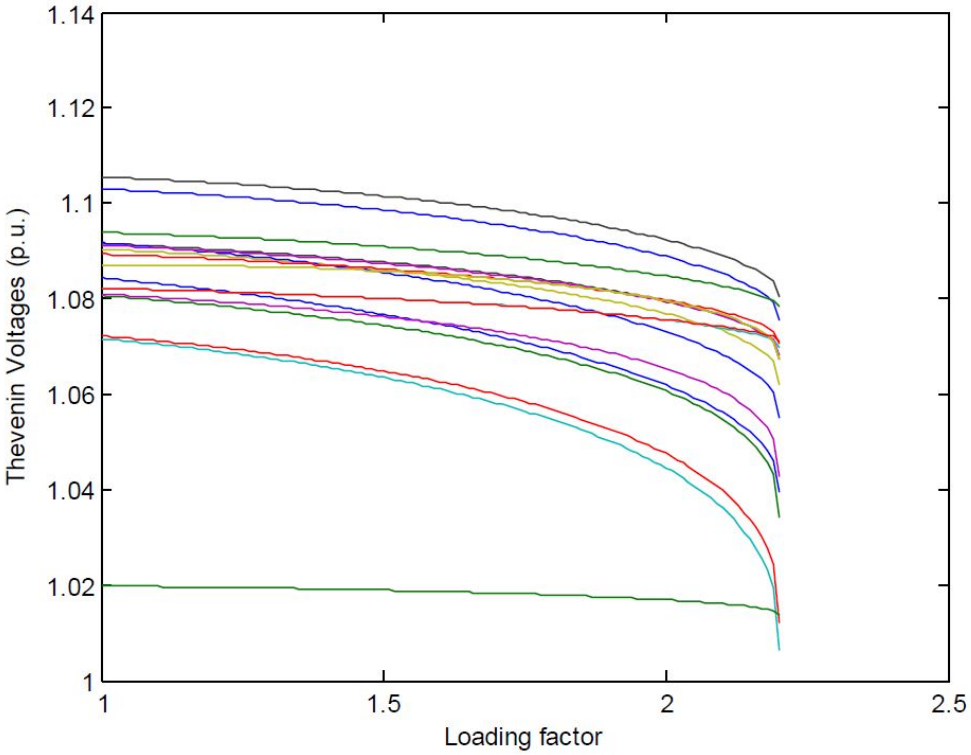

Figure B.4: Thevenin Voltages using a Multi-port model

The normalized bus margins are plotted in figure B.5

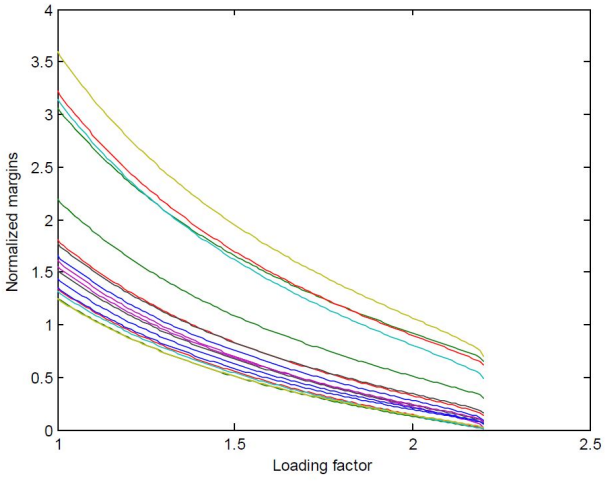

Figure B.5: Bus Margins using a Multi-port model

B.2 Voltage Stability Assessment on Flowgates

For the VIP to produce a meaningful estimate of the stability margin, it is necessary that there are changes on the load side. As pointed out by [75] the VIP algorithm can estimate the correct value of the Thevenin Equivalent when the change happens in the apparent load and it is possible for the VIP to have a wrong estimate if the there is no change in the load or the change in the load impedance is very small. During conditions of near steady state, system conditions do not change appreciably between two consecutive measurement samples. In the absence of any appreciable change in the operating point, which would be the change in load impedance, the VIP evaluation is paused. Change in the system conditions due to transient events can result in false VIP triggering. It thus becomes essential to differentiate system changes caused by transient events as opposed to the ones caused by load changes [3]. Figure B.6 illustrates the limitation of the limitation of the recursive VIP algorithm

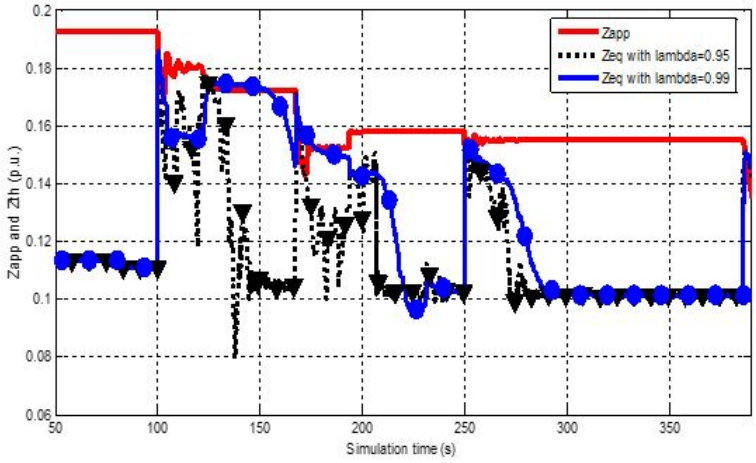

Figure B.6: VIP evaluation using recursive approach for time-domain application [3]

Flowgates are transmission corridors (long lines) with high impedance. In [3] a VIP algorithm which is based on the sets of measurement samples obtained from PMUs for the purposes of monitoring voltage stability in systems with a pronounced longitudinal topology is proposed.

Figure B.7 depicts the flowgate structure connecting two systems. The system is subdivided into subsystem A and B. Subsystem A is provides the transmission path to the electrical energy coming from the source and the subsystem B delivers the energy to the loads.

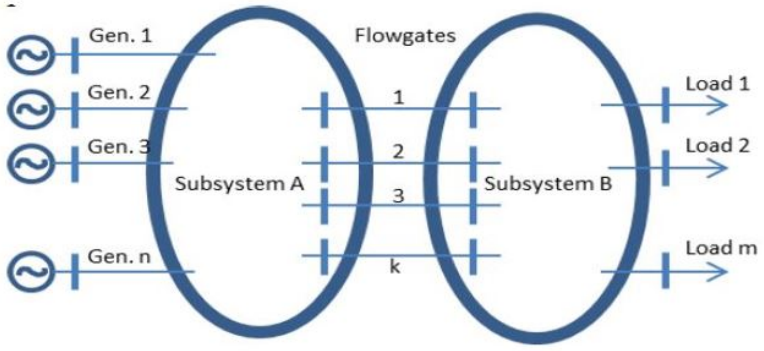

Figure B.7: Model of flowgates connecting the two subsystems [3]

The flowgate VIP calculation is similar to the original VIP calculation except in the use of $S_{flowgate}$ instead of S_{load}. The expression for current becomes

$$I = \left(\frac{S_{flowgate}}{V}\right)^{*} \tag{B.10}$$

The New England system with several modifications is used as the test system for the flowgate VIP algorithm. A total of five transmission flowgates are created by subdividing the original test system into two subsystems. The resulting subsystems are called generator side and load side. In the original system, the branches are modelled as representing short lines. In the flowgate system, the branch parameters are made larger than they originally were. It is observed that all VIP margins show linear dependence to the system load and approach zero at the critical system loading. For this reason, it is suggested that a linear extrapolation of the loading margin can theoretically result in a more accurate fit. Such extrapolation is achieved from the values of the previous two estimated measures of the stability margin. The system critical loading factors thus obtained are shown in figure B.8.

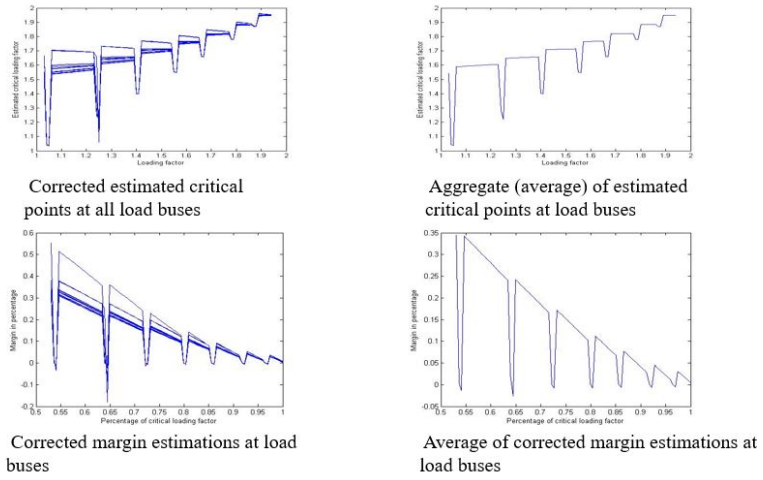

Figure B.8: Estimated Critical Load factors and Estimated margins [3]

B.2.1 Flowgate VIP in remedial action formulation

It has been known that over longer distances the transmission line impedance can be modified by employing series compensation [97]. Such compensation is usually provided by the use of series capacitors. To that extent, when and if some of flowgates reach critical loading thus limiting the transfer of power or even threaten to drive the system in to instability, such series compensation can be carried out to increase the load/power transfer. The order of compensation can be decided by the flowgate sensitivity, with the most sensitive flowgate being compensated first. The sensitivity of loading margin to such series compensation is calculated from the difference in the impedance trajectories.

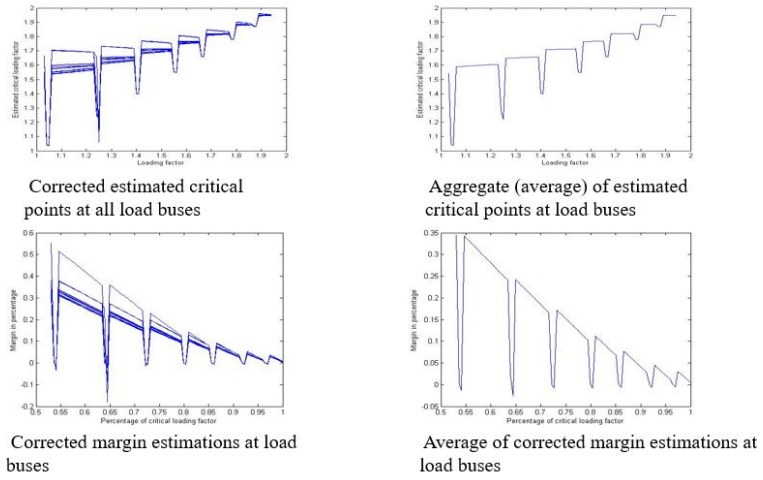

Figure B.9: Trajectories of $Z_L - Z_{Th}^*$ at the receiving end of Flowgates [3]

B.2.2 VIP as trigger for remedial actions

Since the flowgates are the main pathways of power transfer loss of any would dramatically curtail the transfer capacity coupled with a substantial decrease in the loading margin. After any contingency event, it is important to have an update on the loading margin. Reference [98] illustrates the quasi-linearly dependence of the loading margin or even quadratically with respect to various system control parameters. It is possible to derive an empirical relationship between the line admittance and the loading margin. Such a dependence makes it possible to derive a measure of the margin, given two sets of margins and line admittance values $(m1, y1), (m2, y2)$,. With the loss of a flowgate, the estimated new margin can be expressed as

$$m = \frac{m_2 y_1 - m_1 y_2}{y_1 - y_2} \tag{B.11}$$

Extrapolation of critical loading factor for a flowgate contingency at flowgate 1 (all margins are in pu, true critical points after contingency (loss of this flowgate) is 1.52)

Loading factor	No compensation margin	3% series comp. margin	Estimated critical loading factor
1.1	0.6650	0.6688	1.4900
1.2	0.5151	0.5184	1.4938
1.3	0.3699	0.3726	1.5033
1.4	0.2296	0.2318	1.5331
1.5	0.0954	0.0969	1.5337
1.52	0.0694	0.0708	1.5373

Extrapolation of critical loading factor for a flowgate contingency at flowgate 2 (all margins are in pu, true critical points after contingency (loss of this flowgate) is 1.38)

Loading factor	No compensation margin	3% series comp. margin	Estimated critical loading factor
1.1	1.1101	1.1210	1.3353
1.2	0.8440	0.8543	1.3587
1.25	0.7159	0.7258	1.3729
1.3	0.5914	0.6009	1.3883
1.35	0.4709	0.4799	1.4012
1.38	0.4006	0.4093	1.4170

Figure B.10: Critical loading factor for different flowgate admittance values [3]

B.2.3 Multi-port Analysis to Flowgates

As we saw in the multi-port system model, the equation for the voltage vector can be written as

$$\begin{bmatrix} V_{L1} \\ . \\ . \\ . \\ V_{Ln} \end{bmatrix} = \begin{bmatrix} K_{11} & . & . & K_{1m} \\ . & . & . & \\ . & . & . & \\ . & . & . & \\ K_{n1} & . & . & K_{nm} \end{bmatrix} \begin{bmatrix} V_{G1} \\ . \\ . \\ . \\ V_{Gm} \end{bmatrix} - \begin{bmatrix} Z_{11} & . & . & Z_{1n} \\ . & . & . & \\ . & . & . & \\ . & . & . & \\ Z_{n1} & . & . & Z_{nn} \end{bmatrix} \begin{bmatrix} I_{L1} \\ . \\ . \\ . \\ I_{Ln} \end{bmatrix} \tag{B.12}$$

For any flowgate j, voltage can be expressed as

$$V_j = \sum_{i=1}^{p} K_{ji} V_{Gi} - \sum_{i=1}^{q} Z_{LLji} I_{Li} - \sum_{1=q+1}^{q+r} Z_{LLji} I_{Li} \tag{B.13}$$

where $\sum_{1=q+1}^{q+r} Z_{LLji} I_{Li} = V_{d1}$ = Line Drops caused by flowgate loads

$\sum_{i=1}^{q} Z_{LLji} I_{Li}$=$V_{d2}$= Line voltage drop caused by loads in sub-system A

In case of proportional load increase

$$\left(|\frac{V_{d1}+V_{d2}}{I+Lj}|\right) = |Z_{eq}| \tag{B.14}$$

which is constant for all loads.

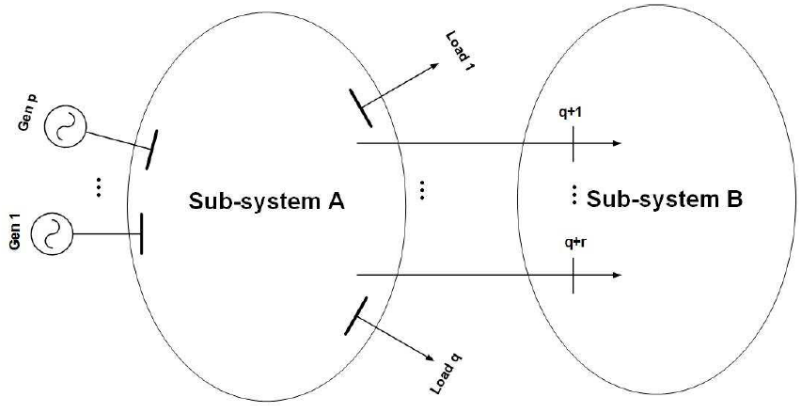

Figure B.11: Line loads and flowgates

Figure B.12,B.13,B.14, plot the Equivalent voltages and Equivalent Impedance as seen from different flowgates.

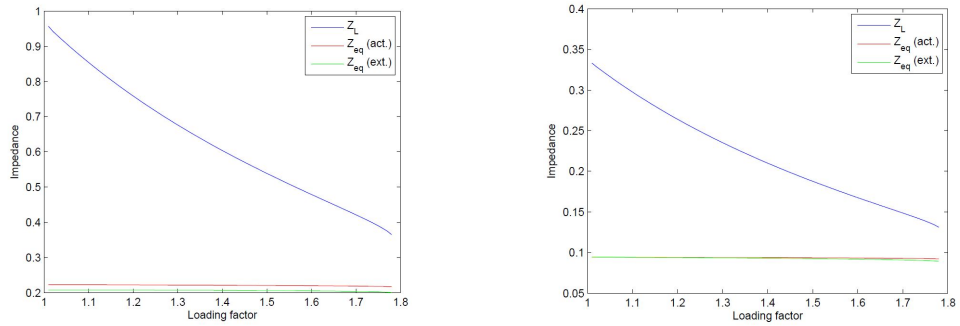

Figure B.13: Equivalent Impedance as seen from Flowgates 1 and 2

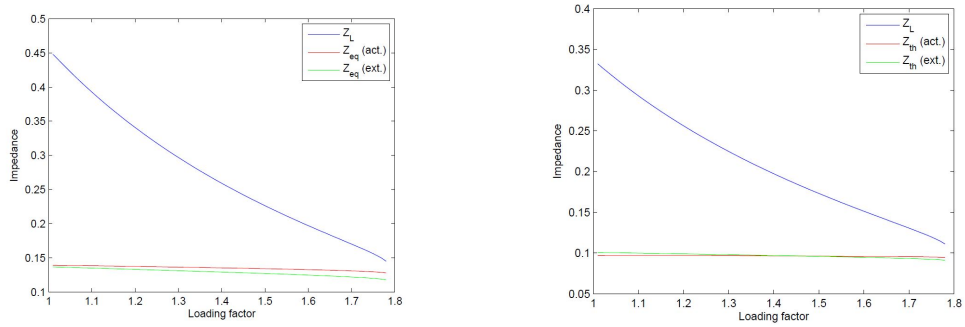

Figure B.14: Equivalent Impedance as seen from Flowgates 8 and 9

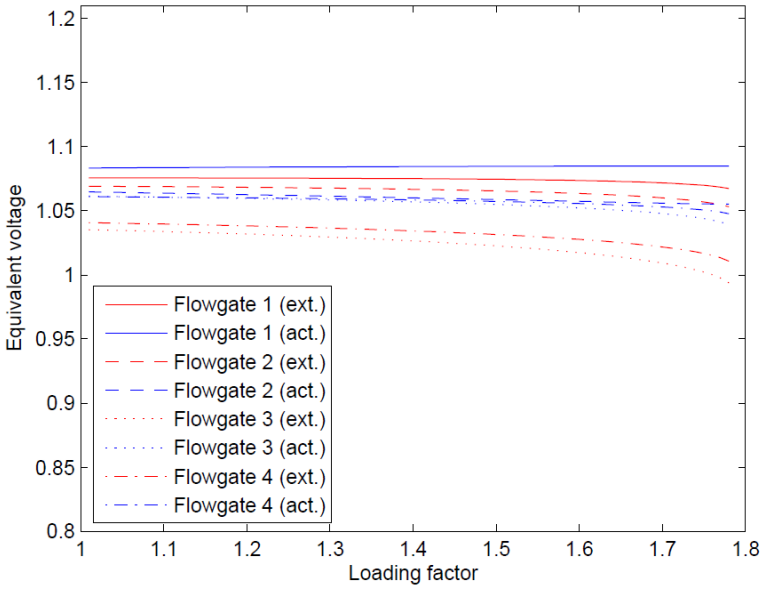

Figure B.12: Equivalent Voltages as seen from Flowgates

APPENDIX C

SOFTWARE PACKAGE

C.1 MATPOWER

MATPOWER [99] is an open source, MATLAB based simulation package that provides a variety of tools targeted towards researchers, students and educators. It is used widely in research and education for AC and DC power flow and optimal power flow (OPF) simulations. It also includes tools for running OPF-based auction markets and co-optimizing reserves and energy. Included in the distribution are numerous example power flow and OPF cases, ranging from a trivial four-bus example to real-world cases with a few thousand buses. MATPOWER consists of a set of MATLAB-m files designed to give the best performance while keeping the code simple to understand and easy to implement. In the study presented in this report MATPOWER has been adapted to include the Q-limits on the generators, and to enable calculating sequence of snapshot power flows, VIP calculation algorithms and other custom-developed routines to simulate the wide area monitoring and control algorithms.

MATPOWER comes equipped with a wide variety of test cases ranging from a simple 4 bus network to a multi-thousand bus real world networks with thousands of generators and tens of thousands of additional user variables and constraints. The six bus system used for simulation in this study is a modified version of the MATPOWER 4 bus system and Table C.1 contains the bus data used and Table C.2 contains the generator data used. Only the bus and generator data was altered while keeping the other constraints the same. Two new branches have been added to this system with similar parameters as that of a 4 bus system. Bus Data

Table C.1: Bus Data used for 6 bus System

Bus	Type	PD	QD
1	3	0	0
2	2	59	23
3	2	59	26
4	1	33	9
5	1	0	0
6	1	18	7

Generator Data

Table C.2: Gen Data used for 6 Bus System

Bus	PG	QG	Q_{max}	Q_{min}
1	0	0	300	-100
2	0	0	42	-14
3	0	0	48	-10

In the IEEE 9 bus system, additional load was added on Bus 8 to simulate the effects on the sensitivity metric. This was done to further check the robustness of the sensitivity algorithm. The Bus data used for the IEEE 9 bus network is presented in Table C.3. The generator data was kept the same.

Table C.3: Bus Data for IEEE 9 Bus System

Bus	Type	PD	QD
1	3	0	170
2	2	0	10
3	2	0	60
4	1	0	20
5	1	90	30
6	1	0	0
7	1	100	35
8	1	10	5
9	1	125	50

All the other test cases used in the study are the original test cases found in MATPOWER. The test cases are provided with MATPOWER and need not be downloaded separately. In the

IEEE 118 bus different test cases were created by fixing the upper reactive limit of generators at 10 MVAr for each unique combination with no other change.

APPENDIX D

PSGUARD-WIDE AREA MONITORING SYSTEMS TOOL

D.1 Wide Area Monitoring System

At its core the idea of a Wide Area Monitoring System lies in the processing of data at a centralized location which is further aimed at evaluating the state of the power system with respect to its stability limits. WAMS is a step in the forward direction towards establishing a future grid with decentralized and distributed power generation. In the modern times the power systems are operated close to their limits, which makes them very sensitive to the disturbances. In such a scenario modern supervision and tools are needed to allow the networks to operate closer to their stability limits while maintaining system security. The data handling in WAMS can be essentially summed up in three stages [100]

- Data Acquisition and Syntheis which is done locally by the PMUs.

- Date Delivery which is done by the communication systems.

- Data Processing; which is done by a central unit.

The dynamics and the non linearities play a significant role and considerably affect the system security limits. For a proper assessment of the system security limits in real time, the data (measurements) must be collected from different locations with high sampling rate and at the same time instant. This is achieved by the use of devices called the Phasor Measurement Units (PMUs).

ABB's RES521 Phasor Measurement Unit is based on a protective relay technology with 18 analog inputs and a selectable transfer rates up to 1 phasor/cycle which is fast enough for VIP. The phasor data is normally sent from the PMU to the data concentrator at a speed of 25/30 or

50/60 samples per channel per second. These speeds are sufficient for measuring changes in the voltage phasors with respect to the changes in the local load of the bus. The reference for the phase angle is the NavStar Global Positioning System which supplies highly accurate time and date information. The applications of PSGuard include phase angle monitoring, voltage stability monitoring, Line Thermal Monitoring, Event Driven Data Archiving, Power Oscillation monitoring, Power Damping monitoring, SCADA/EMS integration and Communication gateway. For voltage stability monitoring it provides information about the power margin to the point of maximum loadability of transmission corridors by using PMU data. The time frame for a possible voltage collapse scenario can be as short as 2 second so the monitoring system should be able to accommodate in such a small time frame. The data communication and processing process should take no more than 1 second. Since the required minimum data rate is 64 kbps per PMU link and the required maximum data latency is less than 0.1s from the physical measurement to data received in PSG828, the aforementioned data communication requirement could be satisfied. PSGuard provides communication to the SCADA/EMS systems which is required since system network and topological information would be needed in the analysis.